AER/AGS Special Report 124

Alberta Energy Regulator

Airborne Geophysics Data Analysis and Interpretation, Central Alberta

AGS
ALBERTA GEOLOGICAL SURVEY

AER/AGS Special Report 124

Airborne Geophysics Data Analysis and Interpretation, Central Alberta

G.P. Lopez, D. McGill, A. Brem and J. McKenzie

Ronacher McKenzie Geoscience Inc.

December 2025

ISBN 978-1-4601-5728-2

Lopez, G.P., McGill, D., Brem, A. and McKenzie, J. (2025): Airborne geophysics data analysis and interpretation, central Alberta; Alberta Energy Regulator / Alberta Geological Survey, AER/AGS Special Report 124, 122 p.

Publications in this series have undergone only limited review and are released essentially as submitted by the author.

Authors address:
G.P. Lopez, D. McGill, A. Brem and J. McKenzie
Ronacher McKenzie Geoscience Inc.
6 – 2140 Regent Street
Sudbury, ON P3E 5S8
Canada

Tel: 705.419.1508
Email: info@rmgeoscience.com

Published December 2025 by:
Alberta Energy Regulator
Alberta Geological Survey
Suite 205
4999 – 98 Avenue NW
Edmonton, AB T6B 2X3
Canada

Tel: 780.638.4491
Email: AGS-Info@aer.ca
Website: ags.aer.ca

Contents

Appendices

Digital Appendix A – Interpretation – GIS files

The appendix is in the accompanying folder entitled 'Digital Appendix A – Interpretation – GIS files,' located in the download zip file.

Digital Appendix B – Airborne magnetic map products

The appendix is in the accompanying folder entitled 'Digital Appendix B – Airborne magnetic map products,' located in the download zip file.

Digital Appendix C – Automatic detection – Fathom Geophysics vector and raster products

The appendix is in the accompanying folder entitled 'Digital Appendix C – Automatic Detection – Fathom Geophysics vector and raster products,' located in the download zip file.

Foreword

The Alberta Geological Survey (AGS) outsourced the geological interpretation of the 2024 high-resolution airborne magnetic surveys conducted by the Alberta Energy Regulator (AER) / AGS in central Alberta. This interpretation focused on modifying the boundaries of known basement domains, dividing domains into subdomains, identifying ductile and brittle structures, and identifying potential intrusions.

All production of geophysical products and interpretation of data were done by Ronacher McKenzie Geoscience Inc. (RMG), as well as the subcontractor Fathom Geophysics LLC (Fathom), with oversight and approval from the AER and the AGS. The 2024 airborne magnetic data were used to create a variety of grid-based filter products as well as three-dimensional (3D) inversions of a select portion of the study area, which were used together to aid in RMG's interpretation. Fathom generated automatic structure detection, radial symmetry detection, depth to basement filters, and other geophysical products. The products were integrated with existing geological data to update previously described basement domain boundaries and, notably, further divide the domains into subdomains. In addition, potential intrusions as well as brittle and ductile structures were identified. This release includes a selection of GIS files, geophysical vector and raster products, as well as the 3D inversion model files.

This work was completed under the Mineral Grant provided by the Government of Alberta dated June 22, 2021.

Geological Interpretation of the 2024 Aeromagnetic Data

Central Alberta

Prepared For:

Alberta Geological Survey

Prepared By:

Gloria Lopez, PhD, P.Geo.
Darcy McGill, P.L. (Geo.)
Arjan Brem, PhD, P.Geo.
Jenna McKenzie, P.Geo.
Ronacher McKenzie Geoscience Inc.

February 7, 2025

TABLE OF CONTENTS

FIGURES

TABLES

APPENDICES

Appendix 1 – Automatic Detection – Fathom Geophysics Report

DIGITAL APPENDICES

Digital Appendix A – Interpretation - GIS files
Digital Appendix B – Airborne magnetic map products
Digital Appendix C – Automatic Detection - Fathom Geophysics vector and raster products

1.0 SUMMARY

The Alberta Geological Survey ("AGS") contracted Ronacher McKenzie Geoscience ("RMG") to provide a geological interpretation of the 2024 high-resolution aeromagnetic surveys conducted over central Alberta.

This report presents the results of the geological interpretation, which includes the central Alberta basement and the overlying Western Canada Sedimentary Basin ("WCSB"). This report supplements the GIS files produced for this project.

The Alberta Energy Regulator ("AER") contracted EON Geosciences Inc., to fly aeromagnetic surveys covering the project area. Data acquisition was completed between September 2023 and March 2024. RMG reviewed the digital data for completeness and data quality. Additional aeromagnetic data from legacy surveys were received to complete coverage of the central Alberta project area.

The new high-quality airborne magnetic data and derivative products enable improved understanding of the 3D architecture of the basement in central Alberta. The observations were integrated with and calibrated against existing results of legacy geophysical studies, geological information, and regional structural interpretations. Care was taken to avoid mistaking potential cultural magnetic response for geology-related anomalies. The following conclusions can be made:

- The higher resolution of the new magnetic data allows for further subdivision of known domains into subdomains in the crystalline basement based on variations of internal magnetic fabrics. Modifications to existing basement domains were made by editing the tectonic domain boundaries of Villeneuve et al., (1993), Ross et al. (1994) and Pilkington et al. (2000) and by dividing known domains into subdomains.
- Rounded anomalies (intrusion detection) were delineated. These range from small single lobe circular anomalies to larger multi-lobe rounded asymmetrical anomalies and may represent potential intrusions.
- Known ductile structures were recognized such as the Snowbird Tectonic Zone and Red Deer Trend; new ductile structures were defined and characterized, including the Eyehill Trend and northern extent of the Vulcan Low.
- The new magnetic data provide further insight and demonstrate relationships between basement features not identified before and the location of linear reef complexes.
- New brittle faults were delineated. Few regional faults of the WCSB reported in literature show a spatial correlation with the magnetic lineaments.
- The interpretation of the new high-quality aeromagnetic data for central Alberta corroborated previous lithotectonic domains defined by previous authors and facilitated the identification of new subdomains and structural lineaments that may help to refine current tectonic models. In particular, the magnetic data suggest that east-central Alberta has more basement complexity than previously recognized and

further investigation is required to understand its lithotectonic history, controls on the deposition of Paleozoic strata, and potential sources, pathways and traps for mineralization.

2.0 Project Overview

The Alberta Geological Survey ("AGS") commissioned Ronacher McKenzie Geoscience ("RMG") to complete a geological interpretation of the 2024 high-resolution aeromagnetic survey over central Alberta conducted by EON Geosciences Inc., with the following regional objectives:

- Define domains for regional tectonic interpretations of the crystalline basement (Western Laurentia).
- Delineate anomalies caused by granitoids.
- Delineate ductile structures in the basement.
- Examine linear anomalies for correlation with brittle fracture zones.
- Identify late brittle faults that may have acted as pathways for fluids (e.g., helium, mineralizing fluids).

RMG completed parallel studies on geophysical data from the Canadian Shield (Lopez et al., 2024a), southern Alberta (Brem et al., 2024), and northern Alberta (Lopez et al., 2024b)

Universal Transverse Mercator ("UTM") coordinates were provided in the datum of WGS 84 zone 11N for all aeromagnetic digital files (vector and map files). Figures herein were projected to NAD 83 zone 11N.

2.1 Previous Regional Studies

Previous regional studies that involve geophysical acquisition and/or geological interpretations include:

- The pioneering work by Hoffman (1988), Ross et al. (1989), and Villeneuve et al. (1993), in which aeromagnetic and gravity data were used to subdivide the basement in Alberta into tectonic domains.
- Misra et al. (1991) provided numerous lineaments based on satellite imagery interpretation. Their work assumed that fractures that outline the fault blocks in the basement control the orientation of faults in the sedimentary cover and hence, the orientation of lineaments appearing on satellite images.
- Burwash et al. (1994) provided a geological interpretation of the basement rocks based on petrography, whole-rock geochemistry, and isotopic age determinations carried out on core samples collected from petroleum wells that had penetrated the crystalline basement. Later the authors provided a metamorphic evolution of the basement of Alberta based on historical and new U–Pb, Rb–Sr, K–Ar, $^{40}Ar/^{39}Ar$ and Sm–Nd geochronology (Burwash et al., 2000).

- Edwards et al. (1998) completed a regional interpretation of magnetic and gravity data in central Alberta using the horizontal gradient to infer the locations of steep basement faults. Results identified distinctive orthogonal sets of NE-, NW and N-S/E-W lineament systems, which may have controlled the deposition and deformation of Phanerozoic sedimentary units.

- The Lithoprobe seismic reflection program was a national research project that studied the 3D structure and evolution of the subsurface in Canada. Lithoprobe data interpretation for central Alberta can be found in Eaton et al. (1995; 1999), Ross and Eaton (2002) and Ross (2002), among others.

- Pilkington et al. (2000) used potential field data and anomaly enhancement methods to emphasize the internal character of domains and refined the basement subdivisions.

- Lyatsky et al. (2005; and references therein) used potential field data and anomaly enhancement methods to identify lineaments in central and southern Alberta. This work supported the conclusions by Eaton et al. (1995) that basement faults have a control on hydrocarbon traps in the Central Alberta basin.

2.2 Recent Advances

New state-of-the-art aeromagnetic and gravity surveys allow better and more accurate analysis and interpretation of the data, particularly since much of the legacy aeromagnetic and gravity data was acquired using very large line spacings and without the spatial accuracy made possible by satellite positioning and navigation systems.

Secondly, over the past two decades, advances in computing power have enabled new geophysical data processing methods and visualization techniques, particularly for large scale datasets. In addition, 3D integration and modelling of subsurface data is now commonplace, enabled by these same computing advances.

2.3 RMG Qualifications

RMG is a Canadian consulting company operating globally. RMG's mission is to use intelligent geoscientific data integration to help mineral explorers focus on what matters to them. We help a growing number of clients understand the factors that control the location of mineral deposits.

With a variety of professional experience, our team's services include:

- Data integration, analysis, and interpretation
- Geophysical services
- Project generation and property assessment
- Exploration project management

- Independent technical reporting
- Project promotion
- Lands management

The primary author of this report is Gloria Lopez, PhD, P.Geo., Senior Geologist at RMG and a geologist in good standing with the Association of Professional Engineers and Geoscientists of Alberta (#181673) and Professional Engineers and Geoscientists Newfoundland and Labrador (#11213). Dr. Lopez has over two decades of experience working as an economic geologist.

A second co-author of this report is Mr. Darcy McGill, BSc, P.Geo. (Limited), P.L. (Geo). Mr. McGill is a Senior Geophysicist at RMG and a geophysicist in good standing with the Association of Professional Geoscientists of Ontario (APGO #2010) and Professional Licensee with the Association of Professional Engineers and Geoscientists of Alberta (#316505). Mr. McGill has worked in geophysical data acquisition, processing, and interpretation for mineral exploration since 1995.

A third co-author of this report is Arjan Brem, PhD, P.Geo., Associate Geologist at RMG and a geoscientist in good standing with the Association of Professional Geoscientists of Ontario (#3798) and with the Association of Professional Engineers and Geoscientists of Alberta (#289121). Dr. Brem has worked globally as a structural geologist in the petroleum and mining industry since 2007.

A fourth co-author of this Report is Ms. Jenna McKenzie, Hons BSc, P.Geo. Ms. McKenzie is the co-founder and Principal Geophysicist to RMG and a geoscientist in good standing with the Association of Professional Geoscientists of Ontario (APGO #1653) and the Association of Professional Engineers and Geoscientists of Alberta (#315719). Ms. McKenzie has worked as a geophysicist since 2001 in the exploration and mining industry on a variety of exploration properties with specific focus on geophysics surveying and interpretation.

Additionally, Fathom Geophysics completed automatic structure detection, depth to basement analysis and radial symmetry analysis for intrusion detection on behalf of RMG.

3.0 PROJECT LOCATION

The project area is located in central Alberta, adjoining Saskatchewan (Figure 3-1). The survey area lies between latitudes 51° and 54°N, and longitudes 110° and 118°W, and is covered by NTS map sheets 72E, 72L, 72M, 73D, 73E, 74D, 82O, 82P, 83A, 83B, 83C, and 83E to 83H. The project area includes the cities of Edmonton and Red Deer.

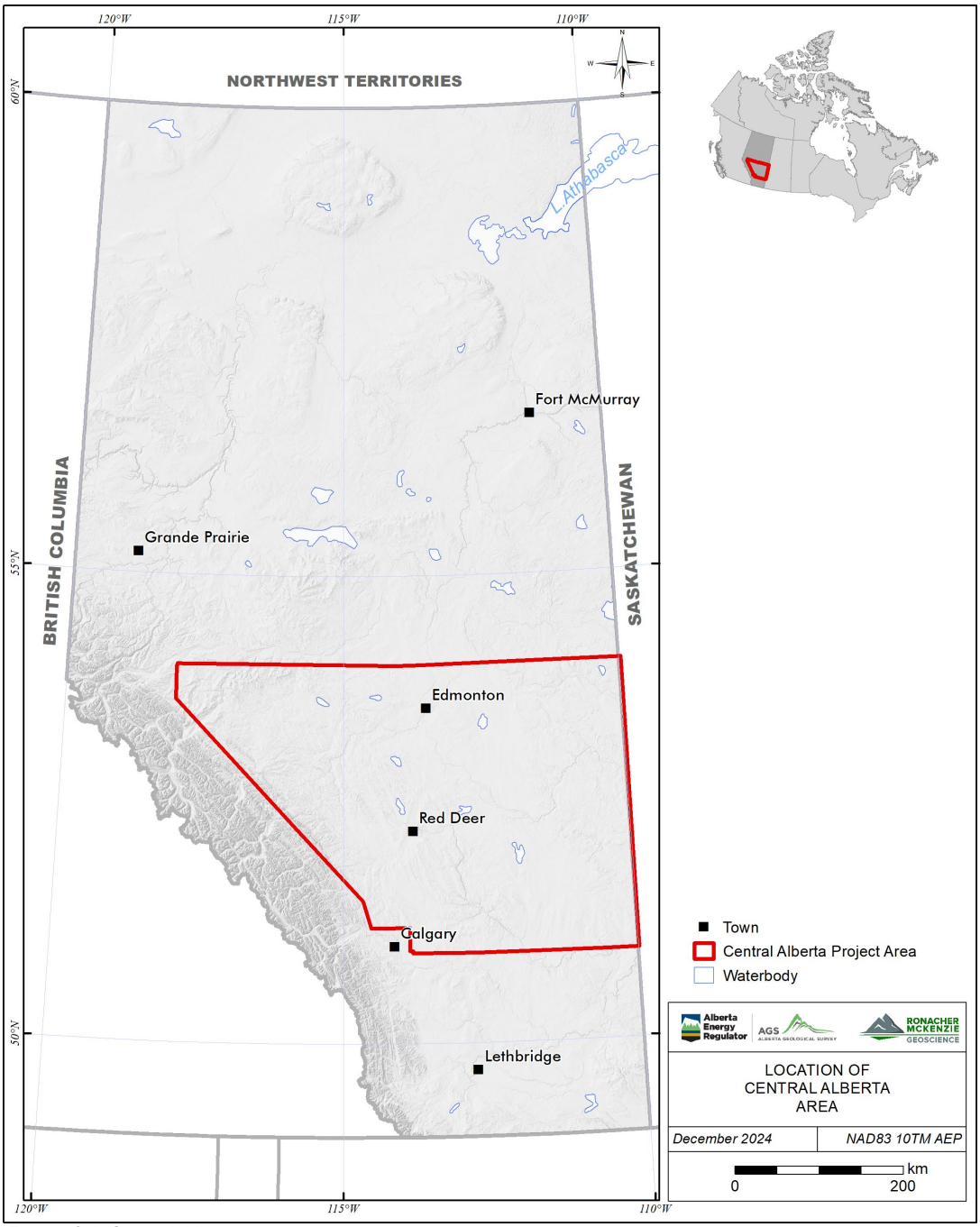

Figure 3-1. Central Alberta survey area location map.

4.0 GEOLOGICAL SETTING

The central Alberta project area encompasses the Central Plains, as well as the northern and central Foothills in the west (Prior et al., 2013). Beneath the Central Plains, the Archean to Proterozoic crystalline basement is overlain by the Middle Cambrian to Cenozoic sedimentary succession of the Western Canada Sedimentary Basin (Figure 4-1).

4.1 Crystalline Basement

Crystalline basement in Alberta is comprised of Archean and Paleoproterozoic domains (Ross et al., 1994; Figure 4-2) that were assembled into Laurentia during the Paleoproterozoic. Together, Ross et al. (1991), Villeneuve et al. (1993) and Burwash et al. (1994) defined these domains based on a combination of potential field data, and petrological and age determinations of drill core samples from basement intersections. They corroborated their interpretation by analogy with geophysical signatures of exposed geologic subdivisions of the Canadian Shield and the earlier subdivisions of Hoffman (1988). Building upon these interpretations, Pilkinton et al. (2000) created an internally consistent compilation of magnetic and gravity data for Alberta (and northeastern British Columbia) and used automated interpretation methods to refine domain boundaries and to further characterize their internal structure.

In central Alberta, tectonic domains include the Proterozoic Chinchaga and Wabamun terranes, Thorsby (Thorsby Low) which is a remnant of oceanic lithosphere, Rimbey (Rimbey High) magmatic arc, Lacombe metavolcanic and metasedimentary back-arc basin, and the Archean Loverna, Matzhiwin (Matzhiwin High) and Eyehill (Eyehill High) domains which are subdivisions of the Archean Hearne Province (Figure 4-3). The compilation of Pană et al. (2021) does not recognize the Matzhiwin domain of Villeneuve et al. (1993) or Pilkington et al. (2000) as a separate domain and included it into the Loverna domain.

The Snowbird tectonic zone (STZ), which separates the Rae and Hearne provinces and extends from the Hudson Bay to the foothills of the Canadian Cordillera, passes through central Alberta as a northeast-trending magnetic low (Thorsby Low) (e.g., Hoffman, 1988; Hope and Eaton, 2002). The STZ has been interpreted either as an Archean or Paleoproterozoic intracontinental transform (e.g., Lewry and Collerson 1990) or as a suture zone (Hoffman, 1989; Hanmer et al., 1995). Pană et al. (2021) outlined the STZ as a main NE-trending deformation zone in the Thorsby domain, plus a northern splay separating the Wabamun from the Buffalo Head and Chinchaga terranes (Figure 4-3).

Other basement features previously recognized in central Alberta are the Red Deer Trend and the northern component of the Vulcan Low. The Red Deer Trend is a narrow northeast-trending positive aeromagnetic anomaly between the Lacombe and Loverna domains first reported by Villeneuve et al. (1993). The northern component of the Vulcan Low is a narrow north-trending magnetic low located between the Loverna and Eyehill blocks. Although the Vulcan domain (Vulcan low, Vulcan structure) is a well-accepted distinct east-trending magnetic low in southern Alberta interpreted as a crustal-scale boundary, Villeneuve et al. (1993) interpreted this north-trending feature lying along the western margin of Eyehill as either a northern component of the Vulcan Low or a younger structure truncating the Vulcan Low. Various tectonic models have been

considered for the Vulcan domain, including rift basin, collision zone, and suture zone (Pană et al., 2021; and discussion therein).

Further characterization of the crustal architecture in 3D has benefitted from integration with Lithoprobe deep seismic reflection studies (e.g., Eaton et al., 1999; Ross and Eaton, 2002). Additionally, lithological and geochronological controls on basement rocks were obtained from the analysis of sparse core samples from nine dispersed petroleum wells by Ross et al. (1991), Villeneuve et al. (1993), and Burwash et al. (unpublished data 1994) (Figure 4-3). Based on the structural interpretation of seismic sections across central Alberta, and available lithology and radiometric ages of the Thorsby, Rimbey, and Lacombe domains, it is suggested that southeast-directed subduction existed along the Hearne Province margin that resulted in crustal derived arc magmatism and development of a back arc basin (Ross, 2002).

Precambrian basement top picks and interpreted basement topography surface are available from the AGS. In the most recent 3D geological framework model (Alberta Geological Survey, 2021), the top of the Precambrian basement is constrained by picks from 50 oil/gas wells in the project area. Elevation of the basement surface ranges from 800 m below sea level in the northeast corner down to 4,533 m below sea level near the Cordilleran deformation front in the northwest of the project area (Figure 4-4).

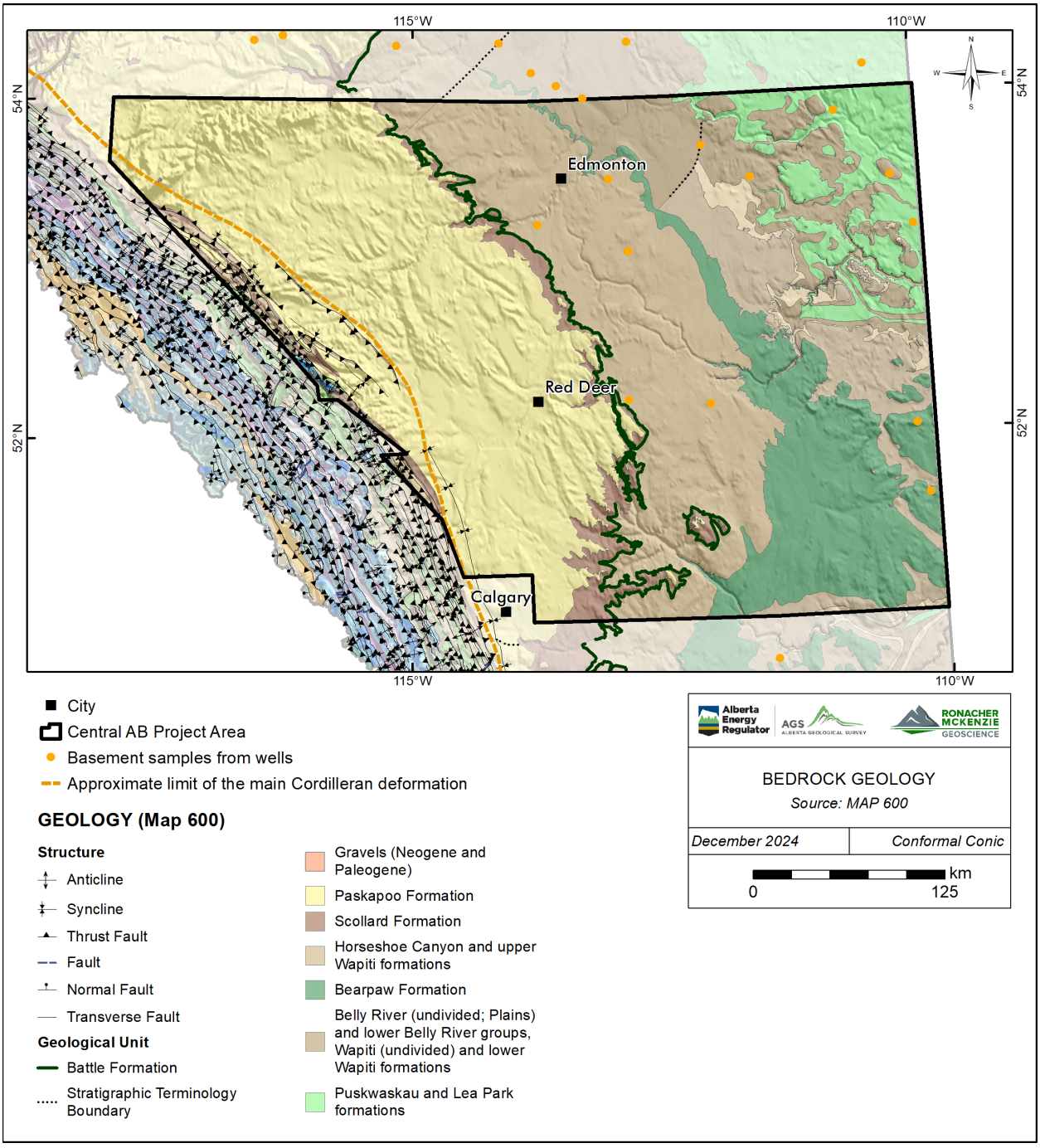

Figure 4-1. Geological map of central Alberta (from Prior et al., 2013).

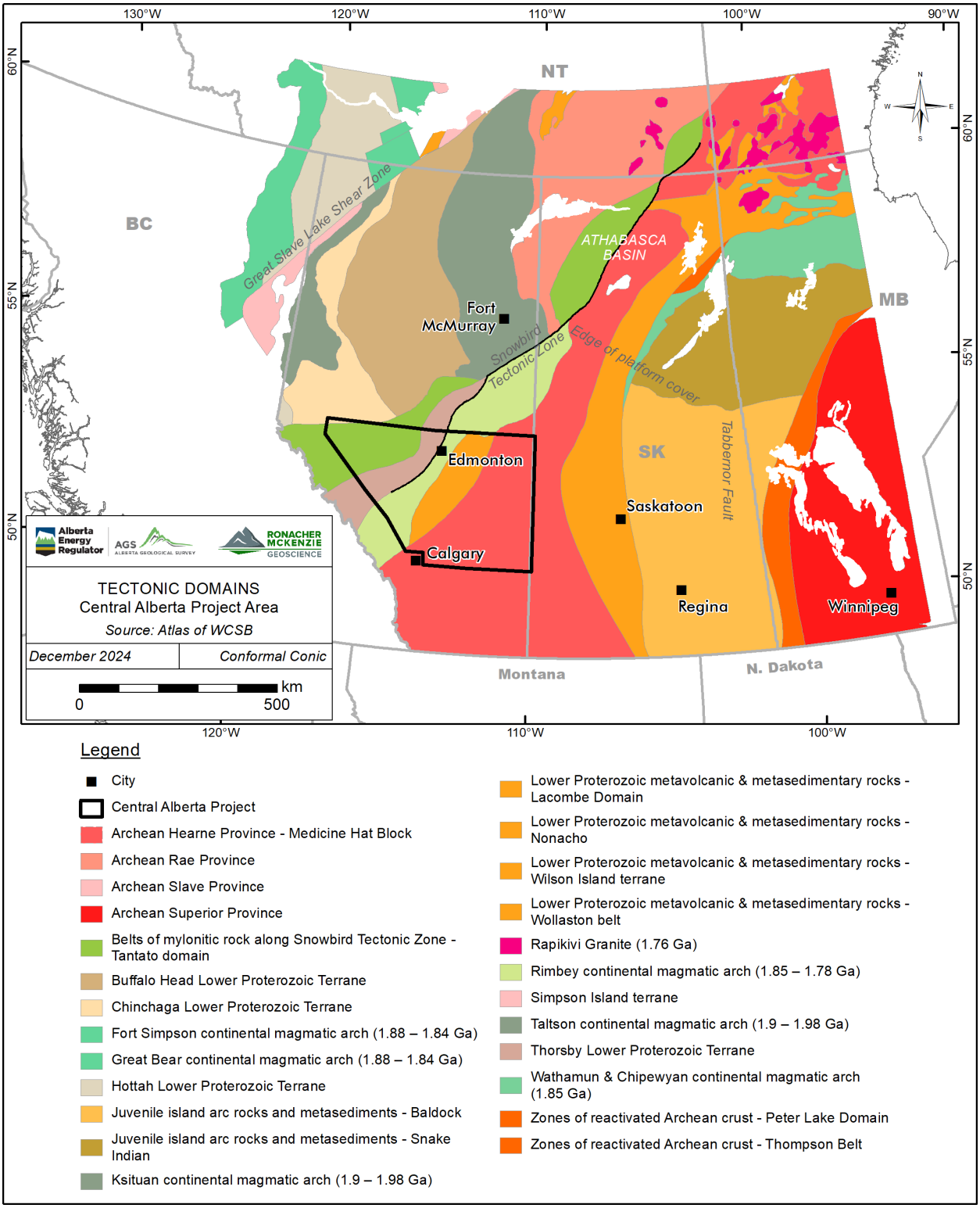

Figure 4-2. Tectonic domains in Western Canada (modified from Ross et al., 1994).

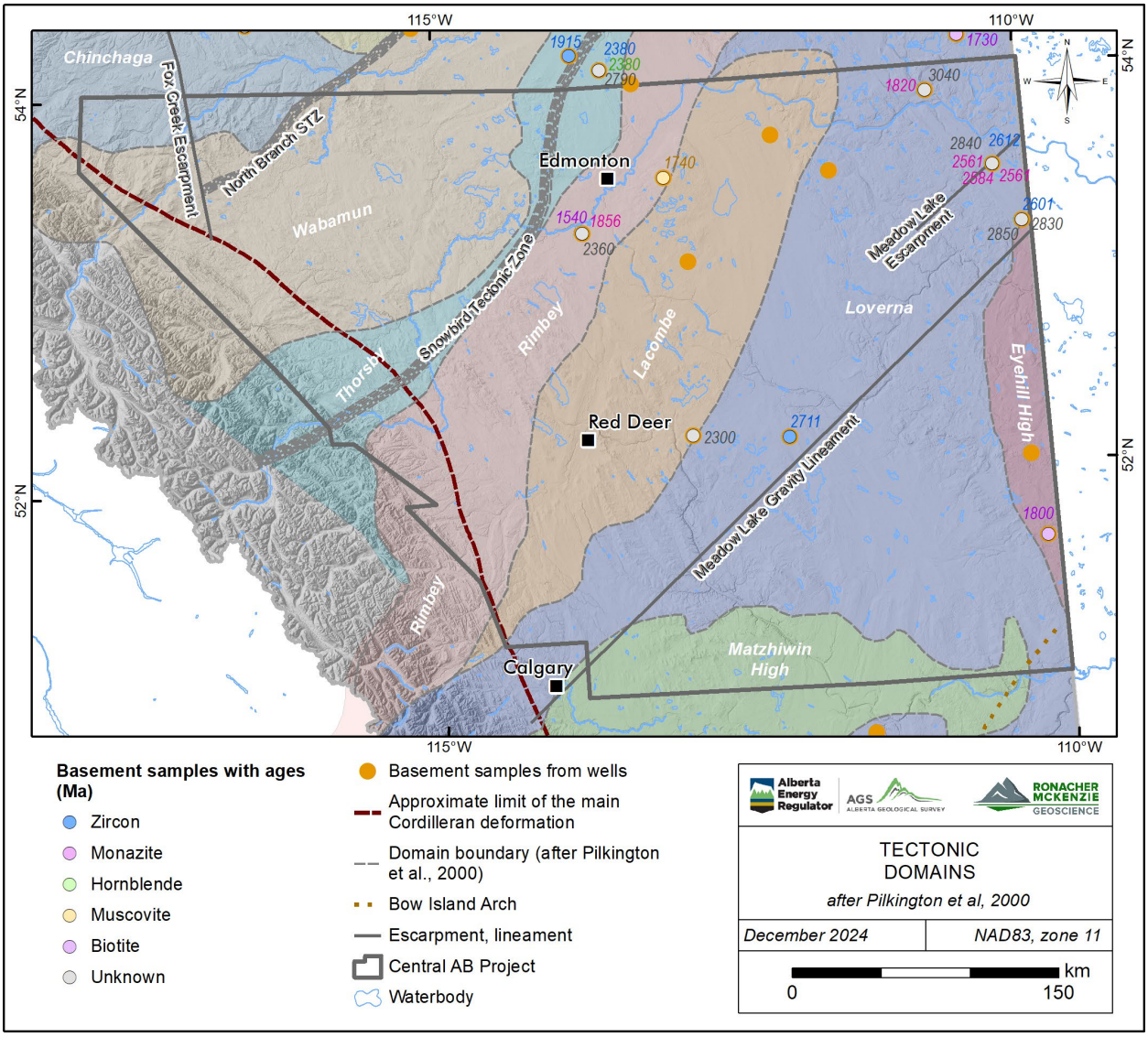

Figure 4-3. Tectonic domains of central Alberta after Pilkington et al. (2000). Selected structural lineaments (grey) from Pană et al. (2021). Radiometric ages from Ross et al. (1991), Villeneuve et al. (1993), and Burwash et al. (unpublished data 1994).

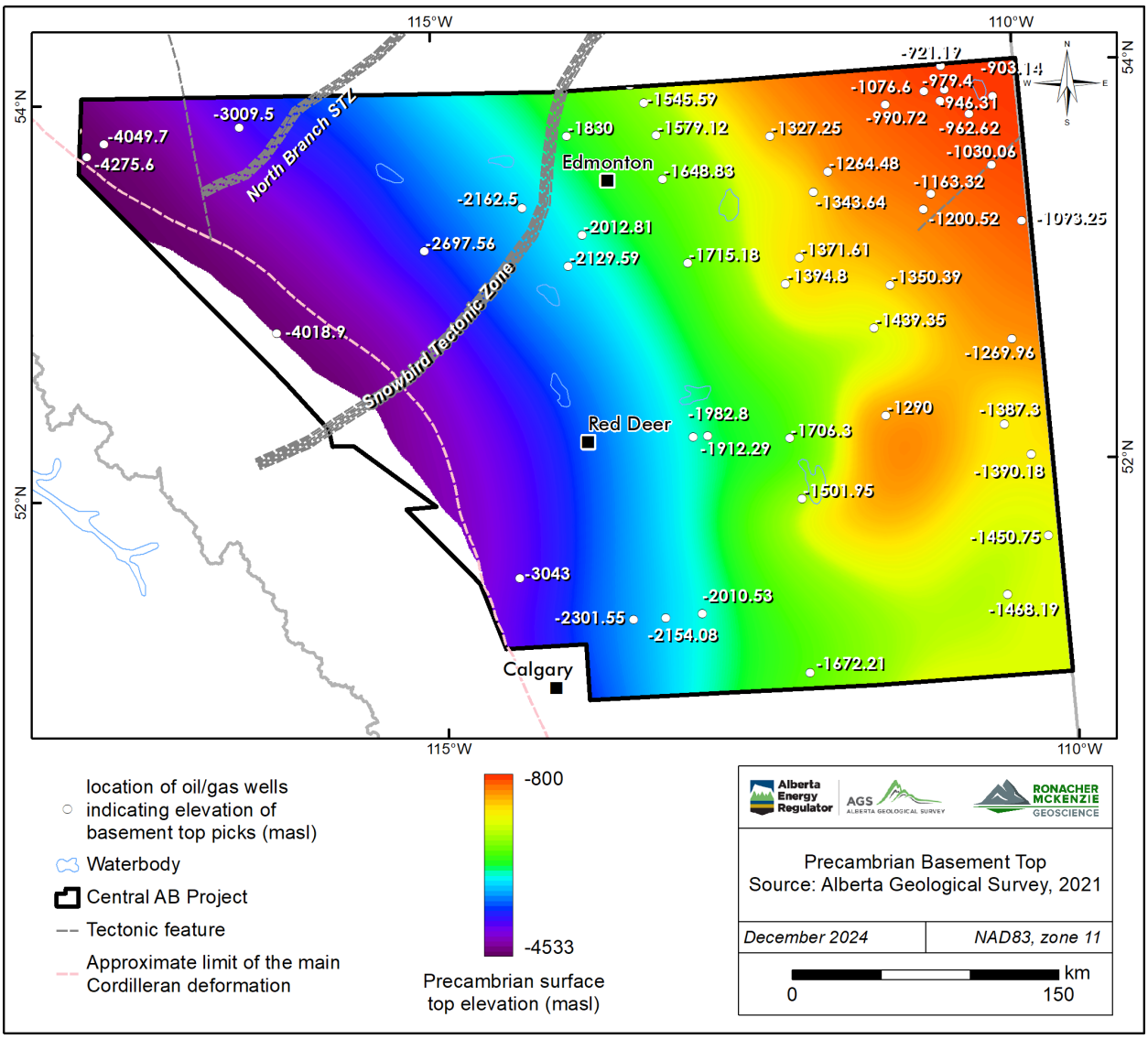

Figure 4-4. Modelled surface of basement top and location of basement top picks in central Alberta. Data from the Alberta Geological Survey. Selected structural lineaments (grey) from Pană et al. (2021).

4.2 Western Canada Sedimentary Basin

In central Alberta, the basement is covered by the Phanerozoic Western Canada Sedimentary Basin ("WCSB"). The thickness of the sedimentary strata increases towards the Rocky Mountains, from its erosional edge in the northeast in the Canadian Shield region to a maximum of approximately 4.5 km in the northwest.

In the project area, the WCSB stratigraphy reflects deposition in two different tectonic settings (Mossop and Shetsen, 1994).

- Cambrian to Middle Jurassic passive continental margin, dominated by carbonates, mudstones and minor evaporites; and
- Middle Jurassic to Oligocene foreland basin dominated by clastic sequences.

Major structural features of the sedimentary basin are the Fox Creek and Meadow Lake escarpments, in the northwest and northeast of the project area, respectively.

The Meadow Lake escarpment is a regionally prominent pre-Devonian erosional feature in east-central Alberta and Saskatchewan. The escarpment trends to the east and northeast and faces north and northwest. To the southeast of the escarpment, Middle Ordovician to Lower Devonian rocks have been preserved, whereas to the northwest, Middle Devonian rocks rest directly on the Precambrian basement (Norford et al., 1994). The escarpment impacted the deposition of Elk Point evaporites to the southeast and aligns with the northeast-trending of the Upper Devonian Killam reef complex (Edwards and Brown, 1999).

The Fox Creek escarpment is an early Cretaceous erosional feature colinear with the basement contact between Ksituan and Chinchaga terranes in northern Alberta (O'Connell, 1994). In the western part of the central Alberta survey area, the Fox Creek escarpment demarcates a sharp westward thickening of the Lower Cretaceous Mannville Group (Hayes et al., 1994). Currently, the inferred location of the escarpment is defined on the paleo-topography of the sub-Cretaceous unconformity (Peterson and MacCormack, 2014).

Other localized structures in the WCSB include astroblemes, the (eroded) remnants of meteorite impact craters. In central Alberta, these include the Whitecourt astrobleme and James River (inferred) crater (Mazur, 1999). The Whitecourt astrobleme is a bowl-shaped structure with a diameter of 36 m and depth of 6 m. It was interpreted to have occurred <1,130 years ago since it affects Quaternary glacial deposits overlying the Paskapoo Formation. The James River structure is a 4.8 km wide circular feature with a raised central uplift, interpreted to have formed in the Late Cambrian to Middle Devonian (Isaac and Stewart, 1993).

4.3 Surficial Geology

The central Plains are blanketed by Neogene fluvial deposits, glaciogenic materials and postglacial sediments of variable thickness and distribution overlying the bedrock surface. Modelled surficial sediment thickness in the project area range from less than 1 m to as much as 224 m (Atkinson et al., 2020). Maximum thicknesses occur in the northeast corner, and in the east-central part of the project area near Wainwright.

5.0 AEROMAGNETIC SURVEY DATA

5.1 Data Review

New data for the central Alberta dataset were collected by EON Geosciences between September 2023 and March 2024 (Figure 5-1) and it is available to the public through AGS's website (Alberta Geological Survey, 2024).

RMG reviewed the digital data available in the AER's archives for completeness and completed a post-survey quality control report for the AER on the 2023-2024 survey (McGill and Vargas, 2024), covering both the raw and final delivered data. No significant quality control issues were found.

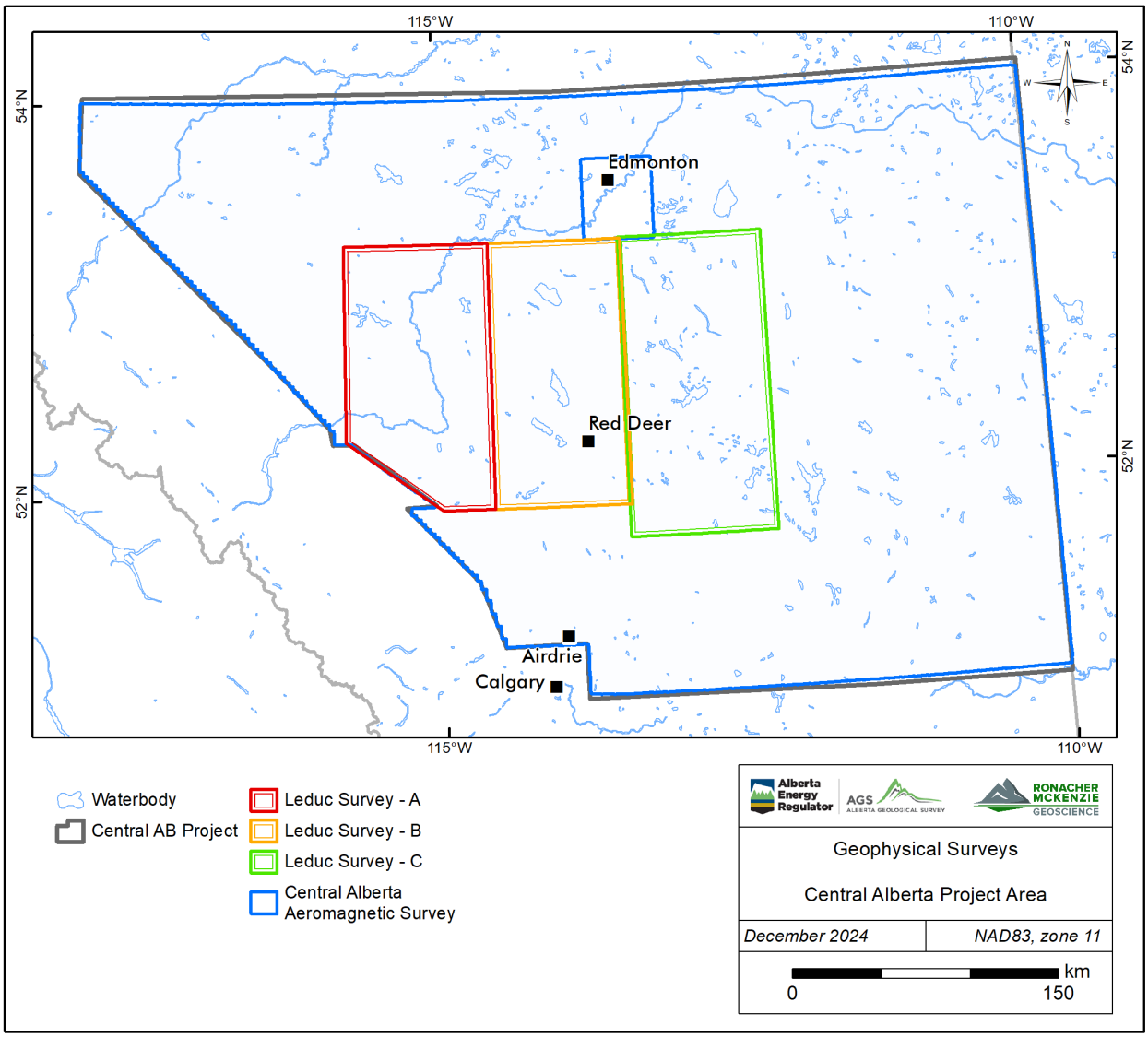

Figure 5-1. Central Alberta airborne survey blocks.

Data from the previously flown Leduc surveys was purchased and integrated with the newly acquired data to create a contiguous magnetic grid for Central Alberta (Figure 5-1).

The airborne contractors performed editing to attenuate cultural effects in the measured data. Cultural effects may not be completely removed but have been attenuated sufficiently to avoid significant problems with calculated filter products.

Flight specifications for each block are summarized in Table 5-1.

Table 5-1. Aeromagnetic survey flight specifications.

Area Name	Contractor	Date	Flying Height (m AGL*)	Survey Line Direction	Survey Line Spacing (m)	Tie Line Direction	Tie Line Spacing (m)
Central Alberta	GDS-EON	2023-2024	200	090°/270°	800	000°/180°	2500
Leduc A	World Geoscience	1997	120	090°/270°	600	000°/180°	1800
Leduc B	World Geoscience	1997	120	090°/270°	600	000°/180°	1800
Leduc C	Spectra	1997	120	090°/270°	600	000°/180°	1800

**AGL: Above ground level.*

5.2 Derivative and Filter Products

Grid-based filter products were calculated from the total magnetic intensity ("TMI") and International Geomagnetic Reference Field ("IGRF")-removed residual magnetic intensity ("RMI") grids (Table 5-2). The various filter products are used to enhance and highlight different features in the measured data to aid in geologic interpretation. RGB ternary images were also created from selected filter products to produce pseudo-structure and pseudo-geology maps.

Table 5-2. Magnetic Filter Products.

Product	Abbreviation	Description
Total Magnetic Intensity	TMI	Measured data.
Residual Magnetic Intensity	RMI	Measured data, IGRF removed.
TMI/RMI, Pole Reduced	RTP	Transform to vertical magnetic field, simplifies anomaly shapes.
X Horizontal Derivative	DX	Highlights near surface features in N-S direction.
Y Horizontal Derivative	DY	Highlights near surface features in E-W direction.
1st Vertical derivative	VD1	Highlights near surface features.
2nd Vertical derivative	VD2	Enhances subtle near surface features.

Product	Abbreviation	Description
Analytic Signal (Total Gradient)	AS	Highlights discrete magnetic bodies and zones of high gradients.
Total Horizontal Derivative	THD	Highlights horizontal changes in the total field.
1st Vertical Derivative of Total Horizontal Derivative	THD_VD1	Enhances THD.
Tilt Derivative	TD	Tilt angle between vertical and horizontal derivatives, highlights magnetic contacts, amplitude independent.
Total Horizontal Derivative of Tilt Derivative	TD_THD	Used with TD to estimate depth of discrete magnetic sources.
Area	AREA	Highlights discrete areas.
Edge	EDGE	Highlights edges of discrete areas.
Geology	GEOLOGY	Pseudo-geology map. Ternary image (RMI/RTP, VD1, VD2) only, no grid data.
Structure	STRUCTURE	Pseudo-structure map. Ternary image (DX, DY, VD1) only, no grid data.
Differential Upward Continuation	DIF_XXX_YYY	Highlights features at selected approximate depths.

Selected filter products are presented in Figure 5-2 through Figure 5-10. All filter products are included in the Digital Appendix B.

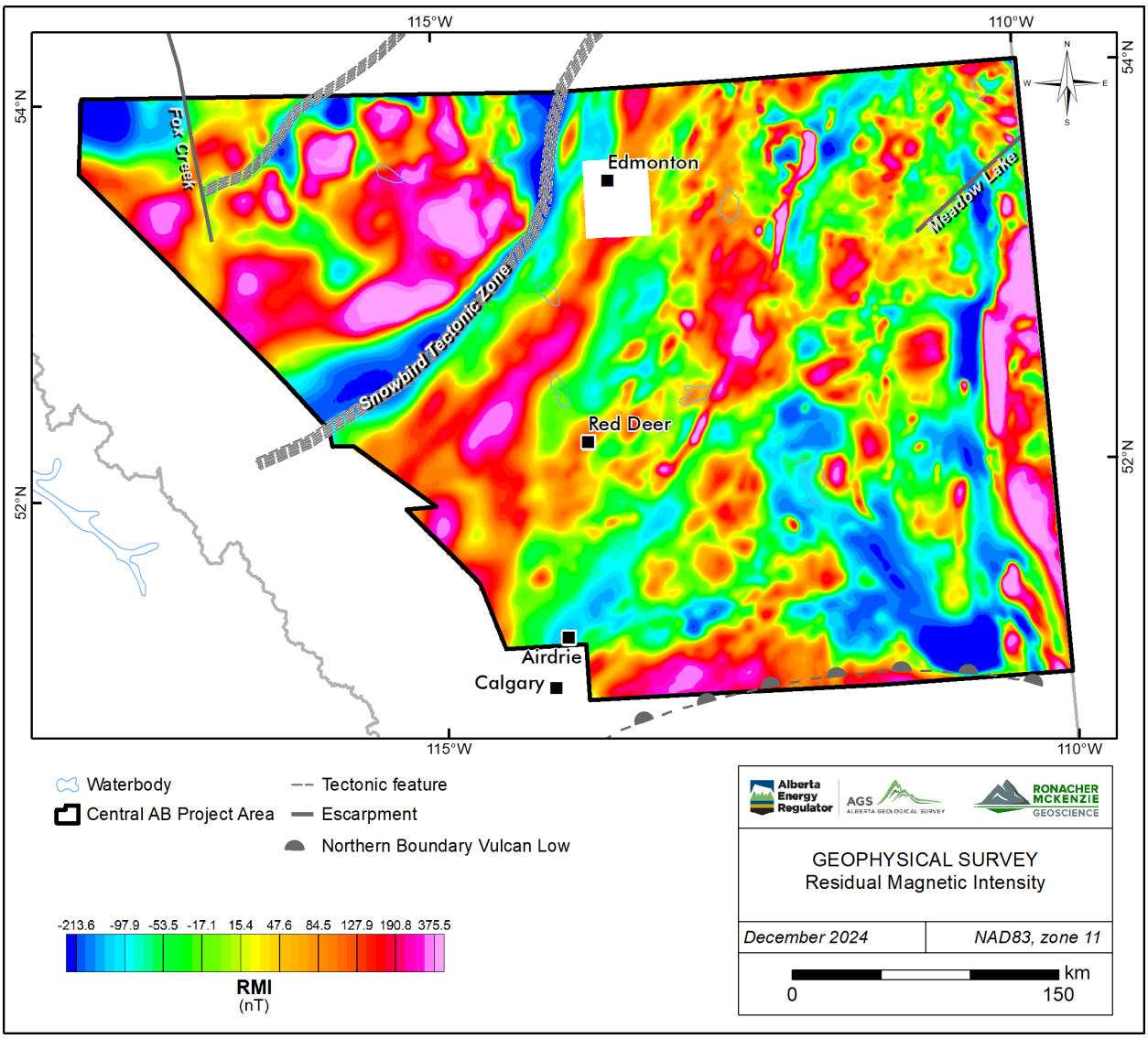

Figure 5-2. Residual Magnetic Intensity ("RMI"). Selected structural lineaments from Pană et al. (2021).

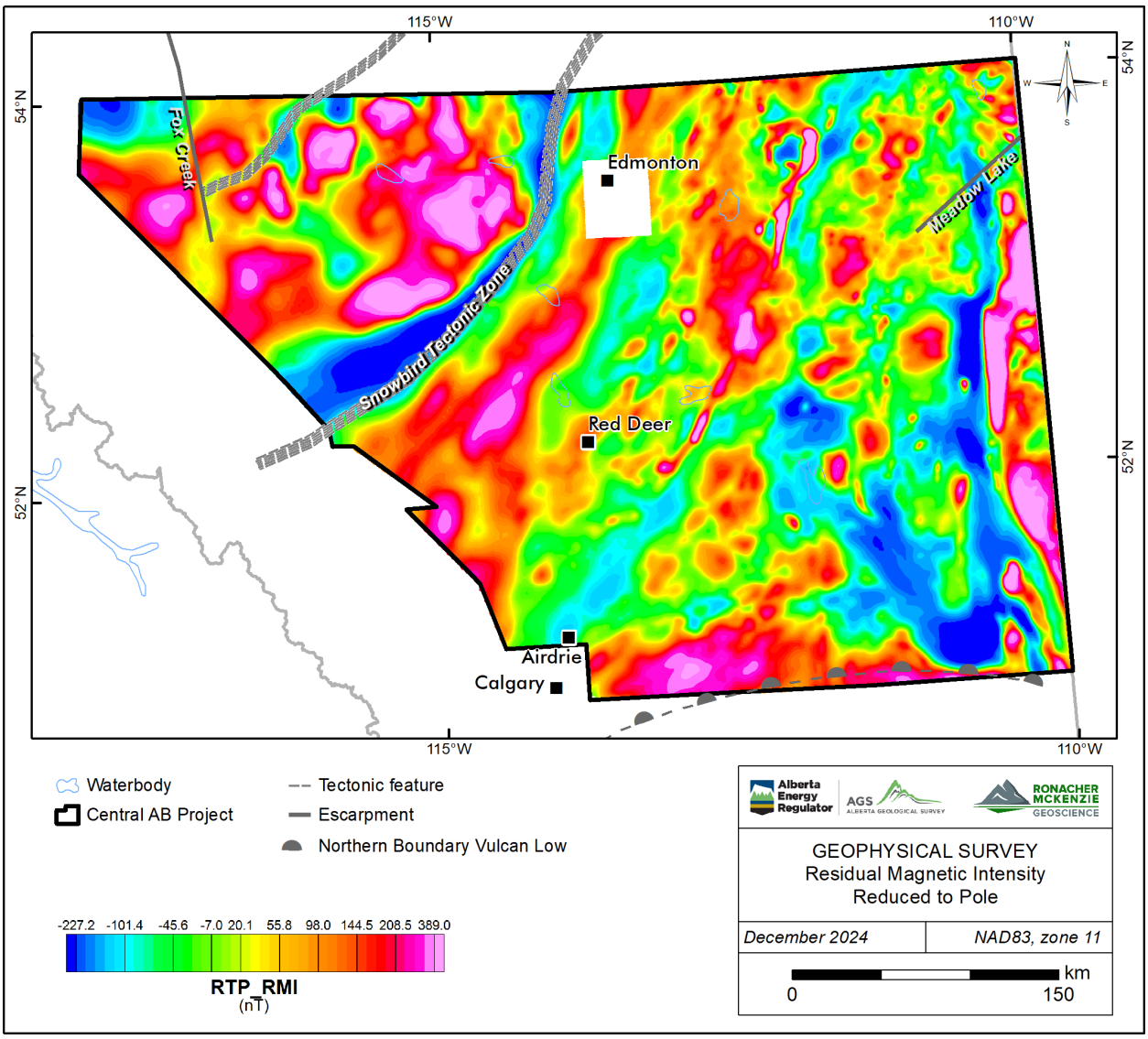

Figure 5-3. RMI, reduced to pole. Selected structural lineaments from Pană et al. (2021).

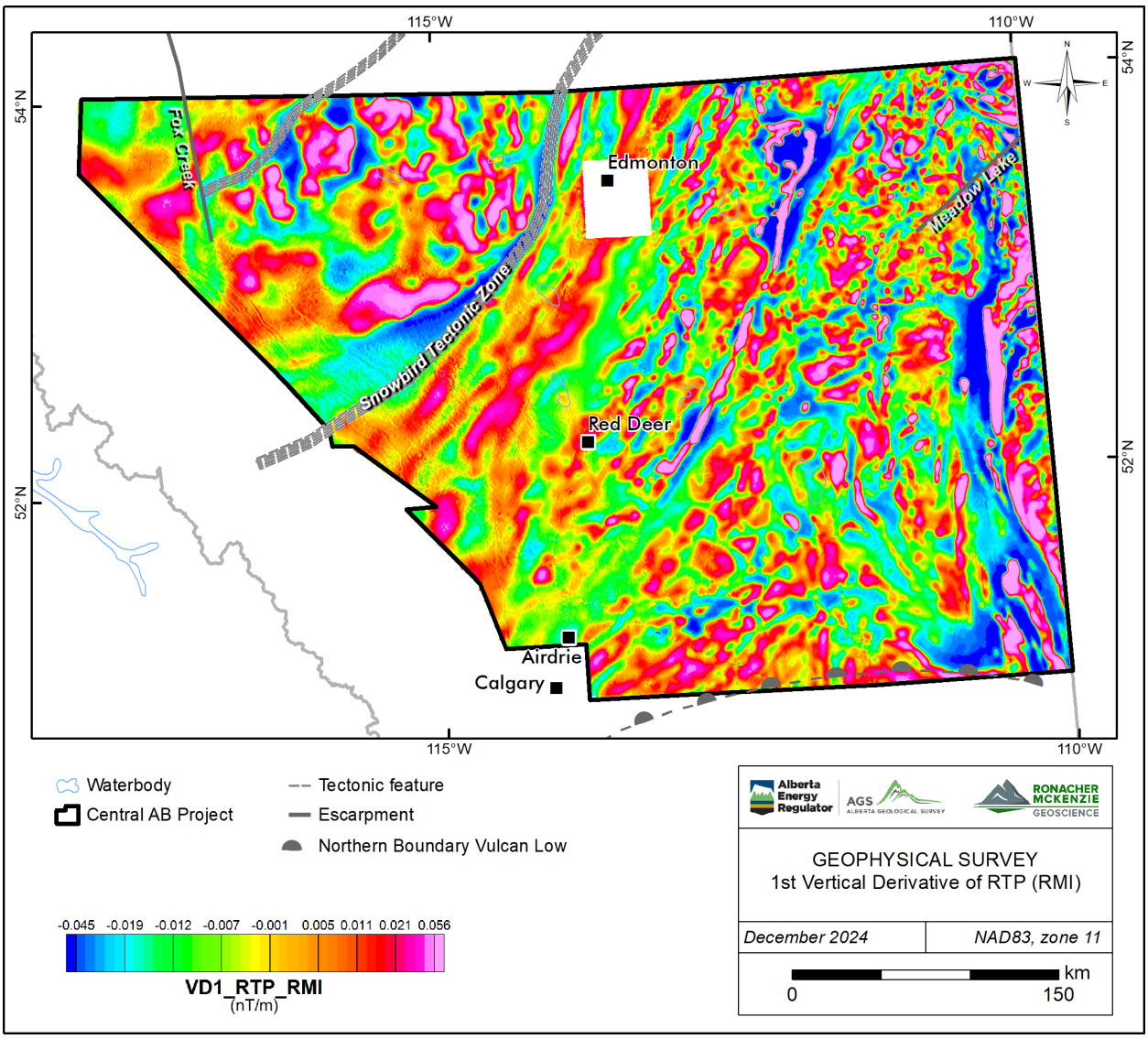

Figure 5-4. RMI, reduced to pole, 1st vertical derivative. Selected structural lineaments from Pană et al. (2021).

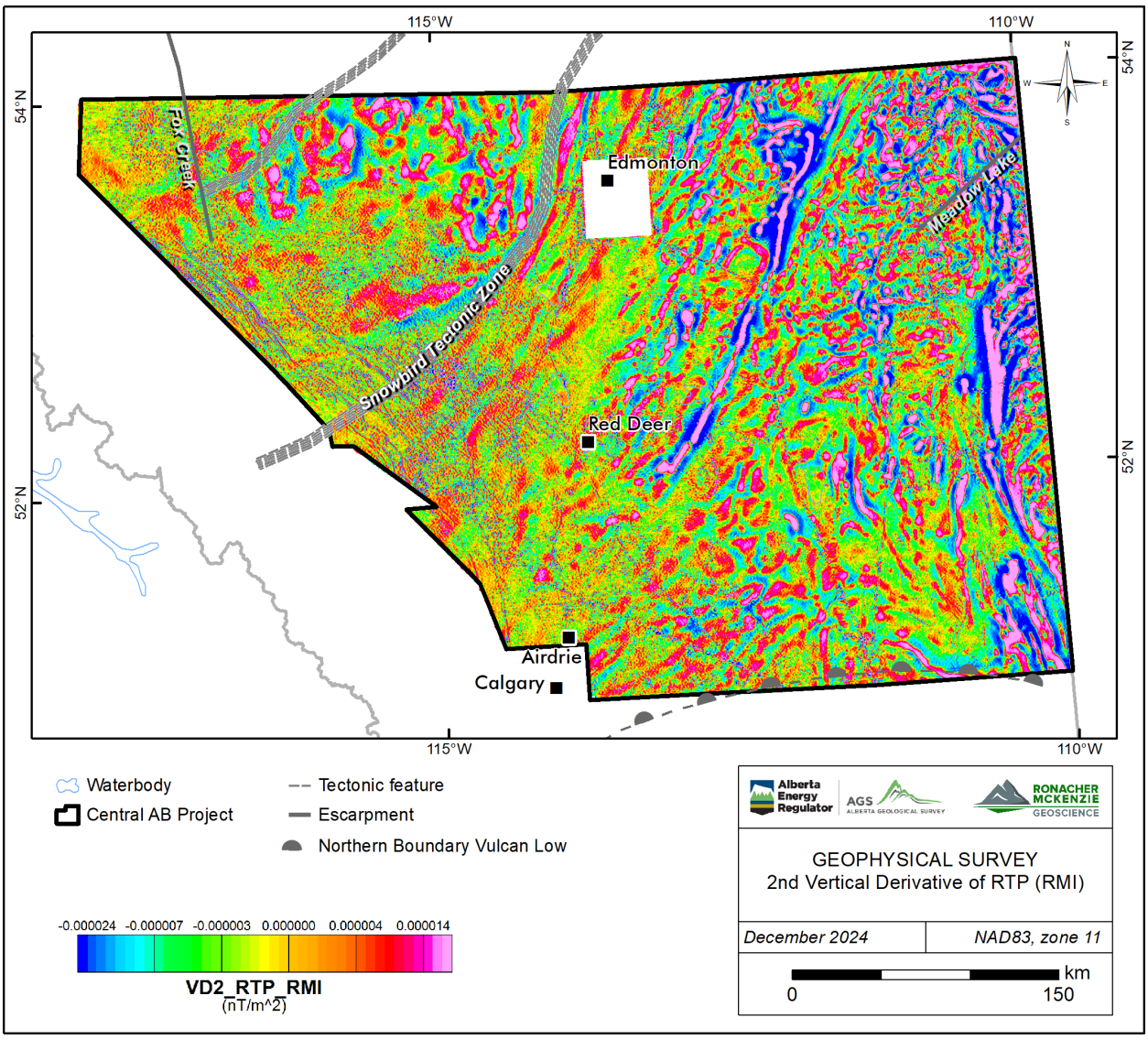

Figure 5-5. RMI, reduced to pole, 2nd vertical derivative. Selected structural lineaments from Pană et al. (2021).

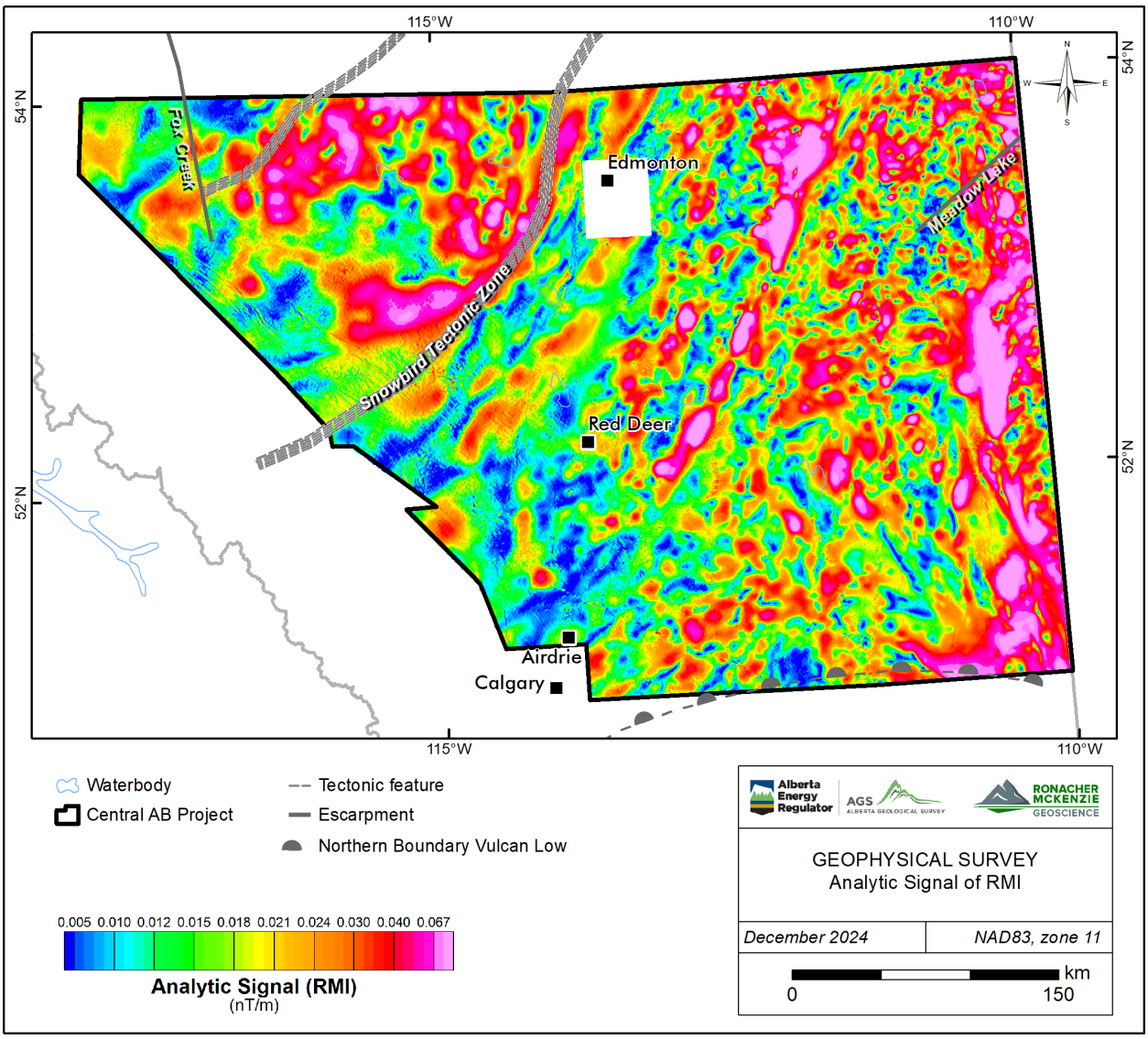

Figure 5-6. RMI, Analytic Signal. Selected structural lineaments from Pană et al. (2021).

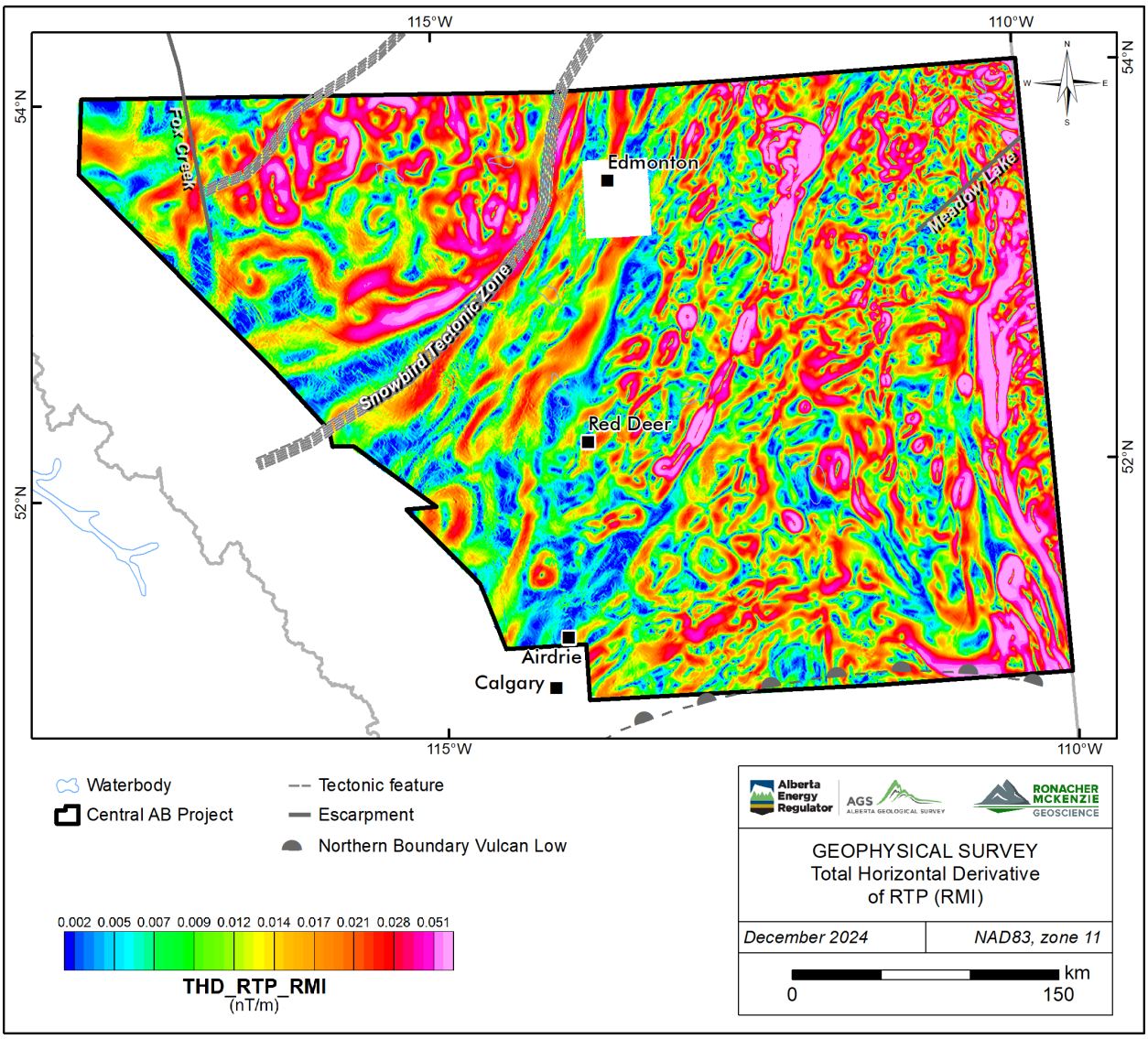

Figure 5-7. RMI, reduced to pole, total horizontal derivative. Selected structural lineaments from Pană et al. (2021).

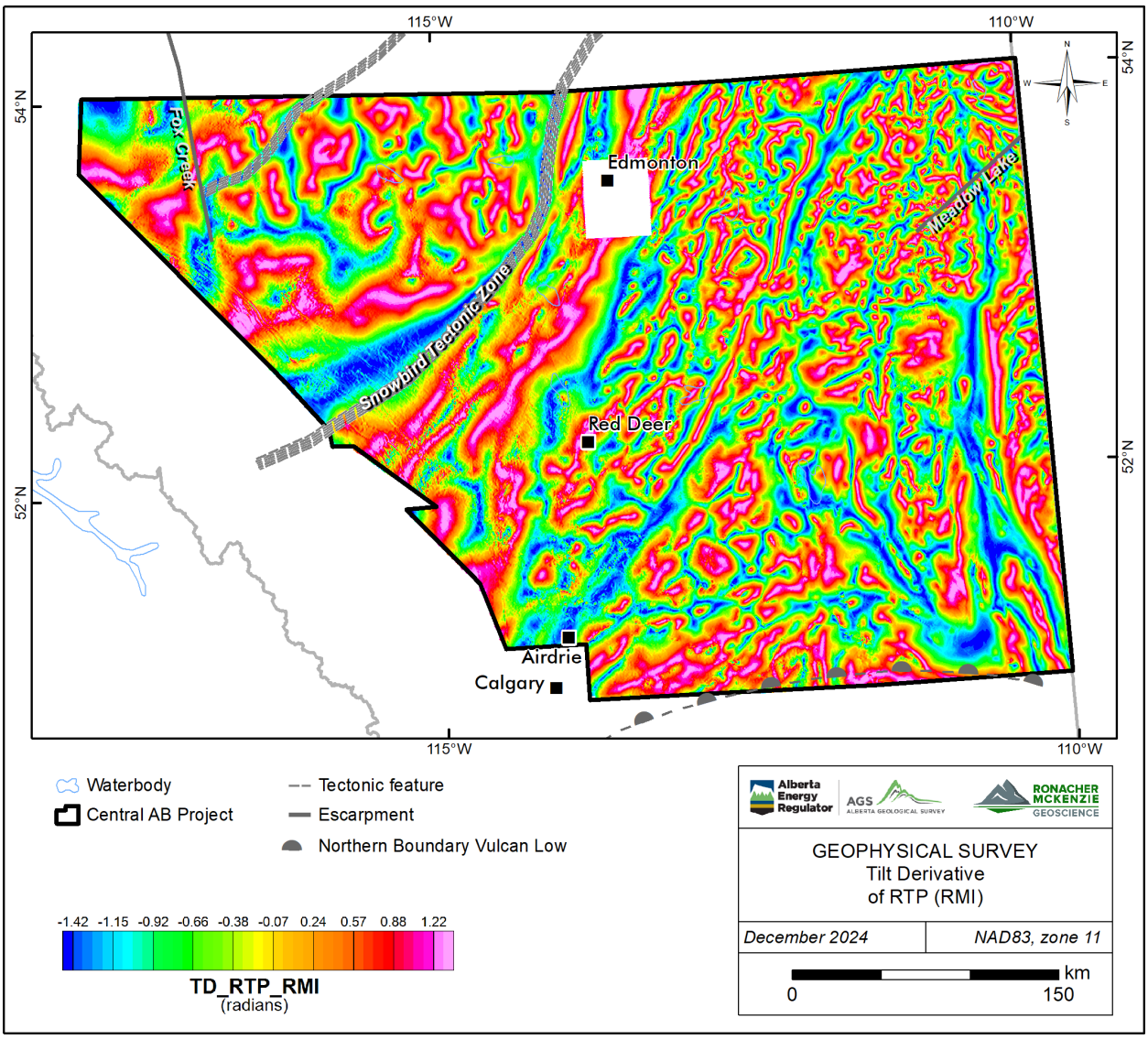

Figure 5-8. RMI, reduced to pole, tilt derivative. Selected structural lineaments from Pană et al. (2021).

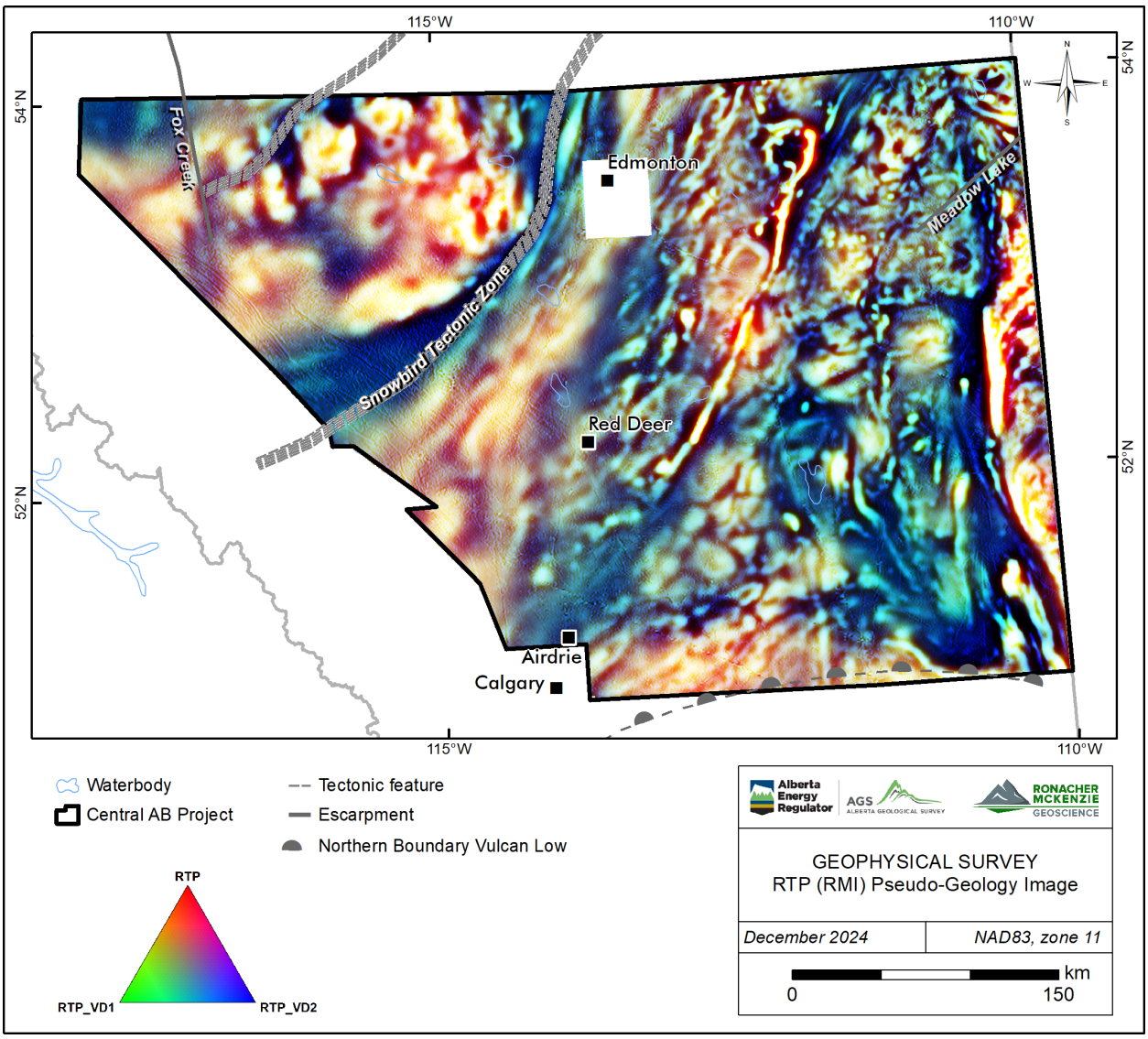

Figure 5-9. RMI, reduced to pole, pseudo-geology ternary image. Selected structural lineaments from Pană et al. (2021).

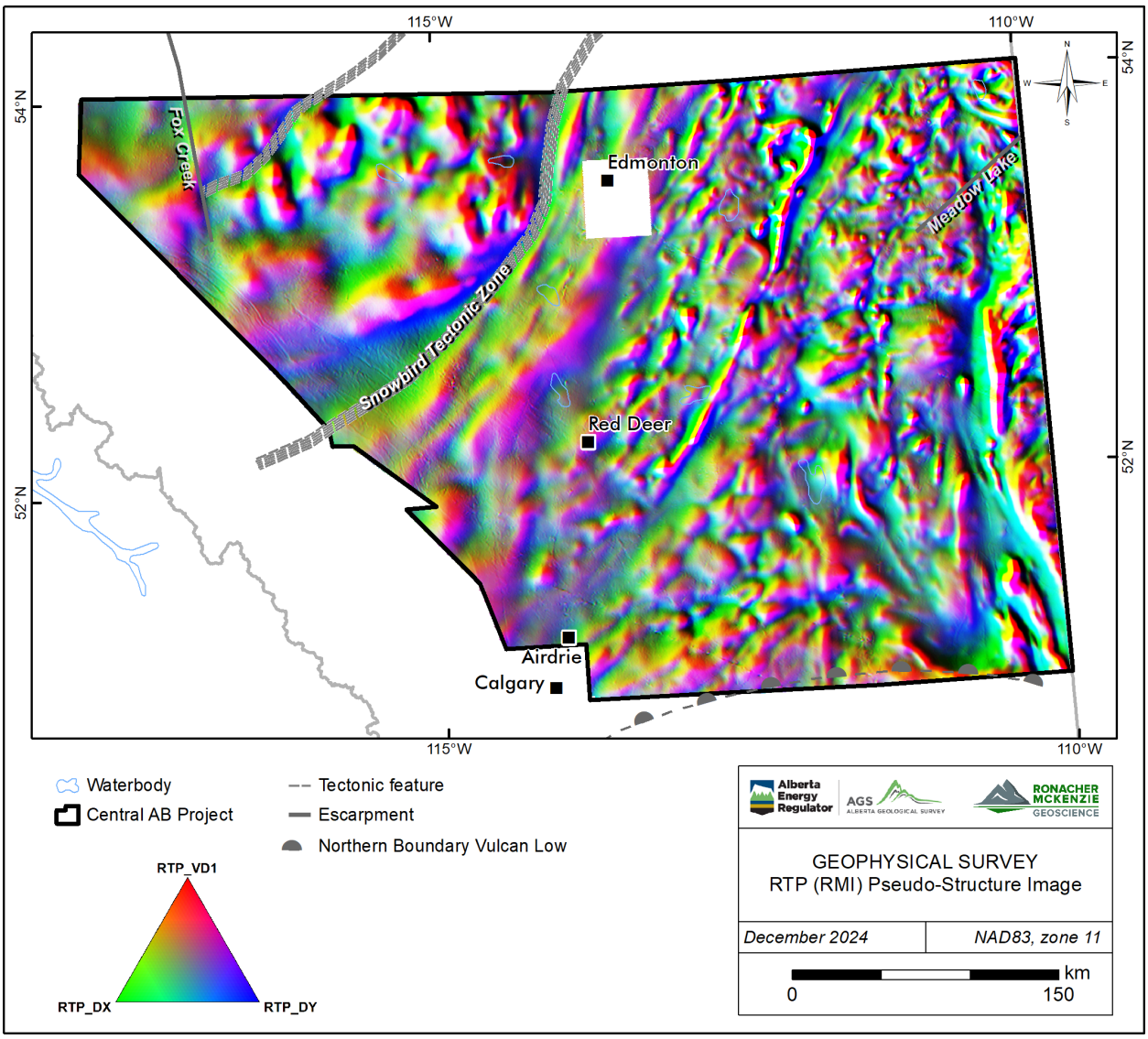

Figure 5-10. RMI, reduced to pole, pseudo-structure ternary image. Selected structural lineaments from Pană et al. (2021).

Differential upward continuation grids were created to extract information from selected approximate depths. Differential grids show information from an approximate depth range equal to half of the upward continuation distances (e.g., the 3000-5000 m differential grid will show information from approximately 1500 to 2500 m depth). Selected differential maps are presented in Figure 5-11 and Figure 5-12.

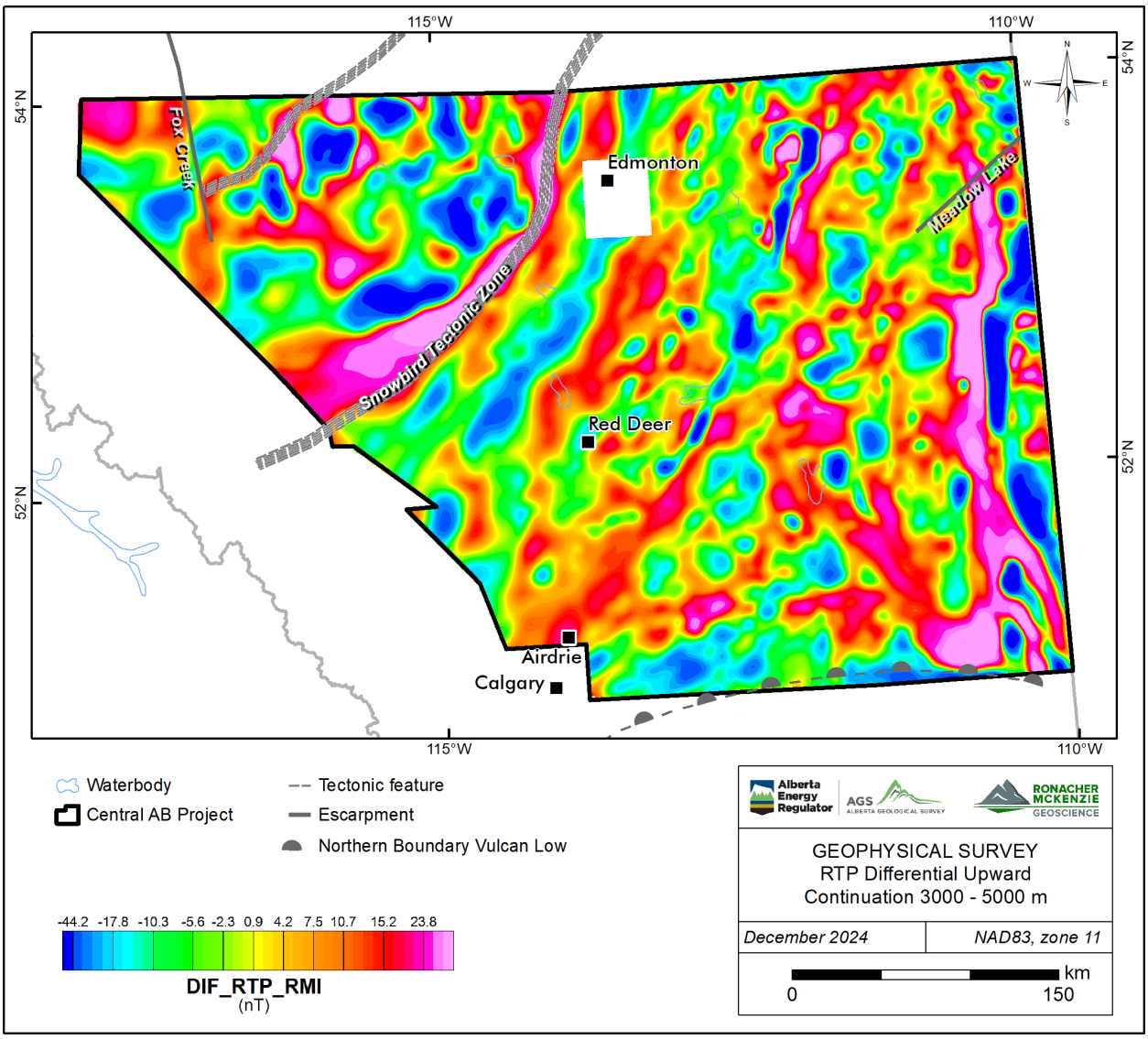

Figure 5-11. Differential upward continuation, 3000-5000 m (1500-2500 m approximate depth). Selected structural lineaments (grey) from Pană et al. (2021).

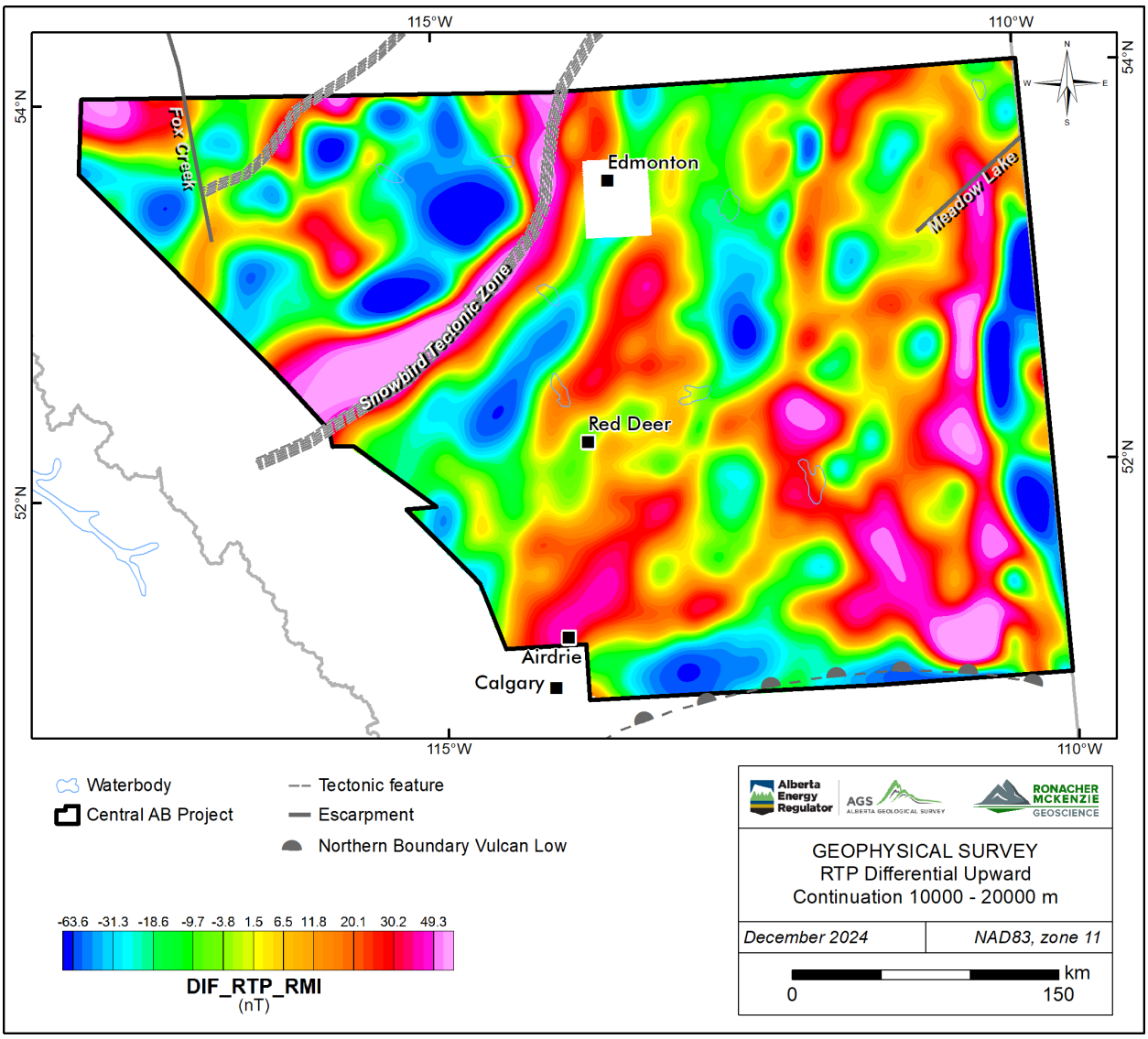

Figure 5-12. Differential upward continuation, 10000-20000 m (5000-10000 m approximate depth). Selected structural lineaments from Pană et al. (2021).

The gridded magnetic data are also displayed using alternate colour distributions to aid in data interpretation (Table 5-3). Different colour distributions are used to help identify structures in the interpretation process. For example, greyscale maps are useful for highlighting high and low areas while minimizing the effects of local amplitudes, and isoluminant palettes (e.g., CET i1 described in Kovesi, 2015) mitigate artificial highlighting caused by perceived brighter colours in commonly used rainbow palettes, particularly in the yellow and green ranges.

Table 5-3. Colour palettes applied to geophysical datasets.

Colour Distribution	Abbreviation	Description
Rainbow	(none)	Standard blue through purple colour palette.
Greyscale	BW	Black to white colour range, often easier to see structures.
Centre for Exploration Targeting (I1)	CET	Isoluminant colour range developed by University of Western Australia. No 'bright spots' in the spectrum to artificially attract the eye.

Selected examples of alternate colour distributions are shown in Figure 5-13 through Figure 5-15.

A complete set of georeferenced gridded data including alternate colour distributions is included in the Digital Appendix B.

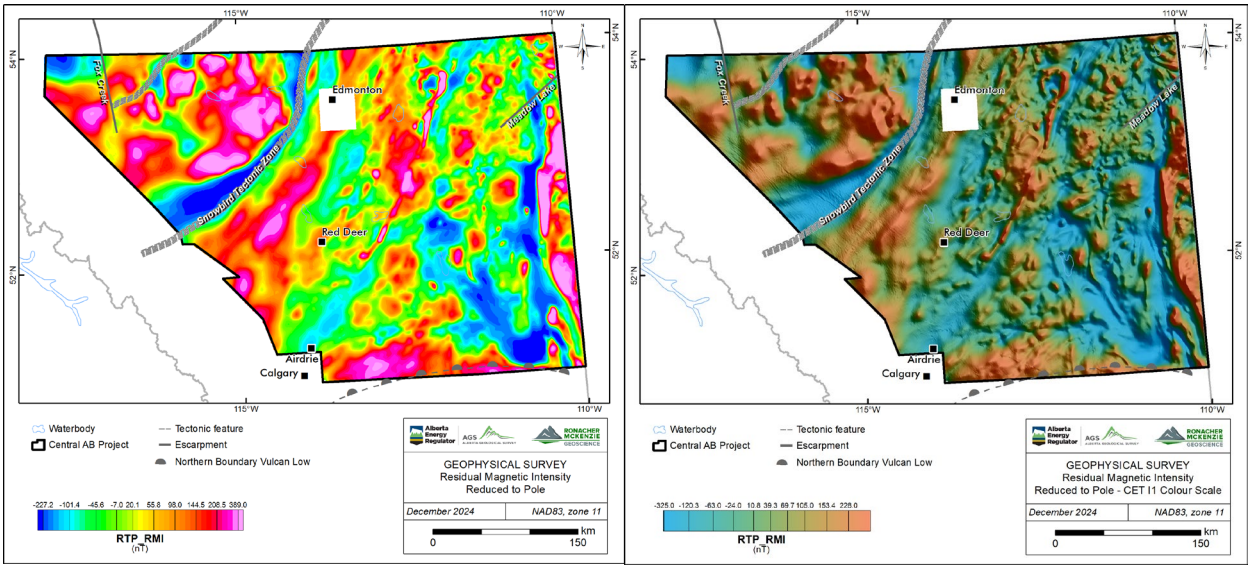

Figure 5-13. RMI, reduced to pole, standard rainbow (left) and CET i1 isoluminant (right) colour distributions. Selected structural lineaments from Pană et al. (2021).

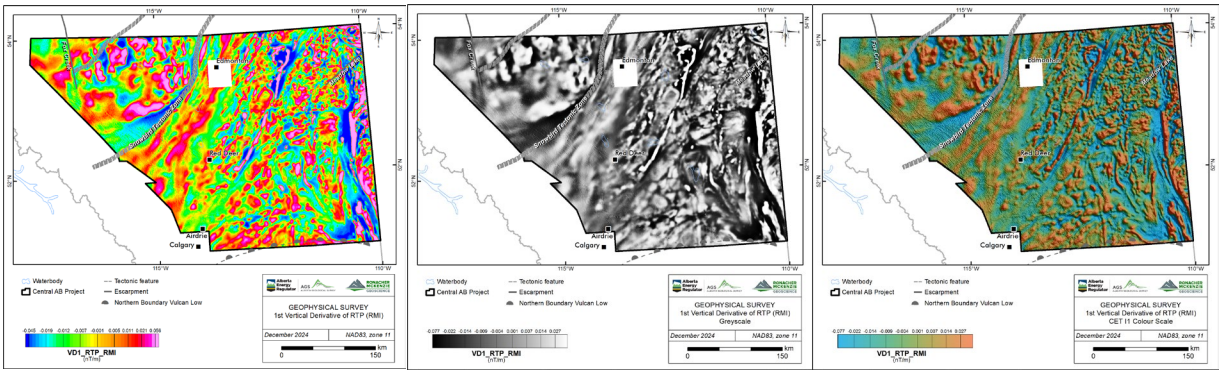

Figure 5-14. 1st vertical derivative (RTP), standard rainbow (left), greyscale (centre), and CET i1 isoluminant (right) colour distributions. Selected structural lineaments from Pană et al. (2021).

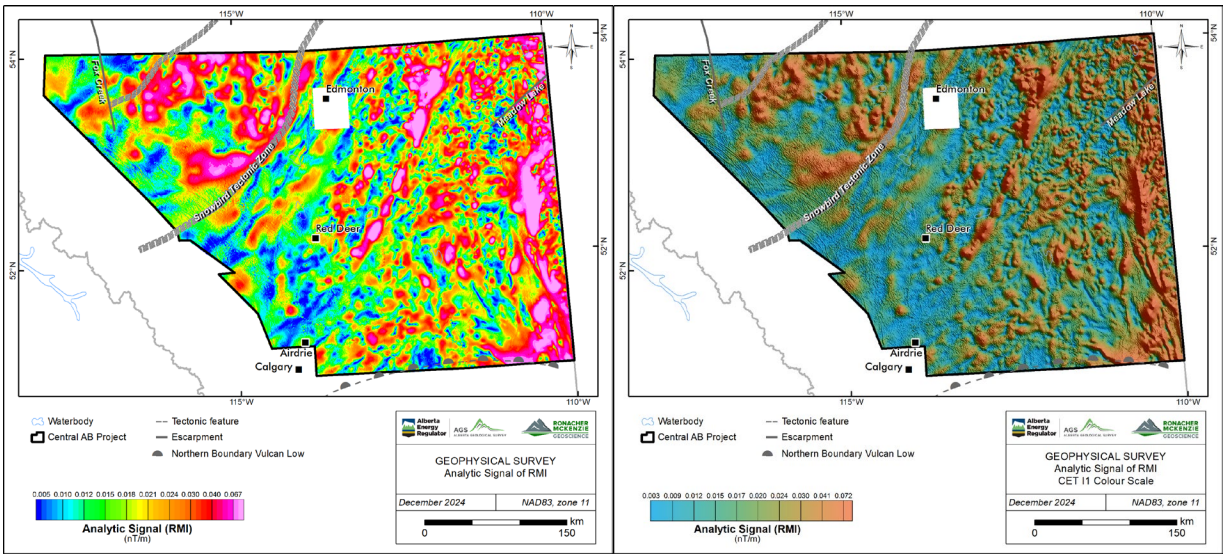

Figure 5-15. RMI, Analytic Signal, standard rainbow (left) and CET i1 isoluminant (right) colour distributions. Selected structural lineaments from Pană et al. (2021).

5.3 Automatic Structure Detection

RMG collaborated with Fathom Geophysics to perform automatic structure detection and to generate additional magnetic products to assist with the geological interpretation of the magnetic basement. Automatic detection was applied to the merged gridded magnetic data for all of Alberta, with the exception of depth to basement, which was only applied to Central Alberta. The processing included application of standard filters as well as Fathom Geophysics' structure detection, radial symmetry, fabric orientation, and depth to basement

filters. Fathom Geophysics' report is available in Appendix 1. Final digital vector and image products were clipped to central Alberta and are available in the Digital Appendix C.

The additional filter and image processing products created by Fathom Geophysics are listed in Table 5-4. An example of an image processing product, a ternary image of 1VD, tilt angle, and horizontal gradient magnitude ("HGM"), is shown in Figure 5-16.

Automatic structure detection is a linear feature detection algorithm used to highlight ridges, valleys, or edges in gridded data. Automated structure detection is a multi-scale phase congruency algorithm in which features are highlighted either in areas of low or high magnetic contrast, irrespective of amplitude. The method also allows inference of the estimated depth of structures between 0.5 and 1 times the filter wavelength, assuming shorter wavelengths are related to shallow structures and longer wavelengths are related to deeper structures (which may not always be the case). Structure detection products are listed in Table 5-5.

Radial symmetry is a filtering process that identifies equant discrete features in the data. The algorithm seeks locations around which data values either decrease or increase in all directions. These features may be related to stocks, batholiths, cupolas, alteration haloes, kimberlites, diatremes, steeply plunging mineralized zones, and breccia pipes. Radial symmetry products were calculated using wavelengths from 250-16000 m, starting from a number of different residuals. Radial symmetry products are listed in Table 5-6.

Table 5-4. Additional filter and image products.

Product	Abbreviation	Description
Filter Products		
Automatic Gain Control (standard deviation = 30)	AGC30	Evens anomaly amplitudes to make subtle features more visible, longer wavelengths are suppressed.
Pseudogravity	PGrav	Useful for highlighting large scale features.
Pseudogravity residual	PGravRes	Difference between 0-2000 m upward continued pseudogravity. Longest wavelength features suppressed to highlight intermediate scale features.
Horizontal gradient of PGravRes	PGravResHGM	Highlights edges of intermediate scale features.
Small-scale residual	Res500_2000	Differential upward continuation residual, 500-2000 m. Highlights sources at 250-1000 m depth.
Medium-scale residual	Res2000_5000	Differential upward continuation residual, 2000-5000 m. Highlights sources at 1000-2500 m depth.
Large-scale residual	Res5000_10000	Differential upward continuation residual, 5000-10000 m. Highlights sources at 2500-5000 m depth.
Vertical derivative minus horizontal derivative	VDMHGM	Accentuates contrast in 1st vertical derivative, aids in highlighting shallow features.

Product	Abbreviation	Description
Vertical integral	VINT	Vertical integral of total field.
Analytic signal of vertical integral.	VIAS	Produces a result with similar amplitudes and wavelengths to total field, with reduced effects of magnetization direction and remanence.
Image Products		
Ternary of directional derivatives	X_Y_Z	Ternary images (CMY+RGB) of 1st X, Y, and vertical derivatives.
Ternary of 1VD, Tilt, HGM	1VD_Tilt_HGM	Ternary images (CMY+RGB) of 1VD, tilt angle, horizontal gradient.
Ternary of residuals	SmRes_MedRes_LgRes	Ternary images (CMY+RGB) of small, medium, large-scale residuals.
Ternary of RTP, VIAS, Asig	RTP_vias_asig	Ternary images (CMY+RGB) of RTP, analytic signal of vertical integral, and analytic signal. Helps identify remanent zones.
Ternary of pseudogravity	Prav_PGravRes_PGravRes HGM	Ternary images (CMY+RGB) of Pseudogravity, pseudogravity residual, and horizontal gradient of pseudogravity residual.

Table 5-5. Structure detection products.

Product	Abbreviation	Description
Fabric Orientation (RTP and AGC)	Fabric_Orientation	Reflects the orientation of long-wavelength features.
Total Structure (RTP and AGC)	StructX_Total	Total structure detected. X = filter wavelength (100 to 3200 m).
Oriented Structural Domains	StructX_OriDom_Th	Total structure (X = filter wavelength), thresholded into orientation domains.
Vectorized Structure	StructX_Total_Vec	Vectorized total structure (X = filter wavelength).
Belt-parallel structure	StructX_Para	Structure parallel to major belts (X = filter length).
Vectorized belt-parallel structure	StructX_Para_Vec	Vectorized structure parallel to major belts (X = filter length).
Belt-crossing structure	StructX_Cross	Structure crossing major belts (X = filter length).
Vectorized belt-crossing structure	StructX_Cross_Vec	Vectorized structure crossing major belts (X = filter length).

Table 5-6. Radial Symmetry products

Product	Code	Description
Radial Symmetry Lows	Res_X_Y_RSymZ_mi_Lows	Magnitude-independent radial symmetry at wavelength Z from X to Y residual, lows. Also vectorized.
Radial Symmetry Highs	Res_X_Y_RSymZ_mi_Highs	Magnitude-independent radial symmetry at wavelength Z from X to Y residual, highs. Also vectorized.
Radial Symmetry Highs and Lows	Res_X_Y_RSymZ_mi_Highs_and_Lows	Magnitude-independent radial symmetry at wavelength Z from X to Y residual, highs and lows. Also vectorized.

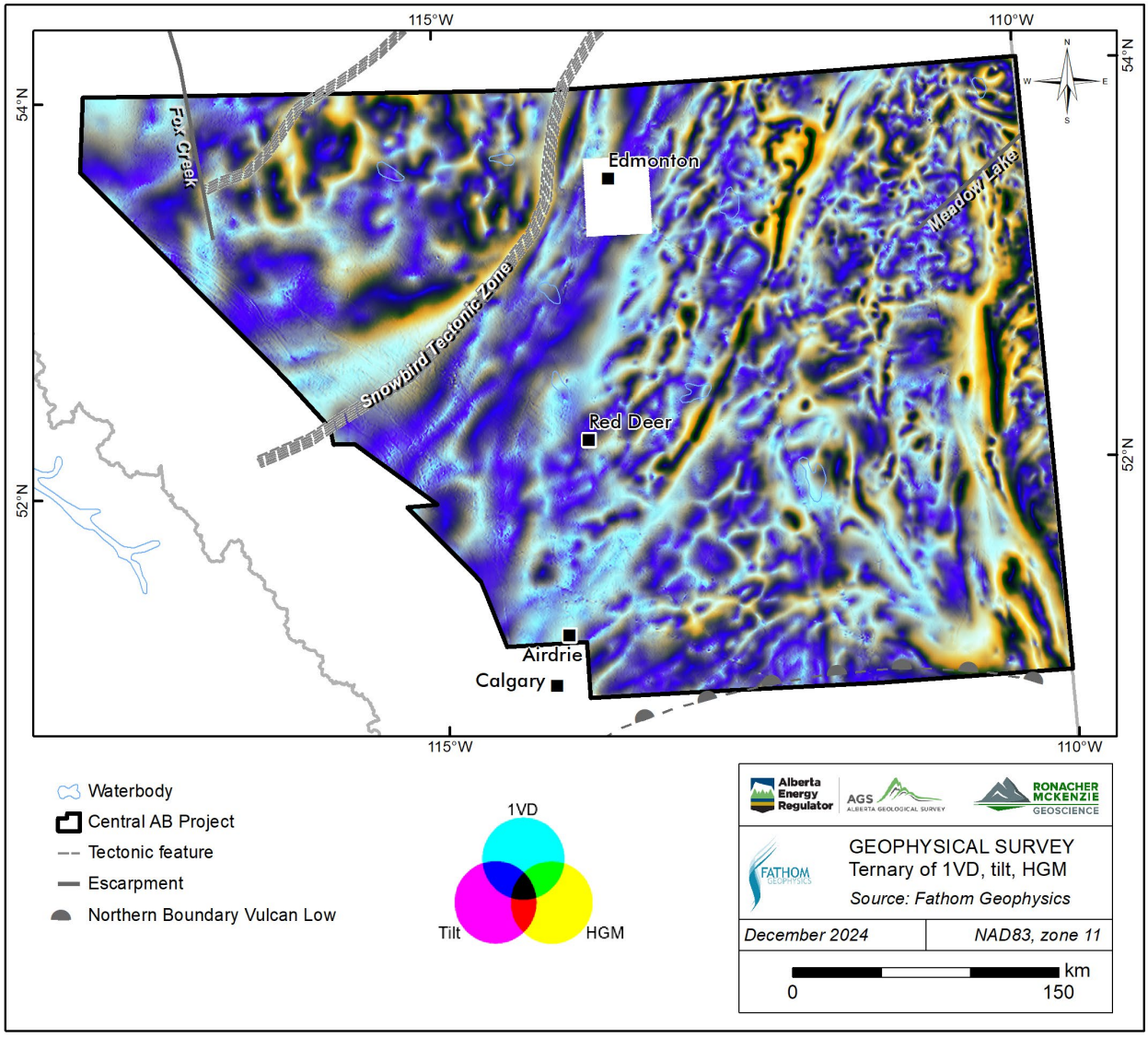

Figure 5-16. CMY ternary image displaying the 1VD, tilt angle, and HGM results from the RTP. Selected structural lineaments from Pană et al. (2021).

5.4 3D Magnetic Inversion

A portion of the central Alberta total magnetic intensity data was inverted using Seequent's VOXI inversion service to produce 3D models of subsurface magnetization. 3D Magnetic Vector Inversion ("MVI") and susceptibility models were obtained for a defined 400 x 100 km 'transect' area of interest. The area selected for inversion is a transect across lithotectonic domains to obtain insights on geometry of tectonic boundaries and depth to magnetic sources to constrain the 3D architecture of the basement. The area chosen is displayed in Figure 5-17.

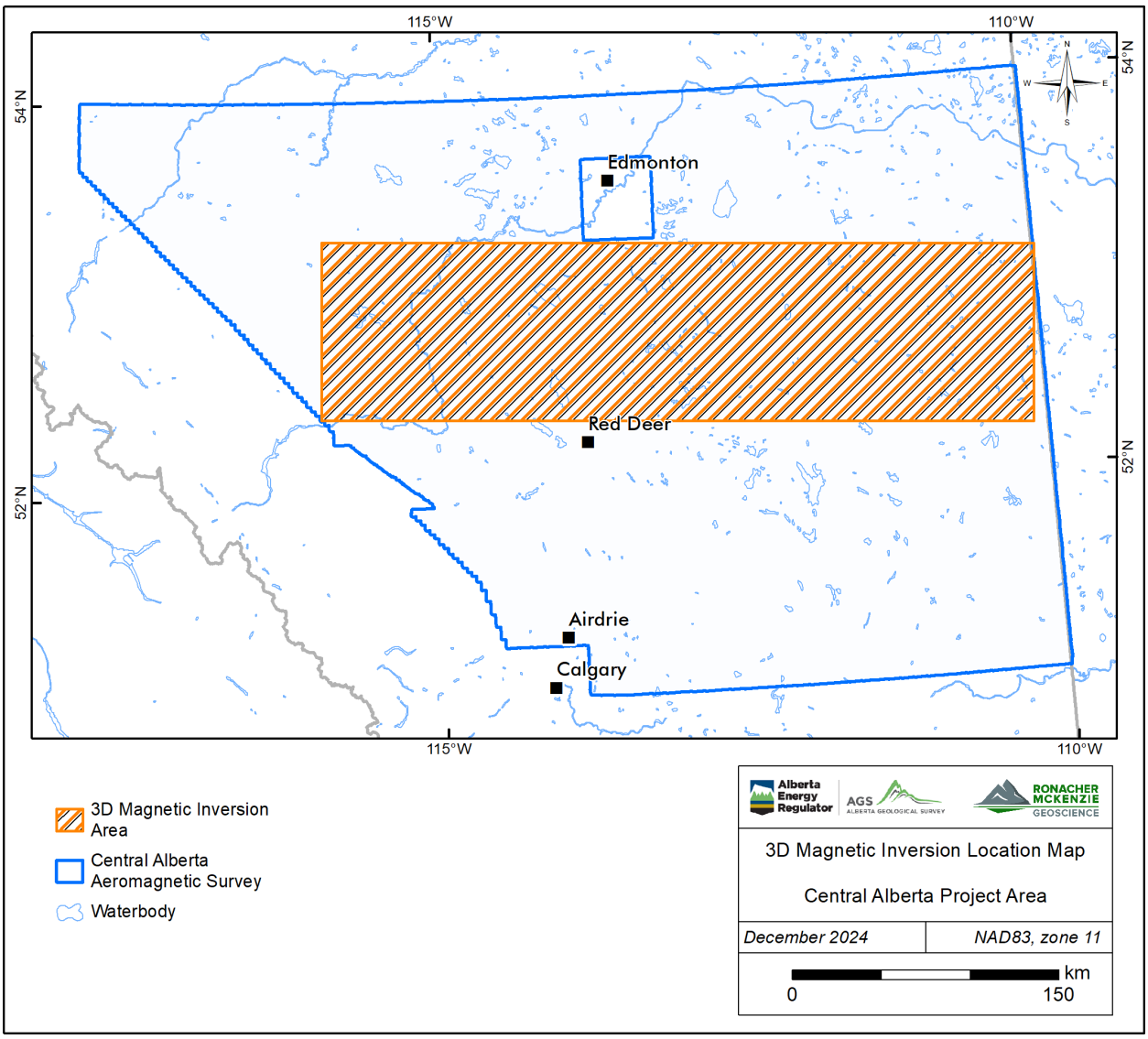

Figure 5-17. 3D magnetic inversion location map.

5.4.1 Data Preparation and Inversion Procedures

Prior to inversion, the data were pre-conditioned to remove long wavelength regional and short wavelength near-surface components, by upward continuation and application of band-pass filtering to the gridded data.

These filtered data were then sampled to a database, which was then de-sampled to the nominal cell size used for inversion. Gaussian noise based on the standard deviation of the low-pass residual of the filtered data was added to create the final data channel used for inversion.

For inversion, an initial error estimate based on the standard deviation of the data was used to generate a first pass inversion model. A new error estimate was calculated based on the misfit from this first pass model and used to run several models to estimate the best regularization parameters for the model. The misfit from the model with the optimal regularization was then used to rescale the estimated error for the final models. For the final models, the inversion was run using the final rescaled error as well as two passes of the VOXI Iterative Reweighting Inversion ("IRI") focus procedure, which helps to sharpen features in the final model and reduce over-smoothing. The IRI models were compared with models run without IRI to ensure that the results are consistent and plausible.

5.4.2 Inversion Results

The parameters used for the inversion area are summarized in Table 5-7.

Table 5-7. 3D Magnetic Inversion Parameters

Parameter	CAB Transect
Horizontal Cell size:	800 m
Vertical Cell size:	400 m at surface, increasing with depth
Upward Continuation applied:	400 m
Band Pass Filter type:	Butterworth, 8th order
Band Pass Filter cutoffs:	Low: 5000 m High: 230000 m
Gaussian Error added to data:	0.68 nT

The final models were trimmed of extraneous cells using SRTM topography from surface to 8 km depth.

The MVI amplitude model reflects only the total magnitude of the magnetization vector, which helps remove effects of ground magnetization not parallel to the Earth's field. The MVI code also returns scalar models of the magnetization vector magnitude parallel to (Eproj) and perpendicular (Eperp) to the Earth's magnetic field. The parallel amplitude (Eproj) is analogous to the result returned from a susceptibility inversion.

A 3D vector model is also generated by the MVI process, showing the direction and amplitude of the magnetization vector in the 3D inversion volume.

For comparison, a susceptibility model was also run, using the same noise and regularization parameters as the MVI inversion (Figure 5-18).

Since the MVI model solves for the magnitude of the magnetic field vector, it is generally less susceptible to effects of remanent magnetization than a susceptibility model which may provide erroneously low values in areas with significant remanent magnetization.

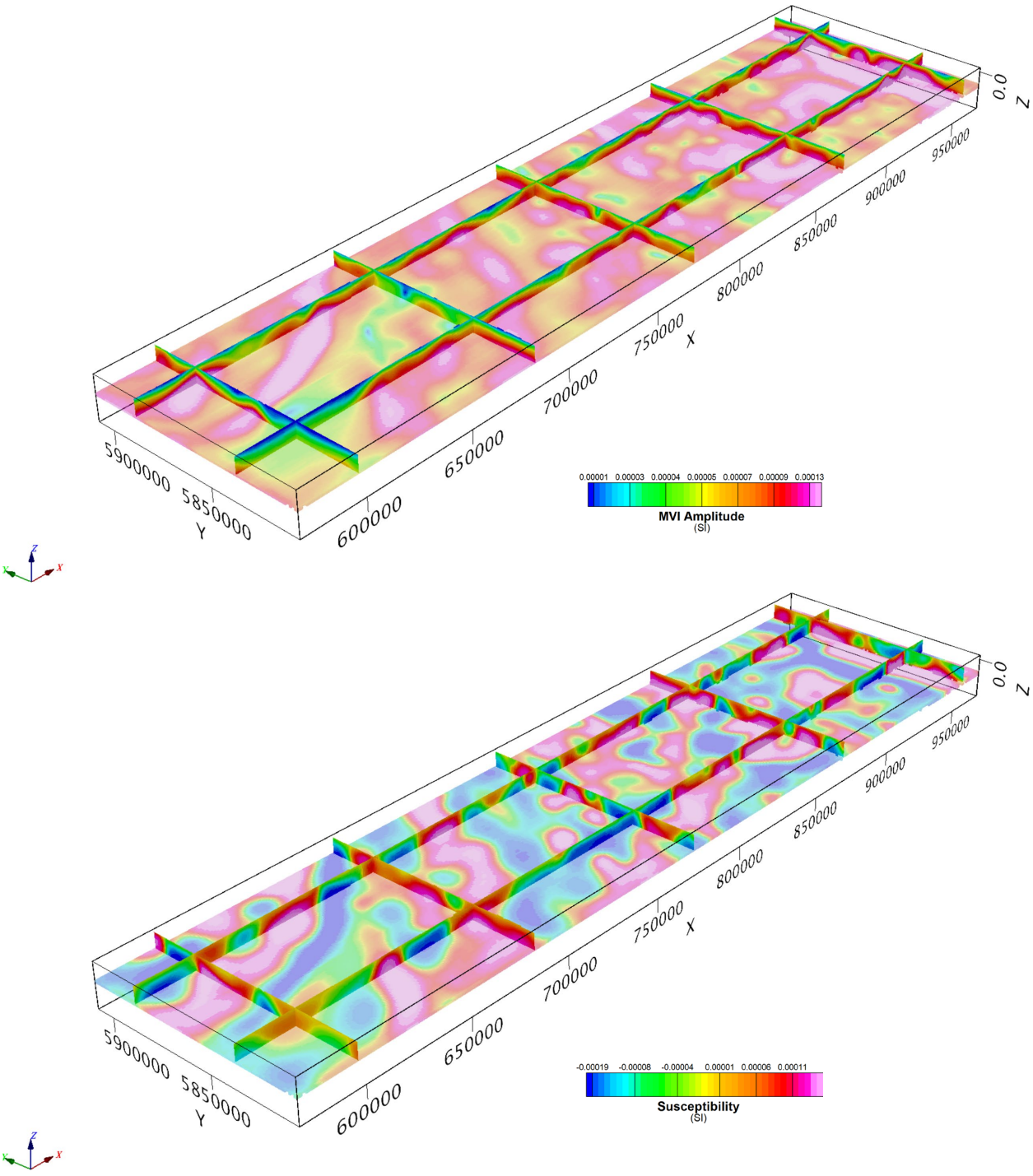

Figure 5-18. MVI amplitude model (top) and susceptibility model (bottom), with sections.

A complete set of inversion products including voxels and elevation plan slices, is included in the digital appendix provided to this report.

6.0 INTERPRETATION METHODOLOGY

6.1 Overview

The airborne magnetic derivative and filter products (Section 5.0) allow for new observations to be made and added to existing studies. Subsequent integration of anomalies allows for new insights in the subsurface in the region, which can steer structural interpretations, tectonic models, and subsurface exploration activities.

6.2 Workflow

The analysis follows the methodology developed by Isles and Rankin (2013), where the interpretation of the magnetic data is completed in three stages: observations, integration, and interpretation. This method is also employed in the associated reports (Lopez et al., 2024a; Brem et al., 2024; Lopez et al., 2024b).

The observation stage is focused on observing features directly from the magnetic filter products (Appendix B) and automatic detection results (Appendix C). The interpreter records magnetic ridges and linear trends as form line features, and magnetic domains from the anomalies that cause them as polygons. Form lines may represent either stratigraphic or structural trends, and line breaks or juxtapositions may represent structural elements (e.g., faults, shear zones, unconformities or intrusive contacts). This stage also includes the definition of domains that outline magnetic characteristics of different regions based on combined form line and magnetic rock unit observations.

The integration stage combines observations with existing geological and other types of data. This stage includes identification of discontinuities and definition of structural elements, magnetic domains, and changes or disruptions in domains with coherent structural or form line trends. Cross-referencing of the observations with other datasets, including Lithoprobe seismic (e.g., Ross et al., 1995; Ross and Eaton, 2002), gravity surveys (Edwards et al., 1998), geology (e.g., Pană, 2013; Prior et al., 2013), geochronology (Ross et al., 1991; Villeneuve et al., 1993; Burwash et al., 1994; Burwash et al., 2000; and Pană, 2010), and structural lineament compilations (e.g., Pană et al., 2001; Pană and Waters, 2016; and Pană et al., 2021) is done in this stage.

The interpretation stage involves the revision or creation of a structural framework that includes inferences of structural and lithotectonic history. This is the final step in generating an integrated geologic and geophysical interpretation of an area to present a final geological interpretation map. The compilation of the domains and structure layers is the basis of the structural framework interpretation.

6.3 Brittle Faults and Ductile Shear Zones

High-pass filter products such as the second derivative, tilt, and automatic gain control (AGC), and the results for short wavelengths from automatic structure detection for cross structures were used to emphasize shallow and detailed brittle structures in the project area. Criteria to identify brittle structures included the following:

- juxtaposition of different form line orientations
- linear features with angular margins

- angular fault jogs or steps
- short subtle curvilinear linear features (for sub-horizontal sedimentary strata)
- narrow zones of demagnetization (due to low temperature oxidation of magnetic minerals)
- offsets of magnetic rock units

Offsets and sense of movement were recorded in the accompanying GIS vector files where possible. Because of the 2D plan nature of magnetic data, interpreted offsets are apparent offsets.

Filters such as vertical and horizontal derivatives and tilt angle (tilt derivative) combined with results from the structure detection for parallel structures completed by Fathom Geophysics were used to identify deeper basin structures and shear zones. The wavelength separation results, particularly the separation of long wavelengths, allows for the interpretation of deeper structures. Furthermore, differential upward continuation magnetic products were useful for discriminating deeper from shallower structures (Figure 5-11 and Figure 5-12).

Shear zones in the project area are characterized by the following:

- broad zones of anastomosing surfaces, with curvilinear margins
- bending of magnetic units or contacts into the shear zone
- magnetic mineral alteration that may be destructive, additive, or both; or
- offsets of units associated with deflection or thinning of magnetic markers as they enter the shear zone

7.0 Interpretation and Results

7.1 Cultural Artefacts

Central Alberta is a highly populated region, including widely distributed infrastructure associated with the oil and gas industry and urban areas such as Edmonton and Red Deer. The survey contractor applied filtering and manual editing to attenuate the effects of culture in the data, but cultural artefacts are still present throughout the survey area. The following cultural features were evaluated against the aeromagnetic images: (1) municipal areas, (2) railways, (3) pipelines, and (4) oil and gas related infrastructure. As these features are all near surface, expected signatures include high frequency anomalies and/or distortion of larger magnetic anomalies. The infrastructure layers were always consulted before mapping features such lineaments or intrusions.

The area of Edmonton presents abundant high frequency features, particularly lineaments related to the pipeline network. The impact of culture is pervasive (Figure 7-1) and upward continued products at an elevation of 250 m were created as a way to filter higher frequency signatures and facilitate manual interpretation of geological features. Larger pipelines do not represent a major challenge in the interpretation of the magnetic images because they show as distinct shallow straight lines and can be easily correlated with infrastructure maps. However, most smaller pipelines do not show a clear magnetic signature at this survey resolution and clusters of pipelines creating a broad magnetic response are difficult to discern from a natural source (Figure 7-1). Overall, the impact of pipelines on the magnetic image is high and therefore, calibration of lineaments with cultural vector files and imagery is highly recommended.

Numerous small (< 5 km^2) rounded anomalies are present throughout the project area that are cultural in nature (e.g., gathering stations, processing plants, power stations). These anomalies may be misinterpreted as small intrusions if they are not correlated with infrastructure vector files or imagery (Figure 7-1). Not all of the high-frequency response is culture and the examples indicated in Figure 7-1 are not exhaustive. It is recommended that smaller rounded magnetic anomalies are carefully evaluated and calibrated with cultural data on a case-by-case basis before assigning a geological meaning.

The regional railroad and powerline networks do not show on any of the aeromagnetic images. The impact of these cultural components is considered negligible.

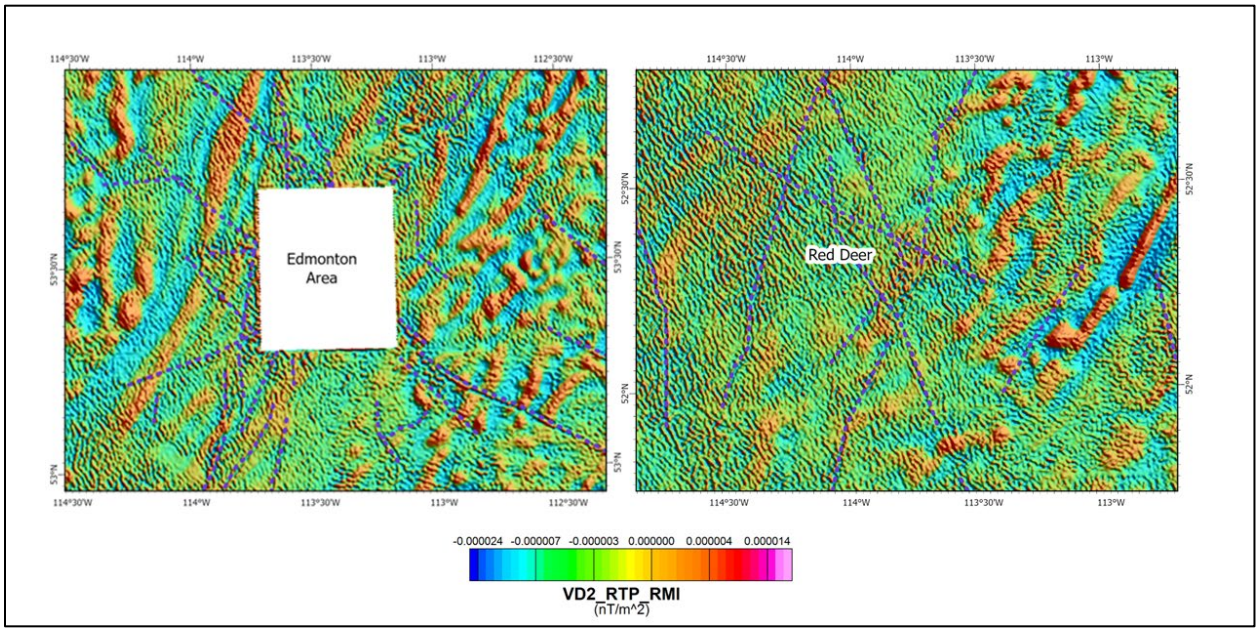

Figure 7-1. Impacts of infrastructure in the greater Edmonton area (left), and in Red Deer area (right) shown on 2nd vertical derivative CET magnetic image. High frequency features represent some urban, industrial site, noise, or geological features. Blue lines represent pipelines.

7.2 Domain Boundaries and Subdomains

In this study, the interpretation of the magnetic derivative and filter products conducted for the project area resulted in the modification of published basement domain boundaries. Many modifications are minor adjustments to the original boundaries; however, due to the higher quality of the new magnetic data some modifications are significant and involve a major relocation of a domain boundary, reintroduction of abandoned domain definitions, or definition of subdomains.

The reduced to pole residual magnetic intensity, analytic signal, first vertical derivative, total horizontal derivative, and ternary magnetic images that highlight geological affinity (e.g., pseudo-geology, pseudo-gravity), are used as the first step to outline domains and subdomains. Existing basement domain interpretations by Ross et al. (1991), Villeneuve et al. (1993) and Pilkington et al. (2000) are used to calibrate and classify domains in this step. Classification follows known basement domains wherever possible, whereas subdomains are defined here for the first time.

In this work, we use the term domain to indicate regions of akin magnetic character outlined by a distinct boundary, although some inferences regarding a tectonic meaning is sometimes offered based on previous studies. Further integration with historical and newly acquired geochronological data, isotope data, and additional geophysical studies is required to conclude that new (magnetic) domains defined herein can be interpreted as tectonic domains involved in the assembly and evolution of western Laurentia.

Basement domains were divided into subdomains based on distinct or contrasting magnetic character within certain domains. Subdomains may be related to a primary heterogeneous magnetic fabric or secondary geological processes that created, introduced, or destroyed magnetic minerals. Boundaries between subdomains are not necessarily tectonic in nature as they represent an internal magnetic variant within a known lithotectonic domain. Basement domains identified herein are shown in Figure 7-2 and Figure 7-3, and subdomains are shown on Figure 7-4 to Figure 7-6.

The main geophysical characteristics of basement domains based on our work are presented below and are also summarized and tabulated (Table 7-1). Petrological and chronological data is taken from unpublished compilations provided by the AGS from Ross et al. (1991), Villeneuve et al. (1993) and Burwash (1994).

- *Chinchaga:* This domain occurs in the northwest corner of the project area and corresponds to the Chinchaga terrane defined by Villeneuve et al. (1993) and Ross et al. (1994), and Chinchaga domain of Pilkington et al. (2000) which largely occurs in northern Alberta. In our study, this domain is characterized by a dominantly magnetic low signature that extends to the north, outside of the project area. In northern Alberta, the low magnetic signature was interpreted to relate to metasedimentary or volcanic rocks (Lopez et al., 2024). In the project area, closer to the contact with the Wabamun domain, the Chinchaga domain displays a localized magnetic high possibly related to effects of the northern splay of the Snowbird Tectonic Zone (Figure 7-2 to Figure 7-6). The magnetic character of the Chinchaga domain is consistent with metasedimentary or volcanic rocks (Lopez et al., 2024), which is consistent with previous studies of Villeneuve et al. (1993) and Ross et al. (1994).

- *Wabamun:* This domain is located between the Chinchaga and Thorsby domains in the western part of the project area and corresponds to the Wabamun High defined by Villeneuve et al. (1993) and the Wabamun domain of Pilkington et al. (2000). Our study shows the Wabamun-Thorsby boundary as a distinct curvilinear positive magnetic ridge. This domain is bounded in the northwest by the north splay of the Snowbird Tectonic Zone. The Wabamun domain shows evidence of magnetic remanence in the northwest (Figure 7-6). Only minor adjustments were made to the previously defined domain boundary. This domain is subdivided based on subtle differences in magnetic trends and subcircular boundaries more clearly seen on the pseudo-structure ternary image (Figure 5-10) and structure detection products (Digital Appendix C). The Wabamun Lake subdomain (Figure 7-4) is an elongate N- and NE-trending region bounded by rounded edges resembling a pluton, with higher frequency NNW- and NE-trending internal magnetic trends. The Wabamun West subdomain (Figure 7-4 to Figure 7-6) presents rounded boundaries in the south end resembling a pluton or zonation rims. Internally, the Wabamun West subdomain consists of large subrounded magnetic high anomalies bounded by linear magnetic lows with variable orientations. The fabric of both subdomains resembles that seen in weakly deformed plutonic belts.

- *Thorsby:* This domain includes the Thorsby Low defined by previous authors (Villeneuve et al., 1993; Ross et al., 1994; Pilkington et al., 2000). In our study, this domain was subdivided into two subdomains, Thorsby Low and Thorsby High (Figure 7-4 to Figure 7-6). The Thorsby Low domain has a homogenous low magnetic signature. A small subdomain, named here as Thorsby High, is identified between the

Thorsby Low and Rimbey domains. The Thorsby High corresponds to a small high amplitude crescent-shaped N-trending magnetic ridge in the west and a trough in the east located on the western edge of the Rimbey domain. According to Pilkington et al. (2000), the Thorsby Low may be the result of demagnetization due to deformation and metamorphism during terrane collision. The Snowbird Tectonic Zone (STZ, see section 7.6.1) runs through the Thorsby Low domain. The Thorsby High magnetic character resembles a small arc and related back-arc basin developed along the Rimbey domain, or alternatively might be a magnetized remnant of the Thorsby Low.

- *Rimbey:* This domain corresponds to the Rimbey or Rimbey High domain defined by previous authors (Villeneuve et al., 1993; Ross et al., 1994; Pilkington et al., 2000). In our study, only minor adjustments to the previously defined domain boundary were made. This domain consists of a prominent northeast-trending curvilinear high magnetic signature between the Thorsby and Lacombe domains. The eastern part of the domain is characterized by NE-trending high amplitude magnetic signature, whereas the western margin presents a penetrative higher frequency NE to NNE-trending and moderate amplitude magnetic fabric, possibly due to deformation (Figure 7-4).

- *Lacombe:* This domain corresponds to the Lacombe domain defined by previous authors (Villeneuve et al., 1993; Ross et al., 1994; Pilkington et al., 2000). Only minor adjustments to the previously defined domain boundary were made. The Lacombe domain is a northeast-trending zone that is internally indistinct in magnetic amplitude relative to the Loverna High subdomain, however it shows distinct fabric orientation and boundaries. The Lacombe domain generally displays as variable in magnetic amplitude and trends, bounded to the east by a sharply defined narrow magnetic high ridge (Red Deer Trend, see Section 7.6.2) along the margin with the Loverna domain, and to the west by the Rimbey domain. The boundary between the Lacombe and Rimbey domains is mostly well defined on the filter products but locally fuzzy where it is crosscut by other lineaments. To the south, the Lacombe domain ends at the confluence of the Red Deer Trend and the Rimbey domain. Internally, the Lacombe domain presents a NNE-trending magnetic fabric, but in the northeast corner it presents a local subrounded negative anomaly with a magnetic high rim resembling felsic intrusions with an outer magnetic rim (Figure 7-6). Three basement core intersections available from this domain include metasedimentary and metavolcanic lithologies; in particular, a low-grade metavolcanic sample collected from the Red Deer Trend yielded just a minimum crystallization age of 1.79 Ga (Villeneuve et al., 1993).

- Matzhiwin: This domain corresponds to the Matzhiwin High defined by Villeneuve et al. (1993) and the Matzhiwin domain of Pilkington et al. (2000). In our study, this domain is a large magnetic high located in the south of the project area. The magnetic amplitude is similar to the Rimbey domain and presents a general NE-trending internal fabric. In the eastern part of the domain the fabric is superposed by a second fabric of N-trending magnetic ridges, resembling parallel dykes, more clearly seen on pseudo-geology and pseudo-structure ternary images (Figure 7-4 and Figure 5-9). Only minor adjustments to the previously defined domain boundary were made (Figure 7-4).

- *Loverna:* This domain corresponds to the Loverna Block of Villeneuve et al. (1993) or Loverna domain of Pilkington et al. (2000). This domain is the magnetically variable region between the Lacombe and Rimbey domains in the west, the Matzhiwin domain in the south, and a magnetic low in the east (defined here as the northern extension of the Vulcan Low). Major boundary modifications to this domain are made, particularly to the eastern side. Previous authors have defined the eastern edge of the Loverna domain in contact with the Eyehill domain. However, in our study, a distinct magnetic low similar to the Vulcan Low of southern Alberta separates the Loverna and Eyehill domains (Figure 7-2 to Figure 7-6). The Loverna domain is subdivided into two subdomains: Loverna High and Loverna Low (Figure 7-4 to Figure 7-6). The Loverna High subdomain is a magnetic high and does not present a preferred internal fabric orientation, except along the northeastern edge where the trends of magnetic ridge lines demonstrate shearing. The Loverna Low subdomain presents generally as a magnetic low with variable NNW-, N- and NNE-trending fabrics and local broad rounded magnetic highs. The edges of the Loverna Low subdomain are fuzzy and it is unclear whether this subdomain relates to the adjacent northern extent of the Vulcan Low North structure or is a separate entity within the Loverna domain that has been affected by secondary processes. Basement core intersections include granites, granite and granodiorite gneiss, and pegmatite in amphibolite (Villeneuve et al., 1993). The Loverna High subdomain displays a NE-trending central discontinuity and attenuation of the magnetic amplitude to the east, whereas the Loverna Low displays a parallel N-trending magnetic lineament also at the centre of the subdomain resembling an extensional structure (Figure 7-5 and Figure 7-6; structure detection products in Digital Appendix C). Both the Loverna High and Low subdomains display high magnetic variability and more internal terrains could be defined, however boundaries are fuzzy.

- *Northern extension of the Vulcan Low (Vulcan Low North):* The Vulcan Low North domain is a distinct narrow north-trending magnetic low lying between the Loverna and Eyehill domains (Figure 7-4 to Figure 7-6). This domain displays a linear NNW- to NNE-trending internal fabric more clearly seen on pseudo-structure ternary image (Figure 5-10), derivative products (Digital Appendix B) and structure detection products (Digital Appendix C). This feature is 15 to 30 km wide and appears to merge with the major east-trending Vulcan Low of southern Alberta (Brem et al., 2024). This merge was also observed by Villeneuve et al. (1993) based on older aeromagnetic data. The merge between the north-trending component and the east-trending Vulcan Low can be observed in the magnetic data from the southern Alberta area (see magnetic products in Brem et al. 2024). The Vulcan Low North subdomain laterally displaces a section of the Matzhiwin domain southward towards the major east-trending Vulcan Low structure in southern Alberta (see magnetic products in Brem et al., 2024). Sharp edges along the boundary with the Eyehill domain and contrasting internal magnetic intensity and fabric in relation to both Eyehill and Loverna domains suggest that this magnetic low zone represent tectonic boundaries. Therefore, the north extension of the Vulcan Low or Vulcan Low North is considered in this work as a distinct tectonic domain (Figure 7-4 to Figure 7-6).

- Eyehill: This domain corresponds to the Eyehill High domain of Villeneuve et al. (1993) and the Eyehill domain of Pilkington et al. (2000). In our study, this domain is a magnetic high located in the east of

the project area near the Alberta-Saskatchewan provincial boundary. The western edge of the Eyehill domain is a curvilinear NNW- to N-trending positive magnetic ridge (see Eyehill Trend in Section 7.6.3), whereas the internal magnetic fabric to the east displays northeast trends that bend towards the south along (or into) the western curvilinear edge (Figure 7-2 to Figure 7-6). Only minor adjustments to the previously defined domain boundary were made.

In summary, major changes to previously defined domain boundaries and their internal characteristics include:

- Subdivision of the Wabamun domain into the Wabamun Lake and the Wabamun West subdomains in central Alberta.
- Major boundary modifications to the Loverna domain, particularly to its eastern side.
- Subdivision of the Thorsby domain into the Thorsby Low and Thorsby High subdomains.
- Introduction of the north-trending component of the Vulcan Low structure as a domain (named here as Vulcan Low North domain) between the Loverna and Eyehill domains.
- Subdivision of the Loverna domain into the Loverna High and Loverna Low subdomains.
- Minor adjustments to the following domain boundaries: Wabamun, Thorsby, Rimbey, Lacombe, Matzhiwin, and Eyehill.

The higher quality of the new magnetic data and derived products allow for the definition of subdomains within known tectonic domains. Reduction of uncertainties to resolve the architecture of the crystalline basement requires further integration with available geological, petrological, chronological, and magnetic susceptibility data.

The GIS files containing the outlines and details of the new interpreted lithotectonic domains and subdomains are included in the Digital Appendix A.

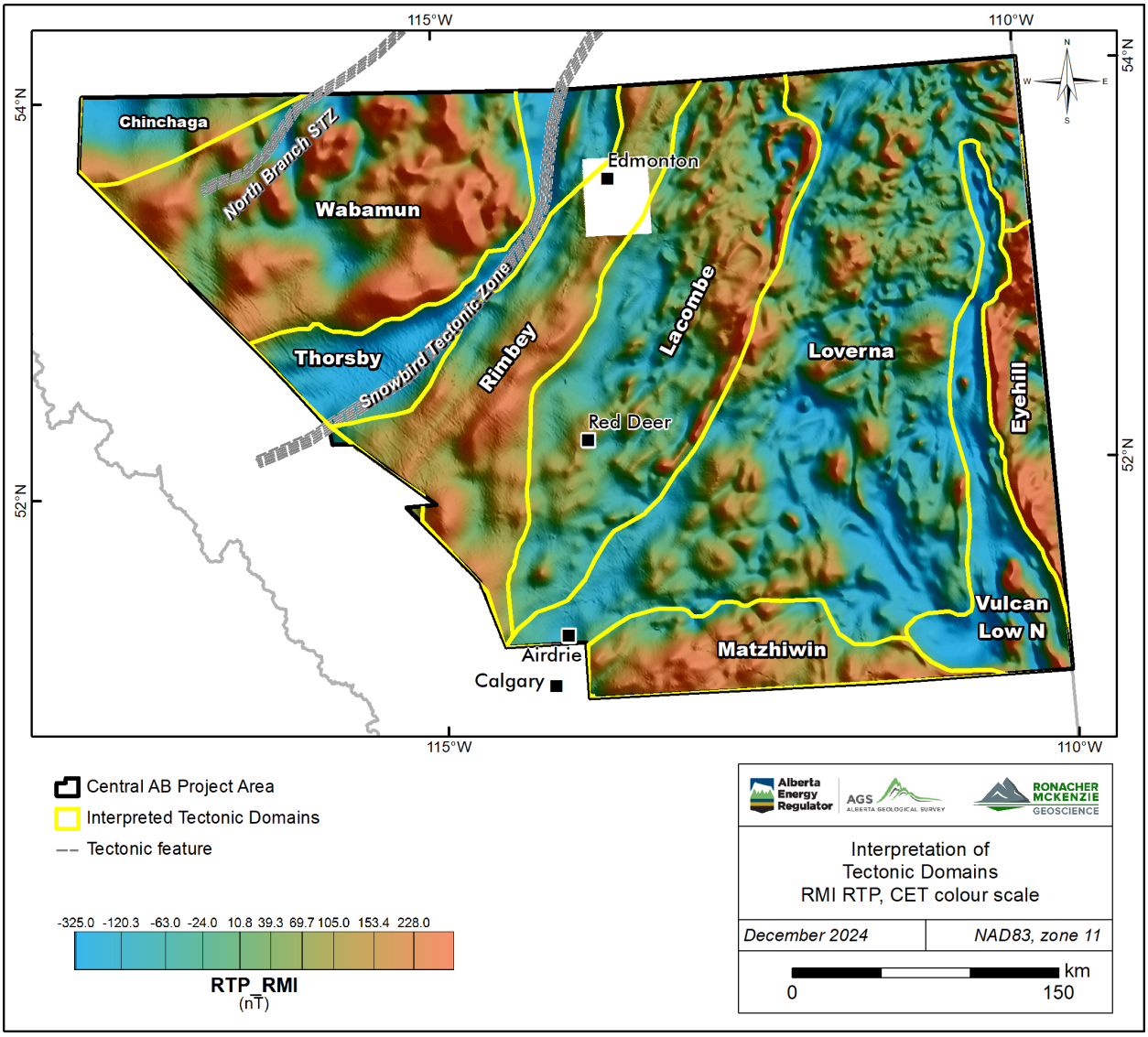

Figure 7-2. Interpreted domain boundaries in central Alberta modified from Pilkington et al. (2000). Selected structural lineaments (grey) are from Pană et al. (2021). Background image: RMI reduced to pole, CET.

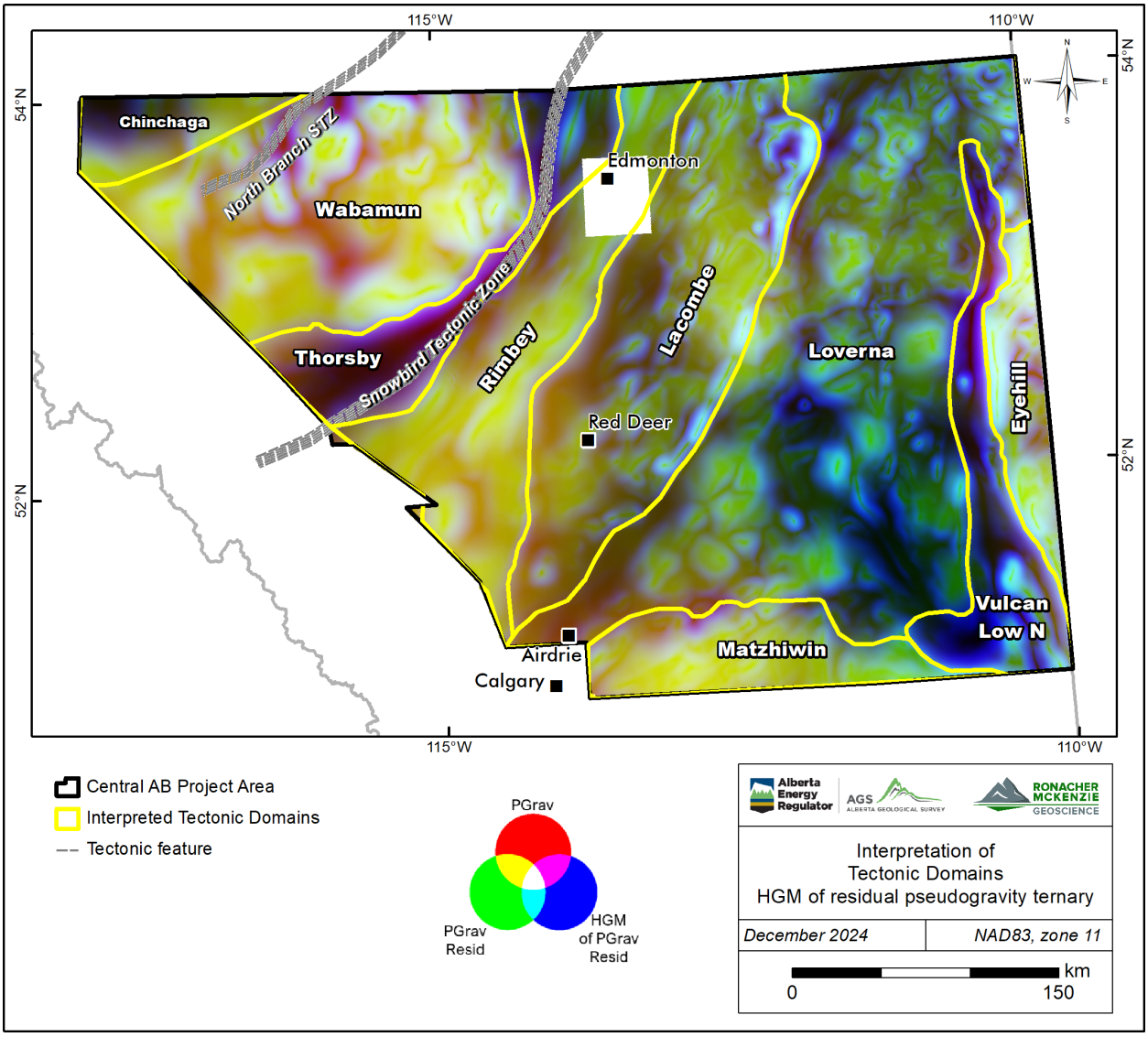

Figure 7-3. Interpreted domain boundaries in central Alberta modified from Pilkington et al. (2000). Selected structural lineaments (grey) are from Pană et al. (2021). Background image: HGM of residual of pseudogravity ternary by Fathom Geophysics.

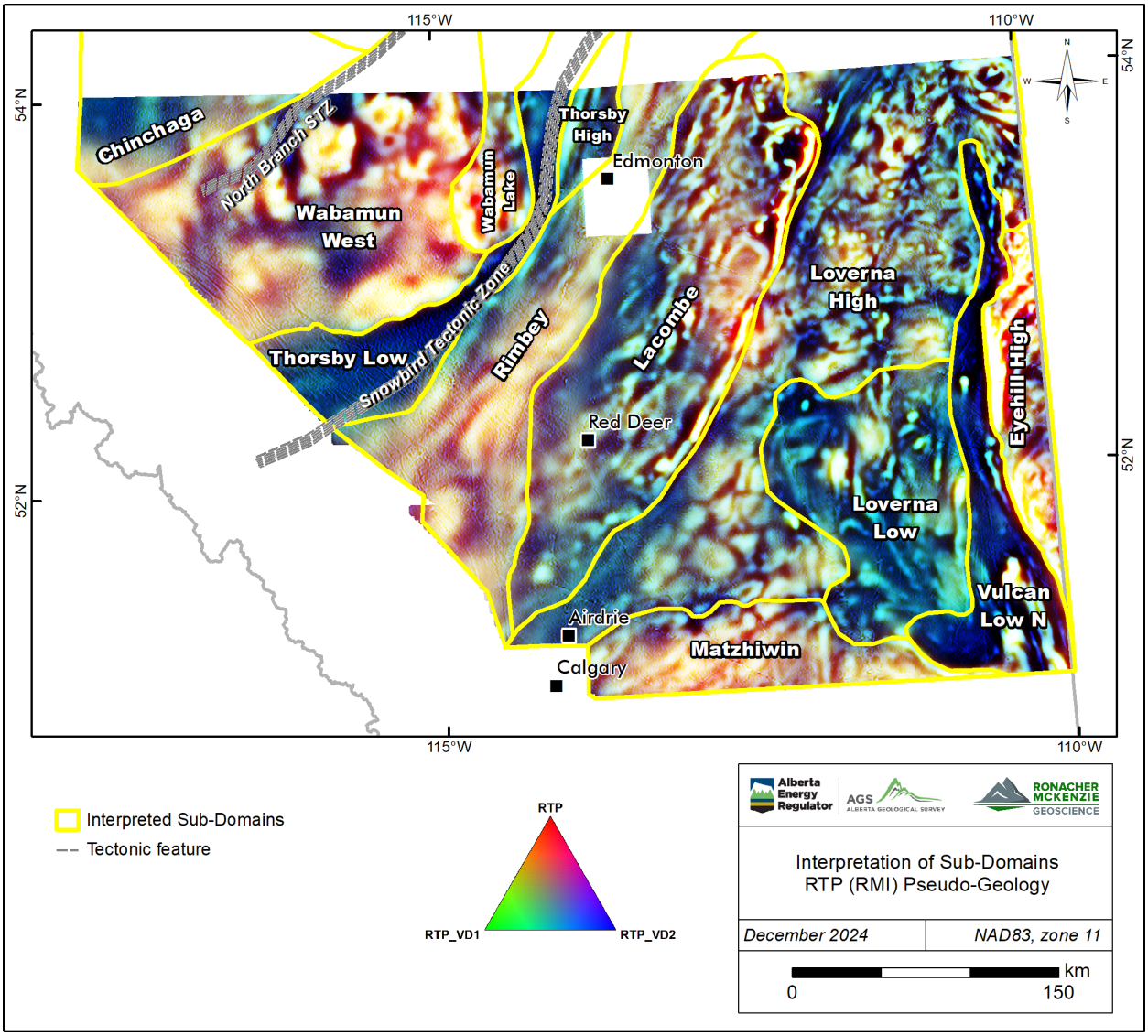

Figure 7-4. Interpreted subdomain boundaries in central Alberta defined for this project. Background image: pseudo-geology ternary.

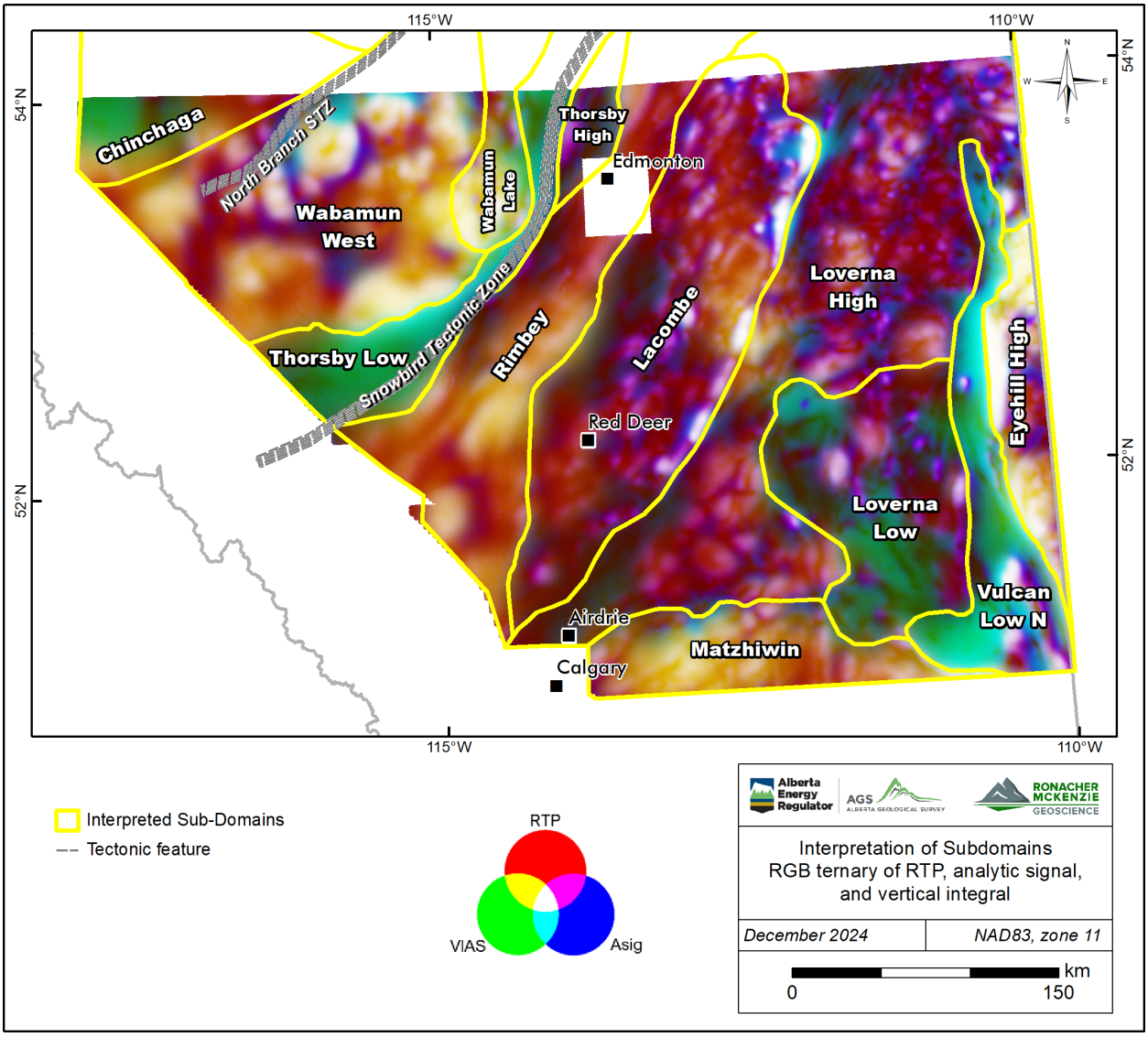

Figure 7-5. Interpreted subdomain boundaries in central Alberta defined by this study. Background image: ternary of RGB RTP, analytic signal of vertical integral, and analytic signal by Fathom Geophysics.

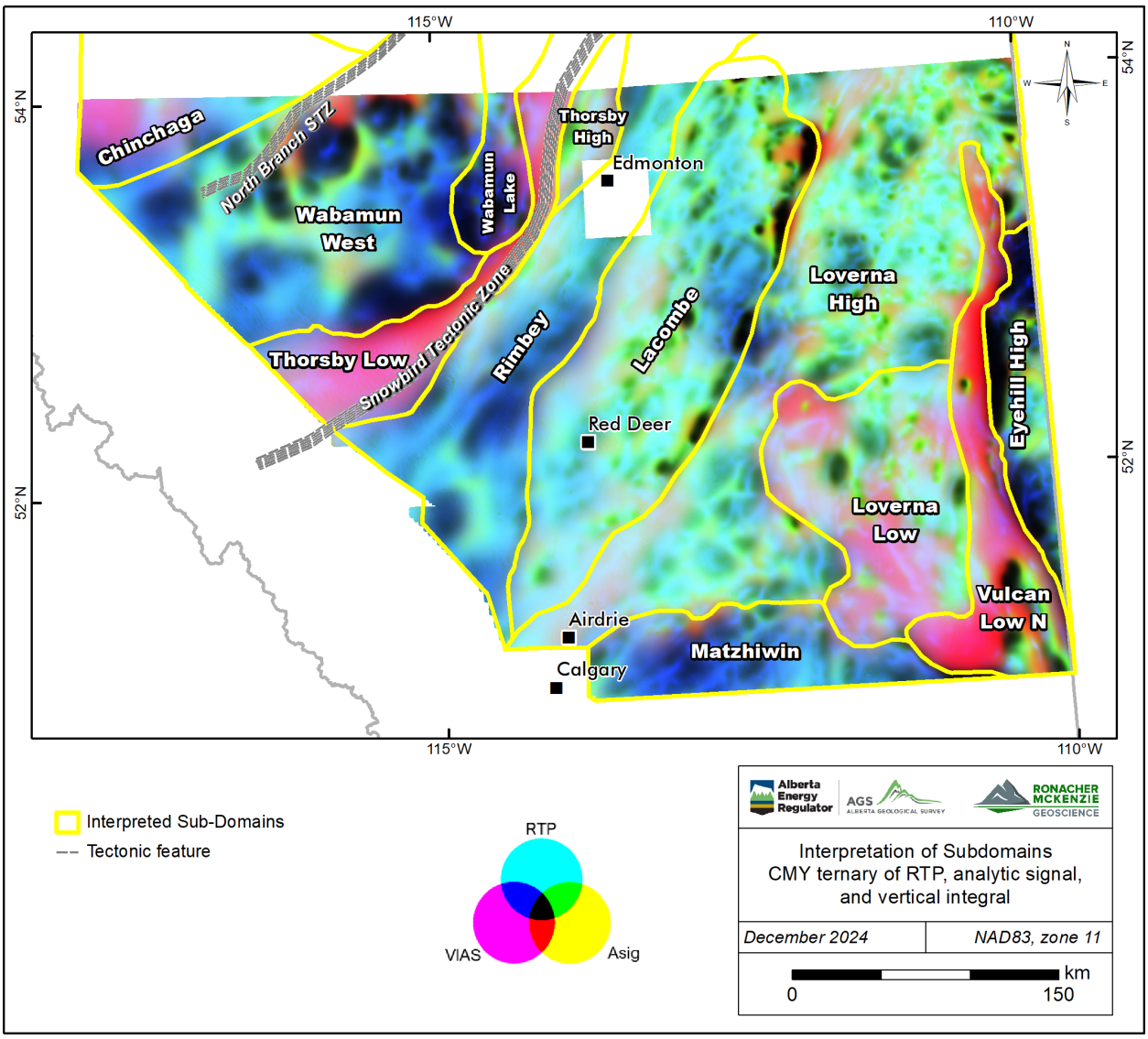

Figure 7-6. Interpreted subdomain boundaries in central Alberta defined for this project. Background image: ternary of CMY RTP, analytic signal of vertical integral, and analytic signal by Fathom Geophysics. Darkest red colour in the Wabamun, Loverna and Vulcan Low North domains indicates areas affected by magnetic remanence.

Table 7-1. Characteristics of basement domains and subdomains.

Domain[1]	Subdomain[2]	Age (Ga)[3]	Type[4]	Amplitude[2]	General Trend[2]	Magnetic character[2]
Chinchaga		2.1–2.2	Paleoproterozoic accreted terrane	Variable, moderate	NW to NNE None	NW to NNE low magnetic trends.
Wabamun	Wabamun Lake	2.3	Paleoproterozoic accreted terrane	Variable, high to low	NNW & NE	NE-trending elongate subdomain with rounded boundaries and internal anastomosing linear trends
	Wabamun West				None	Strong large subcircular anomalies bounded magnetically by low linear trends.
Thorsby	Thorsby Low	1.9–2.4	Remnant of Paleoproterozoic oceanic lithosphere	Low	NNE to none NNE	Strong parallel NE trends curving to the NNE in south boundaries.
	Thorsby High		Trough[2] (?)	High		Crescent-shaped magnetic high trending to the NNE.
Rimbey		1.8	Continental magmatic arc	Variable, high to moderate	NNE	Subcircular anomalies and few NE trends at boundaries.
Lacombe		>1.8	Proterozoic metavolcanic rocks sequence	Variable, high to moderate, locally low	NNE to NE	Moderate to low intensity, NNE to NE internal fabric, bounded in the east by a narrow high magnetic ridge.
Loverna	Loverna High	1.8–2.7	Archean block of Hearne Province	Variable, high to low	NE to ENE	Broad subcircular moderate anomalies and NE trends along western margin.
	Loverna Low			Low	NNW to NNE	Dominantly low magnetic signature with sparse NNW to NNE high magnetic trends, and circular highs in the north.
Matzhiwin		2.5	Magmatic arc[5]	High	ENE	Moderate-intensity, high magnetic signature with little internal fabric.
Vulcan Low North[2] (northern component of Vulcan Low)		2.6	Tectonic boundary between Loverna and Eyehill domains.	Low	NW to N	Dominantly low magnetic signature, and sparse N-trending high magnetic ridges
Eyehill		2.6	Archean block of Hearne Province	High	NE	Internally high to moderate magnetic intensity with NE trends. Western edge is a NNW to N-trending high magnetic ridge.

1. *Domain name after Villeneuve et al. (1993) Ross et al. (1994) and Pilkington et al. (2000)*
2. *This work*
3. *Ages by Ross et al. (1991), Villeneuve et al. (1993), Burwash et al. (1994)*
4. *Type of tectonic domain from structural elements compilation by Pană et al. (2021)*
5. *Type of tectonic domain suggested by Villeneuve et al. (1993)*

7.3 3D Inversion and Correlation to Lithoprobe

The results of the 3D inversion of the magnetic data along an E-W section extracted from the 3D model show the estimated disposition of major tectonic domains up to 6 km of depth (Figure 7-7). Relevant observations include:

- The Wabamun domain is a large east-dipping feature beneath the Thorsby domain,

- The eastern edge of the Rimbey domain is a high magnetic and major vertical crustal-scale feature,
- The Red Deer Trend is a west dipping feature,
- The Loverna domain is divided by a vertical structure of relatively low magnetic magnitude into east and west blocks, and
- The Eyehill domain is bounded in the west by a major magnetic high feature apparently dipping at a high-angle to the east.

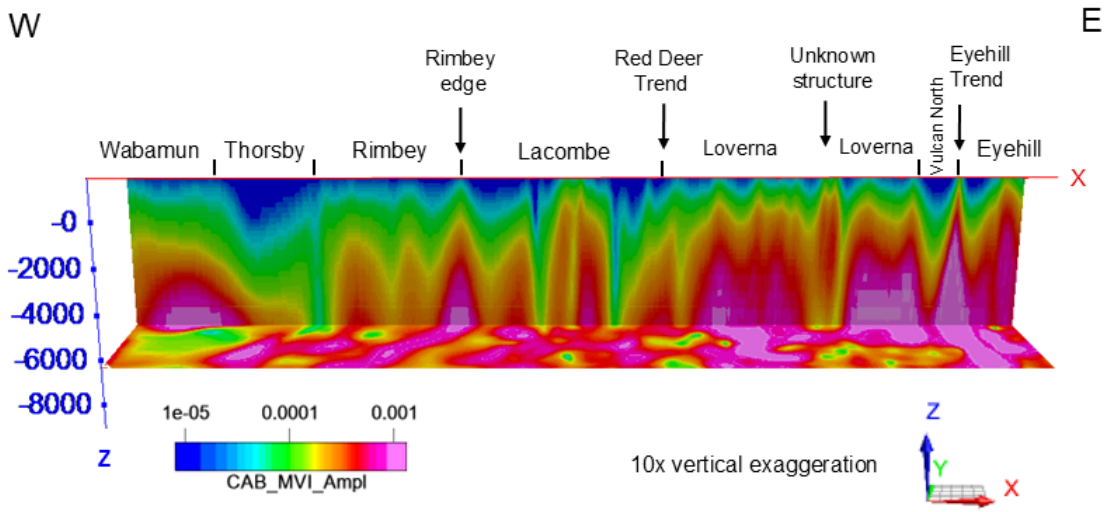

Figure 7-7. 3D magnetic inversion – MVI model, E-W section south of Edmonton and elevation plan at -6000m elevation.

The Central Alberta Transect (CAT) of the Lithoprobe seismic reflection program allows for a first-pass correlation of the magnetic structures with depth. A compilation of the 10 east-west oriented CAT lines is available from previous authors, including Figure 2 of Eaton et al. (1995), Figure 3 of Hope et al. (1999), and Figure 7 of Ross (2002). These compilations show a stratified upper section of the WCSB down to 1.4 - 1.8 s TWT (2-3 km depth). Below the WCSB, the basement can be subdivided into two main regions. Basement in the western region (lines 1-5) is underlain by the Wabamun, Thorsby and Rimbey domains, and is primarily characterized by subhorizontal reflectors, with notable ones at 4-5 s TWT (12-15 km depth). In contrast, the eastern region (lines 7-10), which underlies the Lacombe, Loverna and Eyehill domains, is characterized by numerous easterly dipping reflectors, predominantly in the lower crust (4-12 s TWT; 10-40 km depth).

Loverna – Eyehill boundary: The Vulcan Low North, coincides with an east-dipping reflector on Lithoprobe line 10 (Figure 7 in Ross and Eaton, 2002). There are two other prominent east-dipping reflectors within the Loverna domain on this seismic line, but these appear to have a weaker definition on the magnetic images. The 3D inversion MVI model shows a magnetic low (Vulcan Low North) adjacent to a magnetic high (Eyehill Trend) between the Loverna and Eyehill domains. These features appear to be dipping to the east at a high angle.

The Loverna High subdomain shows complexity as possibly two blocks separated by an unknown structure characterized as a narrow and vertical zone of relatively lower magnetic amplitude (Figure 7-7).

Lacombe – Loverna boundary: The interpretation of Ross and Eaton (2002) indicates that the boundary between the Lacombe and Loverna domains aligns with a "SE dipping thrust zone in the Archean Hearne crust" intersecting the top basement at Lithoprobe lines 08 and 09. Ross and Eaton's (2002) interpretation is not supported by the magnetic data presented in this study. These magnetic data show magnetic anomalies in the 3D inversion MVI model (up to 5 km depth) that are either vertical or dip to the west.

Wabamun – Thorsby boundary: In the western part of the survey area, a distinct magnetic low between the Wabamun and Thorsby regions separates domains with distinct magnetic expressions. This area is inferred to be the subsurface trace of the Snowbird Tectonic Zone (as per Pană et al., 2021). On Lithoprobe lines 2-3, this boundary was interpreted as a west-dipping crustal scale reverse fault that is rooted by an elevated Moho (Eaton et al., 1995). Due to the lack of higher resolution seismic sections, this tenuous interpretation could not be verified. The 3D inversion MVI model shows the Wabamun domain dipping shallowly to the east below the Thorsby domain.

7.4 Magnetic Fabric Orientation

The orientation of the magnetic fabric defined by the orientation of magnetic ridges or form lines was determined by Fathom Geophysics by enhancing (with automatic gain control) the pole reduced residual magnetic intensity and applying an anisotropic diffusion filter to highlight linear features (Appendix 1). The resulting orientations were interpolated and smoothed to generate the image shown in Figure 7-8. On this image, green areas are dominated by WNW to ENE trends; blue and cyan areas are dominated by NE trends; magenta indicates NNE trends and red and orange areas are dominated by NNW to N-trends.

The result of the magnetic fabric orientation shows five main regions with different dominant fabric orientations. From west to east, these regions are

- Chinchaga and Wabamun domains,
- Thorsby, Rimbey, Lacombe domains and western margin of Loverna High subdomain,
- Loverna High subdomain and Matzhiwin domain,
- Loverna Low subdomain and northern extent of Vulcan Low domain, and
- Eyehill domain

The region that includes Chinchaga and Wabamun domains display similarly variable magnetic trends. This variability changes to dominantly NW in the southwest possibly related to Cordilleran deformation. In contrast, the central region including the Thorsby, Rimbey, Lacombe domains and the western margin of the Loverna High subdomain are dominated by N to NNE trends represented by magenta, blue and red colours. The Lacombe domain and the western margin of the Loverna High subdomain display more trend variability relative

to the Thorsby and Rimbey domains, however the dominant magenta colour indicates N to NE trends. These domains also show variations in orientation closer to the Cordilleran deformation front.

The region that includes the Loverna Low and the northern extent of the Vulcan Low (Vulcan Low North) displays dominantly NNW to N trends represented by red and yellow colours suggesting that the deformation related to the Vulcan Low North partially affects the Loverna domain. The region that includes the Loverna High subdomain and Matzhiwin domain displays variable magnetic trends, however, in the eastern portion of the Matzhiwin domain, north magnetic trends represented by magenta and red colours are relatively more dominant. Finally, the Eyehill domain, which is separated from the rest by the Vulcan Low North, displays variable trends.

In summary, the fabric orientation magnetic product shows that the basement of the centre region of central Alberta comprising the Thorsby, Rimbey and Lacombe domains and the western part of Loverna domain underwent a deformation event that resulted in the generation of a general N- to NNE-trending fabric that did not affect neither the Wabamun domains nor the centre of the Loverna domain. The available Archean age (2.7 Ga) for the Loverna domain from Villeneuve et al. (1993) occurs within the Loverna Low subdomain, which appears modified by deformation and metamorphism. The Loverna domain displays subdomains with variable fabric orientations and therefore a complex internal lithotectonic structure that appears to have controlled the deposition of Cambrian-Ordovician strata.

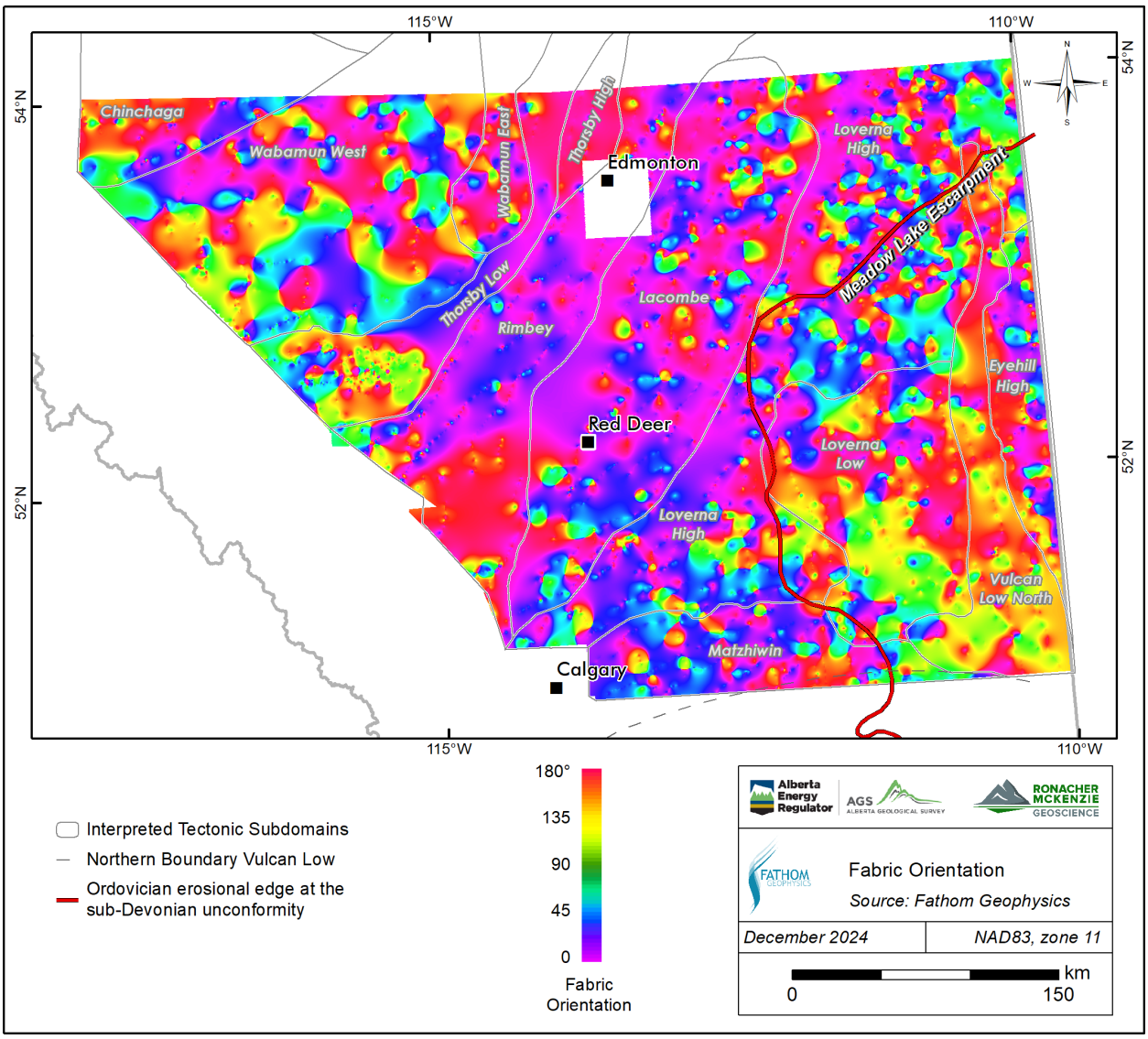

Figure 7-8. Magnetic fabric orientation of the project area. Ordovician erosional edge from Hauck (2020).

7.5 Depth to Basement

Fathom Geophysics generated depth to magnetic source and basement elevation surface grids and images (Digital Appendix C). The method uses the derivative of the tilt angle to estimate the depth of contacts in the data to generate a depth to magnetic basement grid. Then, the magnetic basement surface is generated by subtracting the depth to magnetic source grid from topography data (Figure 7-9). The results for central Alberta show that the basement surface gets deeper to the west and southwest, and shallower in the northeast. The calculated basement elevations are consistently underestimated compared to actual elevations known from basement-intersecting wells.

In the northwest part of the project area, a distinct decreasing elevation pattern occurs parallel to the NE-trending STZ and Rimbey domains, which is attributed to the inherent magnetic lower signature of the STZ. A subtler pattern shows magnetic elevations decreasing towards the southwest for individual domains. This subtle pattern is more consistent with 3D basement surfaces modelled by AGS from top basement picks.

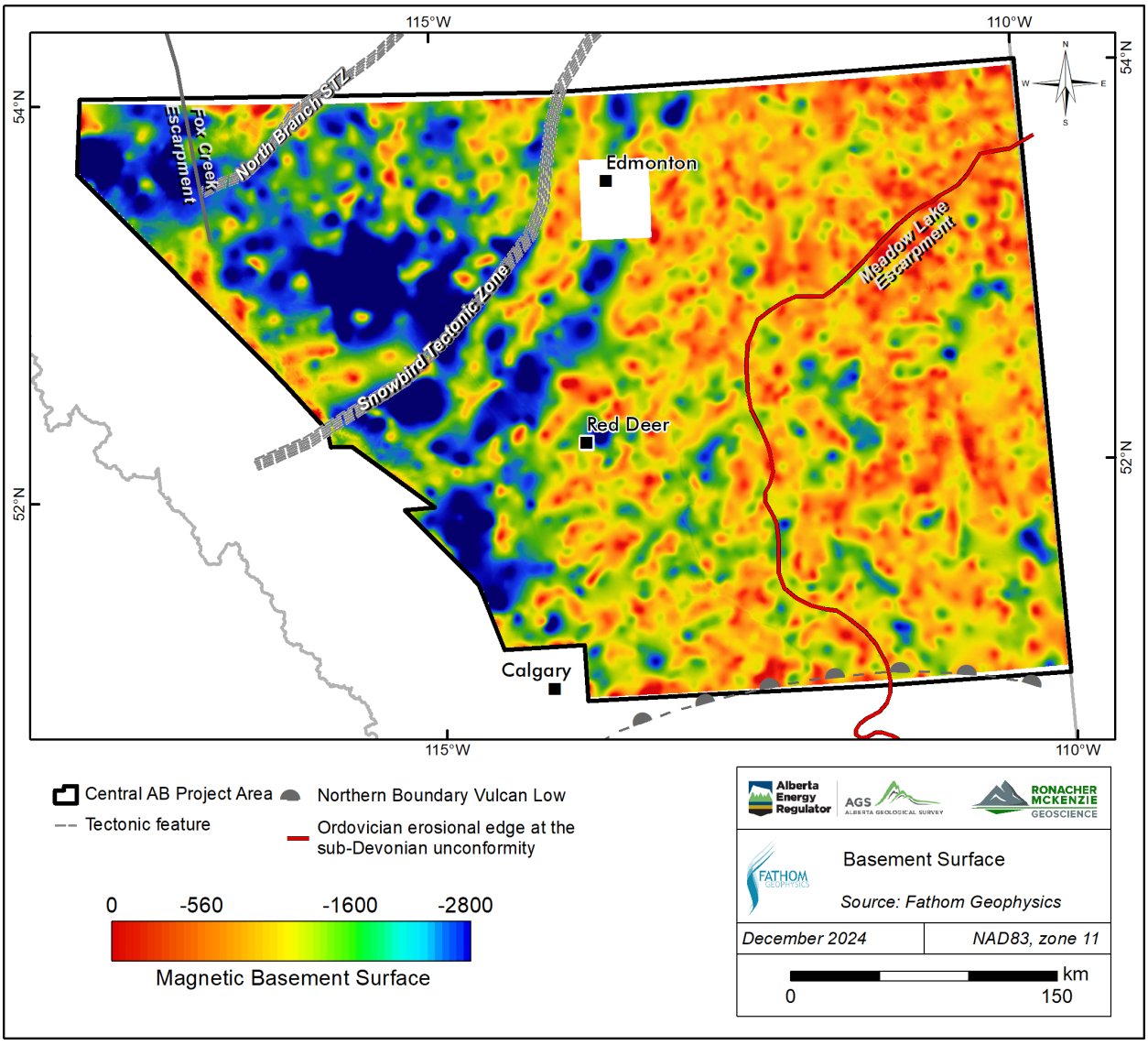

Figure 7-9. Magnetic basement surface product from Fathom Geophysics. Selected structural lineaments (grey) from Pană et al. (2021).

7.6 Structural lineaments

Numerous lineaments were identified using diverse magnetic images (Figure 7-10) and were correlated with the subsurface lineament compilation from Pană et al. (2021). Lineaments were interpreted as ductile shear

zones, brittle faults, thrusts, boundaries, faults (when unclear about ductile/brittle nature), and lineaments (or structural trends). The GIS files containing the interpretation of lineaments and relation to documented structures are included in the Digital Appendix A.

Basement faults and structures can impact the sedimentation of the overlying basin. Therefore, RMG attempted to establish whether faults can be delineated in the WCSB using the magnetic data and/or whether the magnetic lineaments attributed to basement structures have affected the WCSB sedimentary rocks. The interpretation of faults from magnetic data required the search of lateral offsets in magnetic ridges, changes of form line trends across a lineament, change in amplitude or frequency across a lineament, and dimming of magnetic signature to infer uplifted and down-dropped blocks. In addition, the fabric-parallel and fabric-crossing structure detection products by Fathom Geophysics (Digital Appendix C) were used to support lineament interpretations. The fabric-parallel features tend to be contacts or shear zones, whereas the cross structures are more likely to be faults.

A selection from the compilation of regional lineaments from Pană et al. (2021) was compared against the interpreted lineaments. In the central Alberta survey area, Pană et al.'s (2021) compilation includes 1,011 lineaments with interpretations based on one or a combination of the following methods: aeromagnetic, electromagnetic and gravity (e.g. Edwards et al., 1995); surface photo and/or morphological lineament interpretation (e.g. Misra et al., 1991); geophysical logs; seismic; stratigraphic cross-sections; isopach or top surface structural contours of WCSB lithological units (e.g. Wadsworth et al., 2002); and mapped using SEASAT and Thematic Mapper in hydrocarbon-producing areas (Misra et al., 1991). All these methods are based on 2D mapping and infer the presence of a fault, either in the basement or in the overburden, through implied genetic relationships. More than half of the lineaments interpreted in this compilation were derived from historical aeromagnetic data and morphological lineaments. Sixty-eight lineaments from Pană et al. (2021) were selected according to length (> 100 km) for their calibration with the interpreted lineaments from the new magnetic data. The correlation with Pană et al. (2021) was added to the lineament interpretation shapefile which is provided in the Digital Appendix A.

Key interpreted lineaments were also correlated with available Lithoprobe seismic interpretations, stratigraphic thickness and extents of the WCSB using the AGS' 3D geological model (Alberta Geological Survey, 2021).

The most relevant interpreted lineaments identified are described in the subsections below.

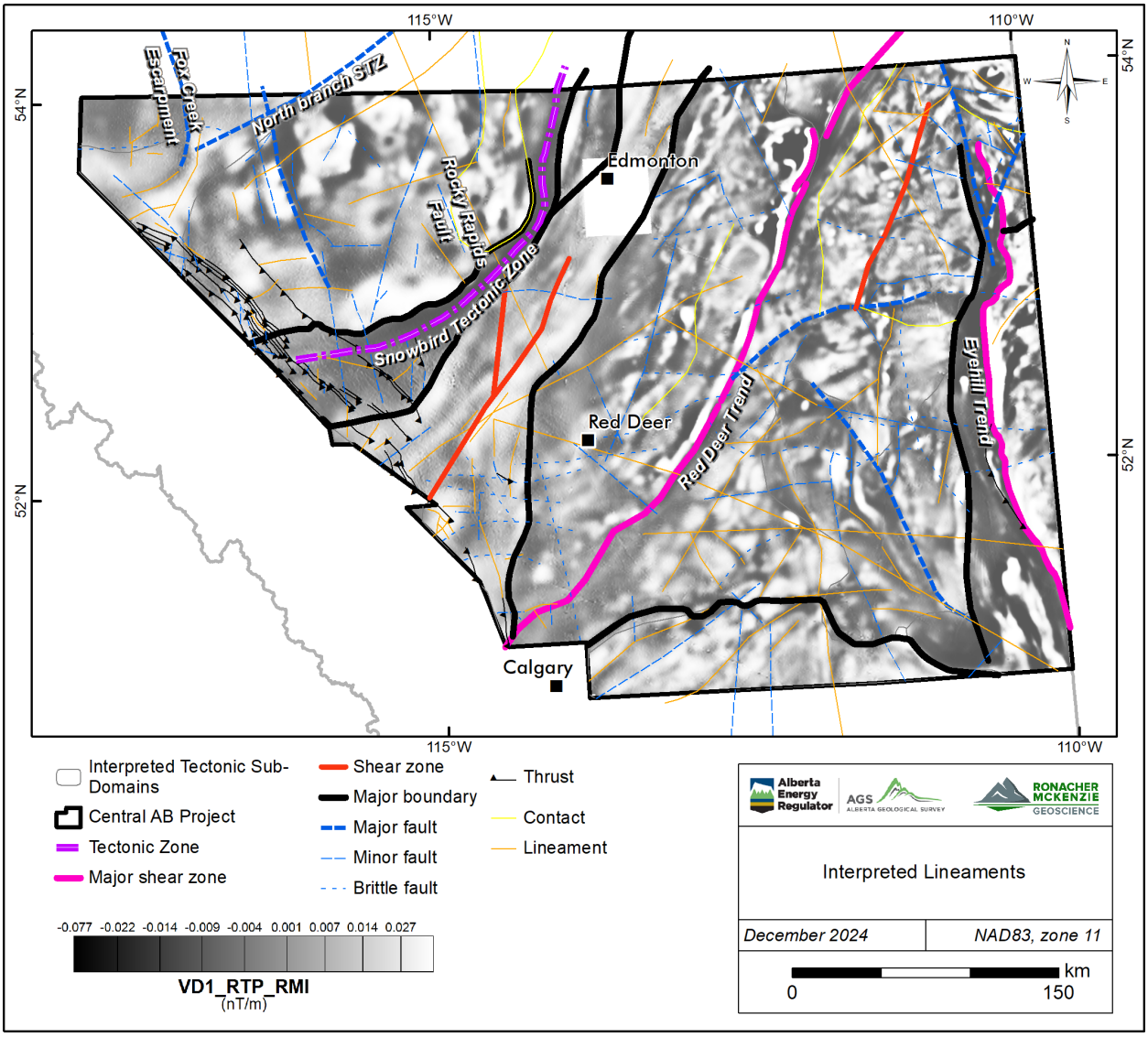

Figure 7-10. Interpreted linear features, including lineaments, faults and shear zones, in central Alberta. Background image: first vertical derivative in black and white colour scheme.

7.6.1 Snowbird Tectonic Zone

Across the western corner of the project area, the magnetic products show the STZ as a NE-trending narrow zone or belt of parallel linear features within the Thorsby domain. A northern linear splay of the STZ separates the Wabamun and the Chinchaga domains (Figure 7-2 to Figure 7-8).

7.6.2 Red Deer Trend

The Red Deer Trend is a NE-trending narrow positive magnetic ridge along the boundary between the Lacombe and Loverna domains (Figure 7-10). To the northeast, the Red Deer Trend runs through the Loverna High subdomain. To the southwest it appears to merge with the Rimbey domain. In this work, the Red Deer Trend is interpreted as a ductile thrust zone because of the following observations:

- continuous and narrow magnetic high along the Lacombe domain margin that can be explained by magnetic mineral addition (centre) and destruction (margins) due to shearing-related metamorphism and/or metasomatism,
- strong NE-trending anastomosing fabric at the northeast and southwest ends, and
- bending of the Loverna domain magnetic fabric towards the Red Deer Trend, suggesting a component of right-lateral movement, although no clear marker is identified to confirm the amount of offset or kinematics.
- magnetic intensities on both sides of the shear zone are different (higher amplitude in western block), suggesting some vertical offset with the western block moved up in relation to the eastern block (Figure 7-10).
- the 3D inversion shows a moderate angle, west-dipping magnetic high bounded in the east by a vertical magnetic low (Figure 7-7), whereas other sections show a vertical magnetic high. The westerly dip direction differs from interpretations from robust seismic data from the Lithoprobe seismic reflection program. Seismic interpretation results indicate that major basement domains in central Alberta are verging to the northwest (Ross, 2002). Further studies are recommended to resolve the dip of the structure.

7.6.3 Eyehill Trend

The western edge of the Eyehill domain is a curvilinear NNW- to N-trending positive magnetic ridge that resembles a shear zone. The 3D inversion resolves this feature as continuing to depth and dipping to the east at high angle (Figure 7-7). The internal magnetic fabric trends in the Eyehill domain bend towards the south into this magnetic lineament.

7.6.4 Brittle Faults and Other Lineaments

Brittle faults

West of Edmonton, Burwash et al. (2000) identified a NW-trending lineament referred to as the Rocky Rapids fault (Figure 7-10). This lineament can be observed on several magnetic images (e.g., Analytic Signal and First Vertical Derivative). Unfortunately, limited resolution of the Lithoprobe section over this area precluded correlation with the magnetics; hence, it is unknown at which depth this fault may be present.

Across the project area, it was observed that many lineaments interpreted by Misra et al. (1991), both NW- and NE-trending, show a reasonable collinearity with the second-order lineaments on the analytic signal and first vertical derivative magnetic images.

In the Cordilleran front, existing thrusts from the bedrock geology map of Alberta (MAP 600, Prior et al., 2013) were extended following correspondent magnetic lineaments and some new thrusts were added. Field reconnaissance is required to confirm the presence of the new thrusts (or back-thrusts) that may be visible in the foothills.

Escarpments

In the northeast of the project area, no collinearity is observed between interpreted magnetic lineaments and the western extent of the Meadow Lake escarpment. Most proximal magnetic lineaments with a similar trend to the Meadow Lake escarpment are interpreted as minor faults, possibly brittle as they interrupt or offset the magnetic fabric. Subtle changes in magnetic linear trends in the Loverna High subdomain suggest a different basement subunit may occur with a trend collinear with the trace of the escarpment, but this is only observed in the structure detection products (Digital Appendix A). However, the western and southwestern edges of the Ordovician strata south of the escarpment delineated in Hauck (2020) clearly correlate with changes in magnetic fabric orientation and boundaries between the Loverna High and Loverna Low subdomains (Figure 7-8).

In the northwest of the project area, a collinearity is observed between a subtle magnetic lineament and the southern extent of the Fox Creek escarpment documented by other authors (Hayes et al., 1994; O'Connell, 1994; Peterson and MacCormack, 2014). A change of magnetic intensity and subtle direction of fabric from NW to NNW in the second vertical derivative magnetic image coincides with the inferred location of the escarpment reported by Peterson and MacCormack (2014). This magnetic lineament is not observable in all magnetic products except the ones that highlight shallower features.

Devonian Reefs

In central Alberta, the connection of Upper Devonian reefs with basement lineaments has been documented by various authors (e.g., Edwards et al., 1995). A degree of parallelism between basement trends and overlying lineaments is to be expected, based on global analogues and sandbox analogue experiments. In central Alberta, some of these reef buildups, including linear reef chains and linear reef edges of more extensive complexes, are aligned with first- or second-order magnetic features. Areal extents of the Leduc Formation reef units were obtained from the AGS 3D geological framework model (Alberta Geological Survey, 2021).

The western edge of the extensive Killam reef complex of east-central Alberta (Alberta Geological Survey, 2021) correlates with the northwest boundary between the Loverna High and Loverna Low subdomains (Figure 7-11), and with changes in magnetic fabric orientation along a NNE trend on the western margin of the Loverna High. This margin is related to the limit of deformation of the Red Deer Trend. In fact, the western margin of the Loverna High subdomain is characterized by strong NNE linear magnetic trends, whereas the central part

of the Loverna High displays variable magnetic trends. Thus, the edge of the Killam reef complex coincides with the edge of the deformation zone related to the Red Deer Trend.

The Upper Devonian Bashaw reef complex overlies a basement high, as interpreted on Lithoprobe line 07 (Eaton et al., 1995). This elongate NNW-oriented reef complex is underlain by distinct NNE-trending magnetic ridges, demonstrating that the primary magnetic lineaments are not representative of faults that have penetrated top basement (Figure 7-11). Locally, the edges of the Bashaw reef tend to align with terminations or dimming of discrete magnetic lineaments. This might be the only signal of the Paleozoic strata and/or basement faults on the magnetic products.

The regional Rimbey-Meadowbrook reef trend of the Upper Devonian Leduc Formation (Woodbend Group) is at approximately a 20° angle with the main regional trend of magnetic ridges and Thorsby-Rimbey domain boundary. This discrepancy in angle suggests that the regional boundary between Thorsby and Rimbey or the Rimbey magmatic arc trend are unlikely to have controlled its location, and the orientation might be related to second-order features or a basement topography that is not evident in all magnetic products. In fact, the magnetic basement surface calculated by Fathom Geophysics shows that the northern half section of the Rimbey-Meadowbrook reef in central Alberta does correlate with a basement topography high trend that starts in the Rimbey domain and extends into the Thorsby High subdomain in the north, but this correspondence disappears in the south for the Homeglen-Rimbey linear portion of the reef and reappears in the southern end (Figure 7-11). Nevertheless, the Homeglen-Rimbey section is unrelated to the basement surface but follows magnetic ridges at or near the Rimbey-Lacombe boundary.

In conclusion, some of the magnetic lineaments are colinear with the Devonian reef build-up, which is consistent with observations by Edwards and Brown (1999). The new magnetic data and derivative products are able to provide further insight due to the higher resolution and add correlations with basement features that had not been identified before.

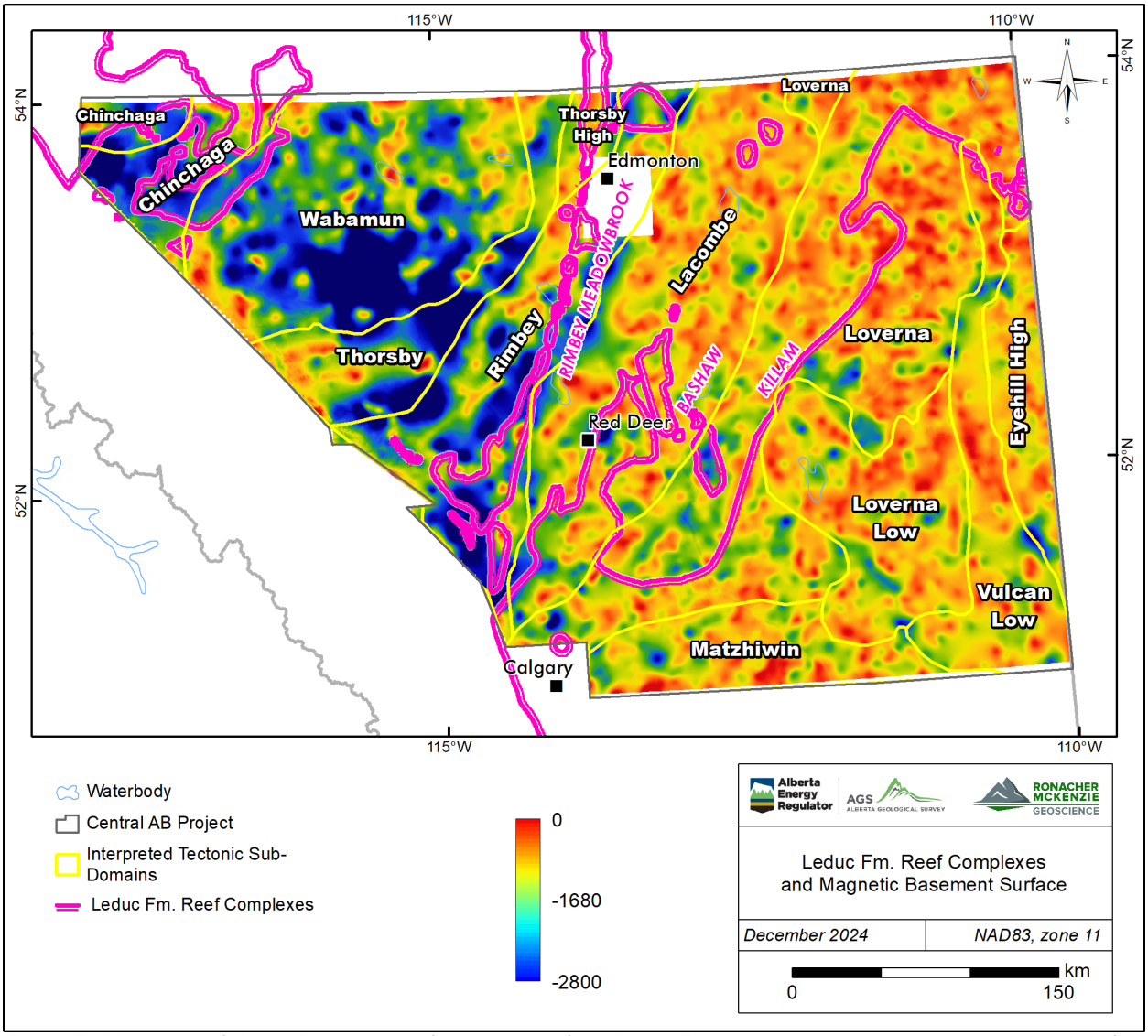

Figure 7-11. Location of Upper Devonian reef complexes of the Leduc Formation relative to magnetic basement surface and subdomains.

7.7 Intrusions

Intrusion detection was conducted in the project area using a combination of manual examination and automatic radial symmetry detection (Figure 7-12). Small and rounded magnetic anomalies were identified that can be interpreted as probable intrusive bodies. These anomalies are noted to be magnetic highs and lows. Following automatic detection, a manual examination was conducted that included calibration with culture such as urban sites and industry infrastructure, and calibration with the known geology. None of these rounded anomalies had been identified by previous studies.

Anomalies interpreted to be intrusions in the project area display the following character:

- single lobe small circular or oblate magnetic anomalies;
- isolated to poorly isolated high frequency smaller (< 5 km^2) circular or asymmetric anomalies;
- larger rounded multi-lobe anomalies; and
- broad rounded anomalies with distinct internal texture.

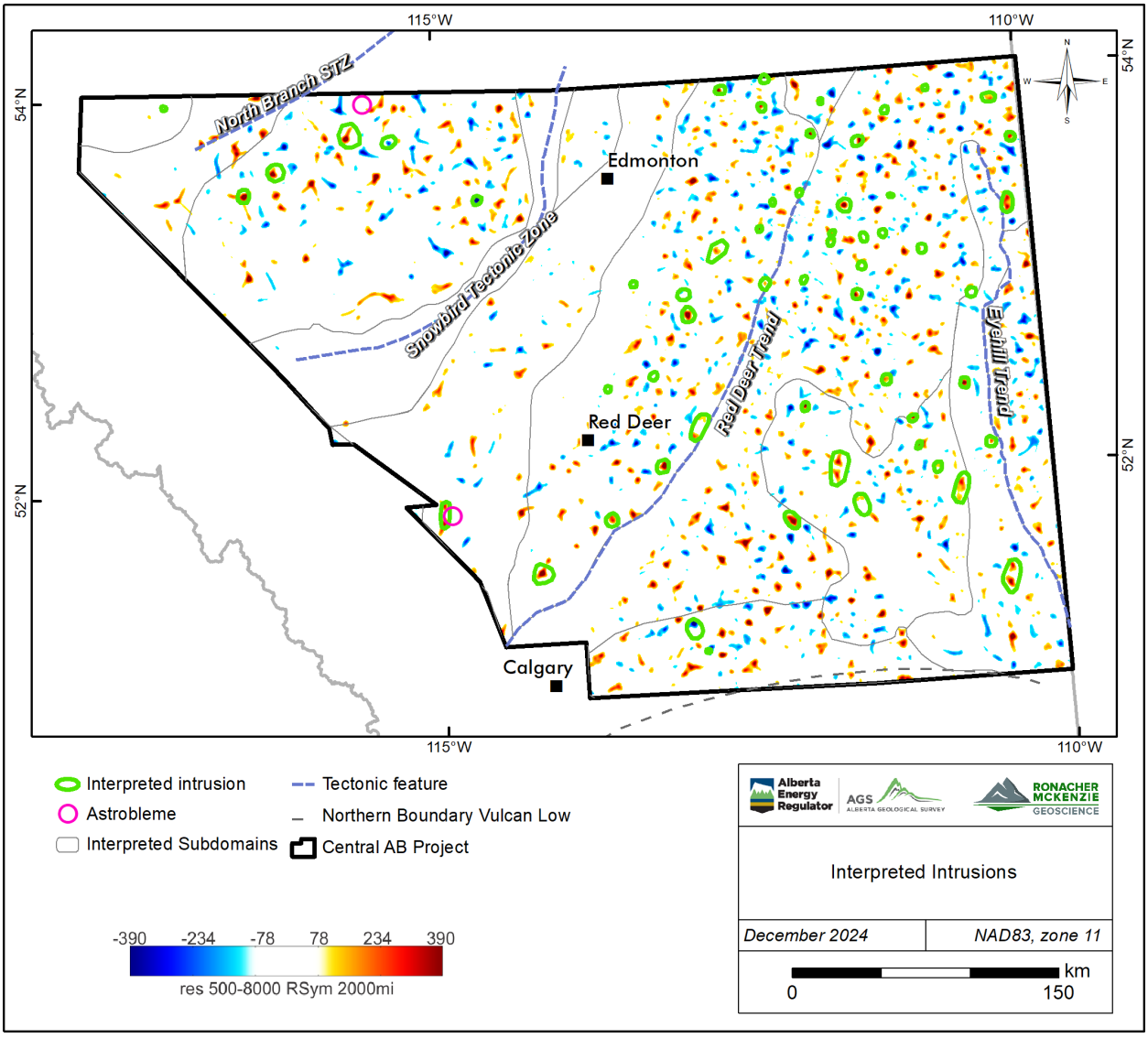

Figure 7-12. Intrusion detection results from Fathom Geophysics' automatic radial symmetry analyses for 2000 m magnitude independent wavelength (red represents rounded magnetic highs, blue represents rounded magnetic lows, and colour bar represents radial symmetry (i.e., how radially symmetric is a high or low).

The magnetic data does not show rounded features related to impact craters on the location of the Whitecourt and James River astroblemes. A broad magnetic high with an oblong shape occurs in the Cordilleran

deformation front near the interpreted James River astrobleme (Figure 7-12). However, this magnetic anomaly is most likely part of the regional magnetic fabric of Rimbey magmatic arc domain, which shows a similar trend and frequency of positive magnetic anomalies to the north.

8.0 CONCLUSIONS

The magnetic filter products and images as well as the automatic detection products derived from the 2024 airborne magnetic survey provide new insights into the basement in central Alberta and overlying sedimentary sequence. The geological interpretation involved a high-level integration with tectonic elements documented in publications.

Care was taken to recognise cultural artefacts (predominantly oil and gas infrastructure) during the interpretation stage.

The following conclusions can be made:

- Modifications to basement domains were made by editing the tectonic domain boundaries of Villeneuve et al. (1993), Ross et al. (1994) and Pilkington et al. (2000) and by dividing known domains into subdomains. The new, higher resolution magnetic data allows for further subdivision of domains in the crystalline basement based on variations of internal magnetic fabrics.
- Known ductile structures were recognized such as the Snowbird Tectonic Zone and Red Deer Trend, and new ductile structures were defined and characterized, such as the Eyehill Trend and northern extent of the Vulcan Low.
- The new magnetic data provide further insight and demonstrate relationships between basement features not identified before, and the location of preserved Ordovician strata and linear Devonian reef complexes.
- New brittle faults were delineated. Some faults of the WCSB reported in the literature show a spatial correlation with the interpreted lineaments.
- Basement anomalies were delineated. These range from small single lobe circular anomalies to larger multi-lobe rounded asymmetrical anomalies and may represent potential intrusions.

The integrated interpretation of the new magnetic data has identified several previously unrecognized features, including subdomains, shear zones, faults, fractures and intrusions underneath the WCSB of central Alberta that will influence future interpretations of the lithotectonic history of the basement. Local interpretations of the magnetic data are required to resolve remaining uncertainties in the geometry of basement structure and gain insights into the shallower structure. In addition, further integration with existing and new petrological, geochronological and rock property data, and integration with regional seismic and magnetotelluric data can improve the interpretation of the nature and architecture of the basement geology.

The interpretation of the new high-quality aeromagnetic data for central Alberta corroborated previous lithotectonic domains and tectonic features defined by previous authors, and identified new structural elements that may help to refine current tectonic models.

9.0 RECOMMENDATIONS

The higher quality of aeromagnetic data for central Alberta allows for further and more detailed interpretations of the basement geology and structure, paleo-topography, and influence on sedimentation patterns and structure in the overlying sedimentary sequence. The magnetic products generated for this work are abundant and suitable for local or case studies to resolve structural uncertainties and better understand both the basement and basin architecture by integrating with additional information available (e.g., seismic data, isopach studies, petrology, lithogeochemistry, geochronology). The following are recommendations to help with the interpretation and correlation with existing geological data:

- Conduct a structural interpretation of available Lidar data and integrate the results with the interpretation from the magnetic data. This is important for the foothills area, close to the deformation front or where the sedimentary cover is relatively thin. Several straight magnetic lineaments were observed near the Cordilleran deformation front, which suggests that they are close to the surface.
- Compile a database (or group of datasets) of basement sample data that integrates and standardizes analytical work from all previous studies, including sample descriptions, petrography, petrological studies, whole rock geochemistry, isotope studies, mineralogical studies, and publication citations. Currently, this information is available from published and unpublished tables created by various authors, which are either incomplete or require onerous standardization prior to use. Methodologies, labs or sources of data are not always listed and the user cannot evaluate the quality of the analytical results.
- Cross-correlation of magnetic products and seismic events (earthquakes) may help in the interpretation of natural and induced seismicity. Local studies are recommended to focus better on resolving the structure of a particular area.
- Reprocess historical gravity products and integrate the findings with the observations from the new magnetic data.
- Conducting additional, local 3D inversions of small regions or particular lineaments of interest can help resolve the 3D architecture of the area. In particular, a local inversion in the west of Central Alberta could better constrain the geometry of Wabamun-Thorsby and Thorsby-Rimbey boundaries, and the geometry of the Snowbird Tectonic Zone.
- Create mineral prospectivity maps by deposit type (not commodity) that use artificial intelligence algorithms (e.g., machine learning) and the mineral systems approach (favorable geodynamics, architecture, and fertility) to generate areas with potential of having generated and preserved mineral deposits.

10.0 REFERENCES

Alberta Geological Survey. 2021. *Geological Framework of Alberta, Version 3 (interactive app and map, methodology, model, dataset, StoryMaps, web maps).* ;Alberta Energy Regulator / Alberta Geological Survey, AER/AGS Interactive Application. <https://gfa-v3-ags-aer.hub.arcgis.com> [January 2025].

Alberta Geological Survey. 2024. *High quality regional airborne geophysical surveys in Alberta, version 3 (data, multiple formats); Alberta Energy Regulator / Alberta Geological Survey.*

Atkinson, L.A., S.M. Pawley, L.D. Andriashek, G.M.D. Hartman, D.J. Utting, and N. Atkinson. 2020. *Sediment thickness of Alberta, version 2 (gridded data, ASCII format).* AER/AGS Digital Data 2020-0023, Alberta Energy Regulator / Alberta Geological Survey.

Brem, A., G. Lopez, D. McGill, and J. McKenzie. 2024. *Airborne geophysics data analysis and Interpretation, southern Alberta.* Special Report 120, Alberta Energy Regulator / Alberta Geological Survey, AER/AGS, 106 p.

Burwash, R.A., J. Krupička, and J.R. Wijbrans. 2000. "Metamorphic evolution of the Precambrian basement of Alberta." *The Canadian Mineralogist* 38: p. 423–434.

Burwash, R.A., McGregor, C.R., Wilson, J.A. and O'Connell, S.C. 1994. "Chapter 5: Precambrian Basement." In *Geological Atlas of the Western Canada Sedimentary Basin*, by G.D. Mossop and I. Shetsen (comp.), p. 48-56. Canadian Society of Petroleum Geologists and Alberta Research Council. https://ags.aer.ca/atlas-the-western-canada-sedimentary-basin/chapter-5-precambrian-basement.

Burwash, R.A., T. Chacko, K. Muehlenbachs, and Y. Bouzidi. 2000. "Oxygen isotope systematics of the Precambrian basement of Alberta: implications for Paleoproterozoic and Phanerozoic tectonics in northwestern Alberta." *Canadian Journal of Earth Sciences* 37: p.1611-1628.

Eaton, D.W., B. Milkereit, G.M. Ross, E.R. Kanasewich, W. Geis, D.J. Edwards, L. Kelch, and J. Varsek. 1995. "Lithoprobe basin-scale profiling in central Alberta: influence of basement on the sedimentary cover." *Bulletin of Canadian Petroleum Geology* 43: p. 65-77.

Eaton, D.W., G.M. Ross, and J. Hope. 1999. "The rise and fall of a cratonic arch: a regional perspective on the Peace River Arch, Alberta." *Bulletin of Canadian Petroleum Geology* 47 (No. 4): p. 346–361.

Edwards, D .L, H. V. Lyatsky, and R. J. Brown. 1995. "Basement fault control on Phanerozoic stratigraphy in the Western Canada." In *in LITHOPROBE Alberta Basement Transects: Report of Transect Workshop, Calgary, April 10–11, 1995, (ed.) G.M. Ross, LITHOPROBE Secretariat, University of British Columbia,* , LITHOPROBE Report 47, p. 181–244.

Edwards, D.J., and J.R. Brown. 1999. "Understanding the influence of Precambrian crystalline basement on Upper Devonian carbonates in central Alberta from a geophysical perspective." *Bulletin of Canadian Petroleum Geology, v. 47, 4,* p. 412-438.

Edwards, D.J., and R. Brown. 1999. "Understanding the influence of Precambrian crystalline basement on Upper Devonian carbonates in central Alberta from a geophysical perspective." *Bulletin of Canadian Petroleum Geology, v. 47, 4, p. 412-438.*

Edwards, D.J., H.V. Lyatsky, and R.J. Broten. 1998. "Regional interpretation of steep faults in the Alberta Basin from public-domain gravity andmagnetic data: an update." *CSEG Recorder* 23, No.1.

Hanmer, S., M. Williams, and S. Kopf. 1995. "Striding-Athabasca mylonite zone: implications for the Archean and Early Proterozoic tectonics of the Western Canadian Shield." *Canadian Journal of Earth Sciences, v. 32,* p. 178–196.

Hauck, T.E. 2020. "The Elk Point Group of Alberta: insights into paleogeography, evaporite karstification, and salt cavern potential based on net-evaporite mapping." Alberta Energy Regulator /Alberta Geological Survey, AER/AGS Report 99, 60 p.

Hayes, B.J.R., J.E. Christopher, L. Rosenthal, B. McKercher, D. Minken, Y.M. Tremblay, and J. Fennell. 1994. "Cretaceous Mannville Group of the Western Canada Sedimentary Basin." in Geological atlas of the Western Canada Sedimentary Basin, G.D. Mossop and I. Shetsen (comp.), Canadian Society of Petroleum Geologists and Alberta Research Council, p. 317–334. URL <https://ags.aer.ca/publications/atlas-western-canada-sedimentary-basin> [January 2025].

Hoffman, P.F. 1989. "Precambrian geology and tectonic history of North America; in The geology of North America–an overview." *A.W. Bally and A.R. Palmer (ed.), Geological Society of America v. A,* p. 447–512.

Hoffman, P.F. 1988. "United plates of America, the birth of a craton, Early Proterozoic assembly and growth of Laurentia." *Annual Review of Earth and Planetary Science Letters* 16: p. 543–603.

Hope, J., and D. Eaton. 2002. "Crustal structure beneath the Western Canada Sedimentary Basin: constraints from gravity and magnetic modelling." Canadian Journal of Earth Sciences, v. 39, p. 291– 312.

Hope, J., D.W. Eaton, and G.M. Ross. 1999. "Lithoprobe seismic transect of the Alberta Basin: Compilation and overview." *Bulletin of Canadian Petroleum Geology* 47, No. 4: p. 331-345.

Isaac, J.H., and R.R. Stewart. 1993. "3-D seismic expression of a cryptoexplosion structure." *Canadian Journal of Exploration Geophysicists,* 29, No. 2: p. 429-439.

Isles, D. J., and L. R. Rankin. 2013. *Geological interpretation of aeromagnetic data.* Australian Society of Exploration Geophysicists, 365 p.

Kovesi, P. 2015. *Good Colour Maps: How to Design Them (colorcet.com).* Accompanying Document, Crawley, Western Australia: Centre for Exploration Targeting, The University of Western Australia. (https://colorcet.com/).

Lewry, J.F., and K.D. Collerson. 1990. "Trans-Hudson Orogen: extent, subdivision, and problems; in The Early Proterozoic Trans- Hudson Orogen of North America." *J.F. Lewry and M.R. Stauffer (ed.), Geological Association of Canada, Special Publication Paper 37,* p. 1–14.

Lopez, G., D. McGill, and J. McKenzie. 2024a. *Airborne geophysics data analysis and interpretation, Canadian Shield, northeastern Alberta.* Special Report 119, Alberta Energy Regulator / Alberta Geological Survey, AER/AGS, 111 p.

Lopez, G.P., A. Brem, D. McGill, and J. McKenzie. 2024b. *Airborne geophysics data analysis and interpretation, northern Alberta.* Special Report 122, Alberta Energy Regulator / Alberta Geological Survey, AER/AGS, 153 p.

Lopez, G.P., J.G. Pawlowicz, J.A. Weiss, and G.M. Jean. 2020. *Metallic Mineral Occurrences of Alberta (tabular data, tab-delimited format).* AER/AGS Digital Data 2019-0026., Alberta Energy Regulator / Alberta Geological Survey.

Lyatsky, H.V., D.I. Pană, and M. Grobe. 2005. "Basement structure in central and southern Alberta; insights from gravity and magnetic maps." Alberta Energies and Utilities Board/Alberta Geological Survey, Special Report 72, 83 p.

Mazur, M.J. 1999. "Seismic characterization of meteorite impact craters." M.Sc. Thesis, University of Calgary, 176 p.

McGill, D., and L. Vargas. 2024. "QA QC report: South-Central Alberta 2024 Aeromagnetic Data." Internal report prepared for the Alberta Geological Survey / Alberta Energy Regulator, 18 p.

McKenzie, J., E. Ronacher, and F. Farahani. 2021. "Interpretation of Geophysical Data, Alberta Geological Survey: He and Li project." Alberta Energy Regulator/ Alberta Geological Survey, AER/AGS Special Report 114, 36 p.

Misra, K.S., V.R. Slaney, D. Graham, and J. Harris. 1991. "Mapping of basement and other tectonic features using SEASAT and Thematic Mapper in hydrocarbon-producing areas of the Western Sedimentary Basin of Canada." *Canadian Journal of Remote Sensing v. 17, 2,* p.137-151.

Mossop, G.D., and I. Shetsen. 1994. "Geological Atlas of the Western Canada Sedimentary Basin." *Alberta Geological Survey.* Canadian Society of Petroleum Geologists and Alberta Research Council. Accessed October 30, 2023. https://ags.aer.ca/reports/atlas-western-canada-sedimentary-basin.

Norford, B.S., F.M. Haidl, R.K. Bezys, M.P. Cecile, H.R. McCabe, and D.F. Paterson. 1994. "Chapter 9 - Middle Ordovician to Lower Devonian Strata of the Western Canada Sedimentary Basin." In *Geological Atlas*

of the Western Canada Sedimentary Basin, G.D. Mossop and I. Shetsen (comp.). Canadian Society of Petroleum Geologists and Alberta Research Council, URL https://ags.aer.ca/publications/atlas-western-canada-sedimentary-basin/chapters/chapter-9-middle-ordovician-lower [November 2024].

O'Connell, S.C. 1994. "Geological history of the Peace River Arch." In *Geological Atlas of the Western Canada Sedimentary Basin, G.D. Mossop and I. Shetsen (comp.)*. Canadian Society of Petroleum Geologists and Alberta Research Council, URL https://ags.aer.ca/publications/atlas-the-western-canada-sedimentary-basin/chapter-28-geological-history-the-peace-river-arch , [November 2024].

Pană, D.I., and E. J. Waters. 2016. *GIS compilation of structural elements in Alberta, version 3.0 (GIS data, line features).* Digital Data 2003-0012, Alberta Energy Regulator/Alberta Geological Survey.

Pană, D.I., and R. Elgr. 2013. *Geology of the Alberta Rocky Mountains and Foothills.* Map 560, Alberta Energy Regulator / Alberta Geological Survey.

Pană, D.I., R. Elgr, E.J. Waters, J.A. Warren, G.P. Lopez, and J.G. Pawlowicz. 2021. "Structural elements in the Alberta Plains." Alberta Energy Regulator/Alberta Geological Survey, AER/AGS Open File Report 2021-01, 33 p.

Pană, D.I., Waters, J., and Grobe, M. 2001. "GIS compilation of structural elements in northern Alberta, release 1.0." Alberta Energy and Utilities Board, EUB/AGS Earth Sciences Report 2001-01, 60 p.

Peterson, J.T., and K.E. MacCormack. 2014. *Paleotopography of the sub-Cretaceous unconformity surface, west-central Alberta.* Alberta Energy Regulator, AER/AGS Map 573. URL <https://ags.aer.ca/publications/MAP_573.html> [January 2025].

Pilkington, M., W.F. Miles, G.M. Ross, and W.R. Roest. 2000. "Potential-field signatures of buried Precambrian basement in the Western Canada Sedimentary Basin." *Canadian Journal of Earth Sciences* 37: p. 1453-1471.

Prior, G.J., B. Hathaway, P. Glombick, D.I. Pană, C.J. Banks, D.C. Hay, C.L. Schneider, M. Grobe, R. Elgr, and J.A. Weiss. 2013. "Bedrock geology of Alberta." Alberta Energy Regulator / Alberta Geological Survey, AER/AGS Map 600.

Ross, G.M. 2002. "Evolution of Precambrian continental lithosphere in Western Canada: results from LITHOPROBE studies in Alberta and beyond ." *Canadian Journal of Earth Sciences, v. 39,* p. 413–437.

Ross, G.M., and D.W. Eaton. 2002. "Proterozoic tectonic accretion and growth of western Laurentia: results from Lithoprobe studies in northern Alberta." *Canadian Journal of Earth Sciences* 39: p. 313-329.

Ross, G.M., B. Milkereit, D Eaton, White, D., E.R. Kanasewich, and M.J.A. and Burianyk. 1995. "Paleoproterozoic collisional orogen beneath the western Canada sedimentary basin imaged by Lithoprobe crustal seismic-reflection data." *Geology* 23: p. 195-199.

Ross, G.M., J. Broome, and W. Miles. 1994. "Chapter 4: Potential fields and basement structure." In *Geological Atlas of the Western Canada Sedimentary Basin*, by G.D. Mossop and I. Shetsen (comp.), p. 41–47. Canadian Society of Petroleum Geologists and Alberta Research Council.

Ross, G.M., R.R. Parrish, M. E. Villeneuve, and S.A. Bowring. 1989. "Tectonic subdivision and U-Pb geochronology of the crystalline basement of the Alberta Basin, western Canada; Geological Survey of Canada." Open File 2103.

Ross, G.M., R.R. Parrish, M.E. Villeneuve, and S.A. Bowring. 1991. "Geophysics and geochronology of the crystalline basement of the Alberta Basin, western Canada." *Canadian Journal of Earth Sciences* 28: p. 512–522.

Villeneuve, M.E., G.M. Ross, R.J. Thériault, W. Miles, R.R. Parrish, and J. Broome. 1993. "Tectonic subdivision and U-Pb geochronology of the crystalline basement of the Alberta Basin, western Canada." Geological Survey of Canada Bulletin 447, 95 p.

Wadsworth, J., R. Blyd, C. Diessel, D. Leckie, and B.A. Zaitlin. 2002. "Stratigraphic style of coal and non-marine strata in a tectonically influenced intermediate accommodation setting: the Mannville Group of the Western Canadian Sedimentary Basin, south-central Alberta." *Bulletin of Canadian Petroleum Geology, v. 50,* p. 507-541.

Appendix 1 – Automatic detection - Fathom Geophysics Report

Processing of the Alberta Merged magnetic survey for Ronacher McKenzie Geoscience

January 2025

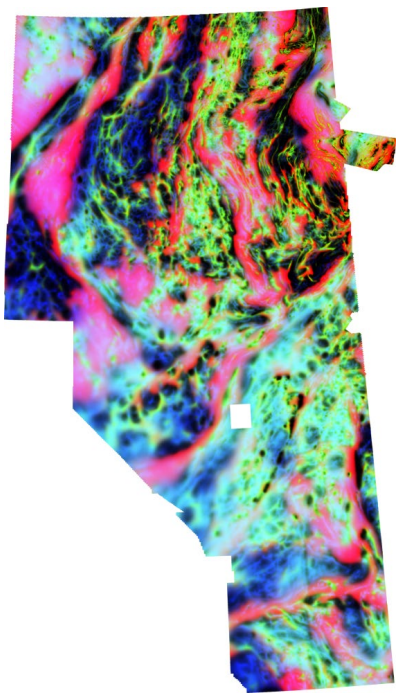

by Dan Core†, Eric Core, and Lisa Lombardi
Fathom Geophysics

†Corresponding author: dan@fathomgeophysics.com

Introduction

The location of the project area is shown in **Figure 1**. The goal of this work is to filter the magnetic dataset over the area to highlight structural features, lithologies, and possible intrusive rocks.

Most of the processing has been applied to a merged grid as indicated by the blue outline on **Figure 1**. The red outline indicates the magnetic survey for Central Alberta. It was processed on its own for the depth-to-source calculation.

The merged grid was provided to Fathom Geophysics by Ronacher-McKenzie Geoscience. The surveys incorporated into the merged grid are the Shield, Southern Alberta, Northern Alberta, and Central Alberta grids. All of these except Central Alberta have been processed individually as part of other projects.

The Central Alberta magnetic data are from a survey flown in 2023 and 2024 by EON Geosciences Inc on behalf of the Alberta Energy Regulator. Gridded data provided with the survey were good quality with some relatively minor cultural artifacts in the western part of the dataset**.** Survey data have 800m line-spacing. All gridded products use a cell size of 200m.

The merged grid also has a grid cell size of 200m (**Figure 2**). This is the native resolution of all the datasets except the Shield dataset. It was down-sampled when it was stitched with the other data.

The merged and Central Alberta grids were supplied to us with coordinates in WGS84 UTM Zone 11N. This coordinate system was used for all our outputs.

The processing completed includes differential reduction to the pole, application of a suite of standard filters and application of Fathom Geophysics' structure detection and radial symmetry filters to the Merged Alberta dataset. Depth-to-source processing was applied to the Central Alberta dataset.

Processing summary — Magnetic data

Differential reduction to the pole

RTP processing produces a magnetic field that is equivalent to what would be generated if the data were collected at the magnetic north pole. This shifts magnetic highs to be directly over their sources and creates symmetric anomalies over the top of symmetric magnetic sources.

We applied a differential RTP (DRTP) filter for this project. The filter uses the appropriate inclination and declination at each point in the project area as apposed to using the mean RTP parameters like a standard RTP would.

The DRTP filter for these data has a median inclination of 76.0° and a median declination of 14.4° (**Figure 3**).

Note that in general RTP processing is not valid for remanent bodies unless the remanence is directly opposed to the present-day field. The dataset almost certainly contains some remanent bodies that will not be corrected properly using the RTP filter. However, it is worthwhile applying the filter because most of the anomalies in the area are normally magnetized or reversely magnetized with relatively few anomalies possessing an apparent magnetization direction at a high angle to the present-day field.

Magnetic standard filtering

The RTP grid was filtered with a suite of standard geophysical filters including the analytic signal and vertical derivative. These grids were imaged using our in-house software to produce shaded images with the sunlight coming from the northwest (NW in the filename) and northeast (NE in the filename). Unshaded images were also produced so that the geographic location of pertinent features in the data can be readily defined (because shaded images can ‘fool the eye’ in this respect).

Figures 4 to 22 show images of most of the standard filtering results supplied. Standard filtering results have been included in this report because of their capacity to help the reader who might be new to the delivered processing results files to quickly grasp the project area’s overall magnetic susceptibility changes/contrasts.

Processing summary — Magnetic data (continued)

Magnetic total structure detection

Structure detection was applied to highlight edges in the RTP magnetic data and the AGC of the RTP data. Edges in potential field data are locales that are more likely to be faults, contacts or other structures. The structure detection algorithm and processing are described in more detail in **Appendix 1**.

Representative images of the total structure detection filtering are shown in **Figure 23** and **Figure 26**. Further results files were delivered in addition to those visualized within this report, and we urge the reader to explore the entire series of results files to ensure full familiarity with the results of total structure detection processing and their possible exploration ramifications.

Total-structure detection filtering was applied to the RTP grid at minimum wavelengths of 250m, 500m, 1000m, 2000m, 4000m, and 8000m. Structure intersection images were supplied alongside structure images.

This filtering was also applied to the AGC grid at minimum wavelengths of 250m, 500m, 1000m, 2000m, 4000m, and 8000m. Structure intersection images were supplied alongside structure images.

The results show that different orientations of structure are dominant in different parts of the area. The N has dominantly N-S features with ENE being the most prominent cross structure orientation. A relatively sharp break separates this fabric from the NE-trending fabric in the central part of the area. The central cross structures are mainly W to NW-trending.

The south has a less pronounced dominant structural orientation. The major structural orientation in the far south appear to be NW to NNW-trending. These structures end at an ENE-trending break in the data. North of this break, the NE-trending fabric of the central area begins.

Processing summary — Magnetic data (continued)

Magnetic belt-parallel and belt-crossing structure detection

In many heavily deformed belts, the fabric-parallel and fabric-crossing structures can be different structure types and may have different timing. The fabric-parallel features tend to be contacts or belt-parallel shear zones. The cross structures are usually not contacts and are more likely to be faults. Any sense of motion is possible on the cross structures. If clear lateral offset of the units is present, the faults are likely strike-slip faults. Normal and reverse faults are often represented by a change in amplitude or frequency content of the magnetic data.

The first step in extracting fabric-parallel and fabric-crossing structures is to extract the fabric orientation. The AGC was used for determining the fabric orientation because it was better at delineating the different structural domains than the RTP did (**Figure 27**).

The results show several domains in the area with different orientations. Most of the far north is dominated by a NNE trend. This orientation bends around to a NNW trend to the south. In the central part of the area, there is an abrupt change to a NE trend. The far south of the dataset is complex and shows several different orientations.

Representative images of the results of parallel and cross structure detection are shown in **Figures 28 to 31**. Further results files were delivered in addition to those visualized within this report, and we urge the reader to explore the entire series of results files to ensure full familiarity with the results of belt-parallel and belt-crossing structure detection processing and their possible exploration ramifications.

The fabric parallel features highlighted by this method are typically either lithological contacts or fabric-parallel shear zones. The AGC results appear to be very good for highlighting lithological boundaries. The RTP results are better for highlighting longer-wavelength features and those are more likely to be major faults.

The fabric-crossing features are more likely to be faults than the fabric-parallel features, but they are also more affected by noise in the data. The most reliable results will come from moderate to long-wavelength results on the RTP data.

It can often be useful to display relatively high-frequency fabric-parallel features with lower-frequency fabric-crossing features. This can be done using the vector outputs for each product.

Processing summary — Magnetic data (continued)

Magnetic radial symmetry

The radial symmetry detection filter can highlight discrete, equant magnetic features with different radii. Radial symmetry detection was completed on the RTP data. The radial symmetry algorithm is described in greater detail in **Appendix 2** of this report.

Representative images of the radial symmetry results are shown in **Figure 32**. Further results files were delivered in addition to those visualized within this report, and we urge the reader to explore the entire series of results files to ensure full familiarity with the results of radial symmetry analysis processing and their possible exploration ramifications.

When applied to the RTP grid, radial symmetry detection processing was applied in magnitude-independent mode at minimum-radius runs of 1000m, 2000m, 4000m, 8000m, and 16000m. Radii greater than these did not appear to be useful on this particular data grid. Both magnetic highs and magnetic lows represent meaningful/useable results and therefore are presented in images.

The radial symmetry results show high-frequency features concentrated in the NE of the area. This is to be expected as that area has less cover, so more high-frequency information is in the data.

The moderate frequencies show a large concentration of features in the north with a gap in the middle of the dataset in an area dominated by very linear features. The south has a significant number of moderate wavelength features as well.

The long-wavelength features are roughly evenly distributed throughout the area. These features have the most uncertainty as far as whether they are intrusions. The causative bodies for the anomalies could be quite deep making ground truthing difficult even if there was outcrop present.

Processing summary — Magnetic data (continued)

Depth to magnetic source

Many algorithms can be used to estimate the depth to magnetic sources. Most are based on at least second order derivatives making them significantly influenced by any kind of noise in the data. This dataset presents some significant challenges for these algorithms due to high frequency noise that occurs where cultural features are present in the data. These features are mostly due to oil and gas infrastructure in the area. While the airborne contractor took steps to mitigate the noise caused by these features, the effects were not completely removed. These features are most abundant in the western part of the dataset.

In order to smooth out these features, a localized Gaussian filter was applied only where the high-frequency noise was a problem. This had to be done rather than using a global filter because a global filter would have smoothed out real detail in the east.

The method that was used for the depth to source is that of Cooper (2014). It involves looking at the derivative of the tilt angle to estimate the depth of contacts in the dataset. The resulting depths were then interpolated to generate a continuous distance to magnetic source grid. The average altitude of the aircraft was subtracted off to generate a depth to magnetic basement grid.

The results of the depth to magnetic source processing are shown in **Figure 45**. The smoother parts of the dataset show greater depth to source as is expected. The results show that the basement surface gets deeper to the west and shallower in the east. The basement does not appear to be exposed anywhere.

The average depths observed in the depth to source processing are similar to those observed in wells that have pierced the basement in parts of the area. The correlation between the well depths and the calculated basement depths are reasonably good indicating that the depth to source appears to be a good estimate. The results correlate well with depth to source completed on the Alberta North grid but have significant mismatches with the results for the Alberta South grid. The Alberta South results are probably incorrect due to insufficient suppression of cultural noise. That dataset could be revisited to improve the results.

The depth to magnetic source grid was subtracted from the topography data to generate a top of magnetic basement surface (**Figure 46**)**.** The magnetic basement surface looks almost like an inverse of the depth to source grid. This is expected given the relatively small amount of topographic variation in much of the area.

**Cooper (2014) The automatic determination of the location, depth, and dip of contacts from aeromagnetic data. Geophysics, v79, pp J35-J41. https://library.seg.org/doi/10.1190/geo2013-0181.1*

File formats and image types delivered

The grids for this work have been delivered in ER Mapper ERS format. All images have been provided in GeoTIFF format with associated MapInfo TAB files and ESRI world files. Vectors have been delivered in ESRI shapefile format.

Structure detection results have been supplied as grids, images (GeoTIFF), and polylines (vectorization of the gridded results). The polylines have been attributed with the values from the structure detection grid and the orientation of the structure calculated based on the vectorized result.

Structure images were made in an unshaded fashion using a warm color bar (yellows through to reds) and a linear color stretch. Dominant orientation images use a wraparound colorbar palette that produces the same color for 0 and 180 with a rainbow distribution for colors in between. Those orientation images that have been thresholded display only significant features and are white in locales that essentially lack structure.

Radial symmetry ‘lows and highs’ images were made using a blue-and-red color bar possessing no intermediate colors. Highs-only images use the red side of that same color bar, and lows-only images use the blue side.

Several ternary images were also created for this work. These images are generated using three separate grids to represent the red-green-blue (RGB) or cyan-magenta-yellow (CMY) channels of the output image. RGB ternary images involve color addition, analogous to how different-colored light beams combine on a performance stage. When all three channels are present in full strength, pure white is the result. (Pure black indicates all three channels are absent.) CMY ternary images involve color subtraction, similar to colors resulting from the mixing of paint pigments. When all three channels are present in full strength, pure black is the result. (Pure white indicates all three channels are absent.) **Figure 17** explains in more detail how to interpret the full gamut of colors that can turn up in ternary images.

See also the list of abbreviations and acronyms supplied in this report to help decode the information contained within a given grid/image filename.

List of acronyms and abbreviations

agc	automatic gain control (appears in delivered file names)
Agc20	AGC when standard deviation=20 (in file names)
Alberta	Project area (appears in file names)
asig	analytic signal (appears in delivered file names)
colorbar	numerical values associated with image's color range (in file names)
CMY	cyan-magenta-yellow ternary (appears in delivered file names)
gray, grayscale	grayscale image (appears in delivered file names)
hgm	horizontal gradient magnitude (appears in delivered file names)
Highs	positive anomalies-only radial symmetry image (in file names)
HSI	hue, saturation and intensity (appears in delivered file names)
HTh	hysteresis thresholding was used during vectorization (in file names)
Int	structural intersections image (appears in delivered file names)
LgeRes	large-scale residual (appears in delivered file names)
lin	linear-stretch image (appears in delivered file names)
Lows	negative anomalies-only radial symmetry image (in file names)
LowsAndHighs	negative and positive anomalies radial symmetry image (in file names)
md	magnitude dependent radial symmetry result (in file names)
MedRes	medium-scale residual (appears in delivered file names)
mi	magnitude independent radial symmetry result (in file names)
OriDom	dominant orientation image (appears in delivered file names)
Pgrav	pseudogravity (appears in delivered file names)
PgravRes	residual of pseudogravity (appears in delivered file names)
PgravResHGM	HGM of residual of pseudogravity (appears in delivered file names)
res	residual (appears in delivered file names)
res25_100	25m-100m residual (appears in delivered file names)
RGB	red-green-blue ternary (appears in delivered file names)
RMI	residual magnetic intensity (appears in delivered file names)
RSym	radial symmetry image (appears in delivered file names)
RSym100	100m minimum radius radial symmetry image (in file names)
RTP	reduced-to-pole (appears in delivered file names)
SmRes	small-scale residual (appears in delivered file names)
Struct	structure image (appears in delivered file names)
Struct100	100m minimum wavelength structure image (in file names)
tern, ternary	ternary image (appears in delivered file names)
Thresh, thr, Th	image made via thresholding (appears in delivered file names)

List of acronyms and abbreviations (continued)

tilt	tilt angle (appears in delivered file names)
TMI	total magnetic intensity (appears in delivered file names)
Total	total structure image (appears in delivered file names)
vd	vertical derivative (a.k.a. 1VD) (appears in delivered file names)
vdmhgm	vertical derivative minus HGM (appears in delivered file names)
Vec	vectorized results file (appears in delivered file names)
Vert, V	shaded image where ‘sun’ is directly overhead (in file names)
vias	analytic signal of vertical integral (appears in delivered file names)
vint	vertical integral (appears in delivered file names)
X	directional derivative along X axis (appears in delivered file names)
Y	directional derivative along Y axis (appears in delivered file names)
Z	directional derivative along Z axis (i.e., vertical derivative) (in file names)

Project location map

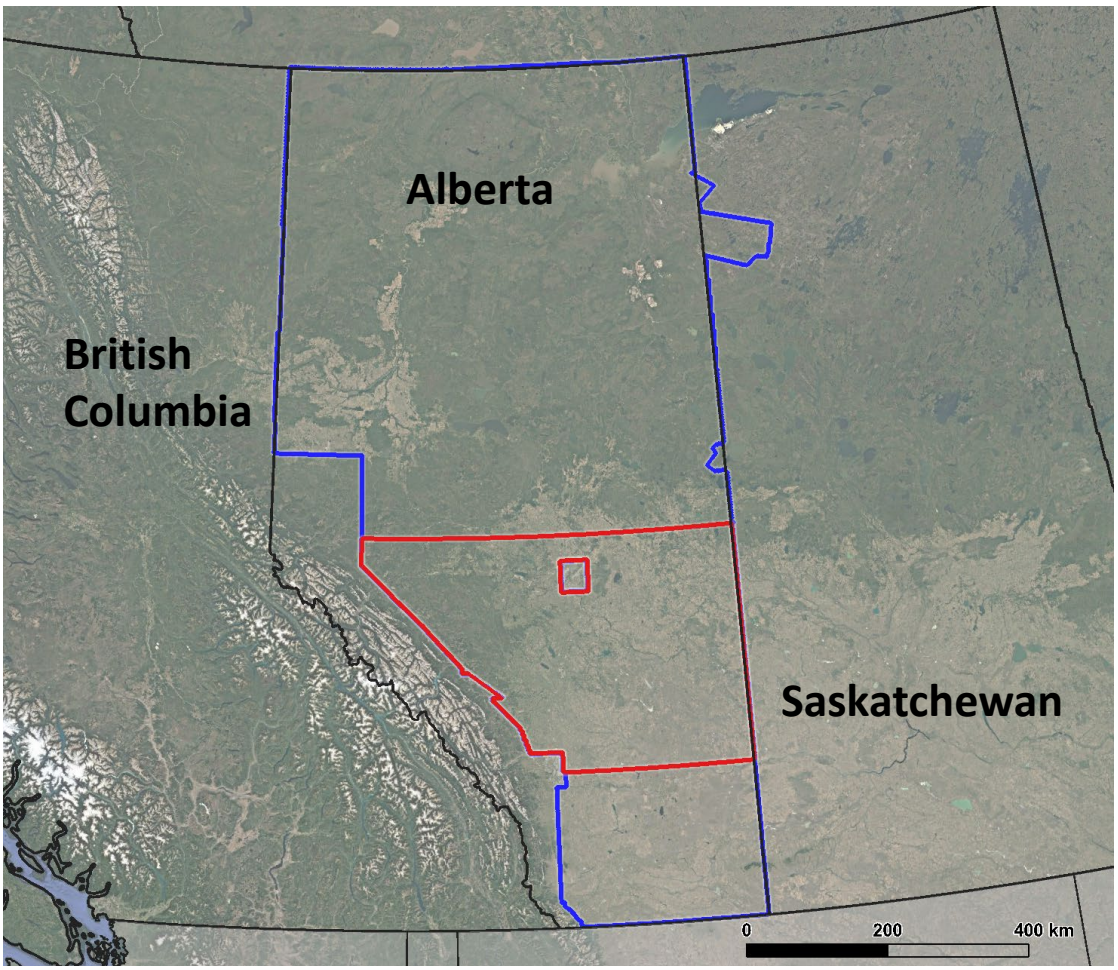

Figure 1: Location map for this project. The blue polygon indicates the outline of the merged Alberta magnetic dataset. The red polygon indicates the outline of the Central Alberta magnetic dataset.

Magnetic data-processing results images
▶ Total magnetic intensity (TMI)

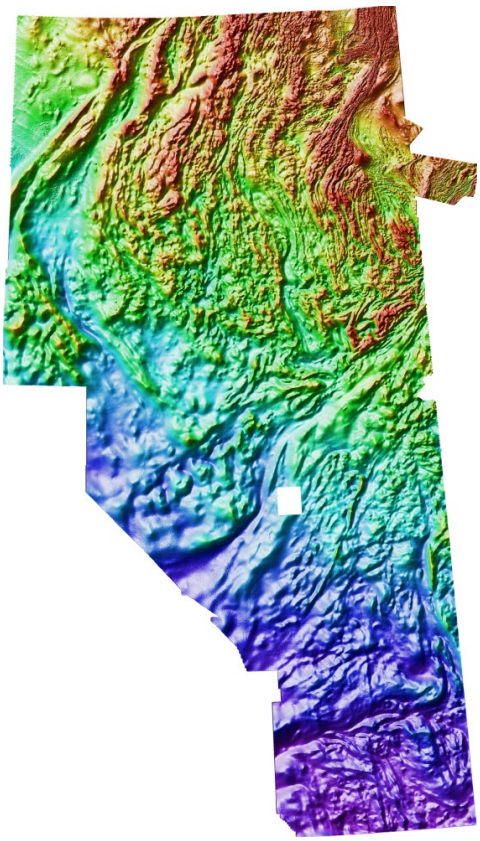

Alberta_TMIfinal_HSI_NW

Figure 2: Total magnetic intensity data for the project area. The indicative colorbar shown applies to all magnetic data-processing results images involving the HSI (hue, saturation, intensity) color display system.

Magnetic data-processing results images
▶ Reduction-to-pole (RTP)

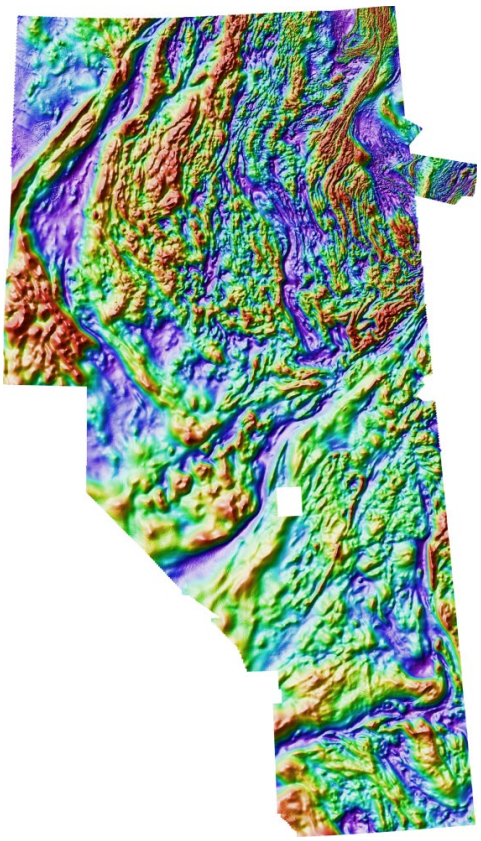

Alberta_RMIfinal_DRTP_HSI_NW

Figure 3: Reduced-to-the-pole magnetic data for the project area. The RTP filter attempts to produce the magnetic field that would be expected if the data were collected at the magnetic pole.

Magnetic data-processing results images (continued)
▶ Standard filtering — First vertical derivative

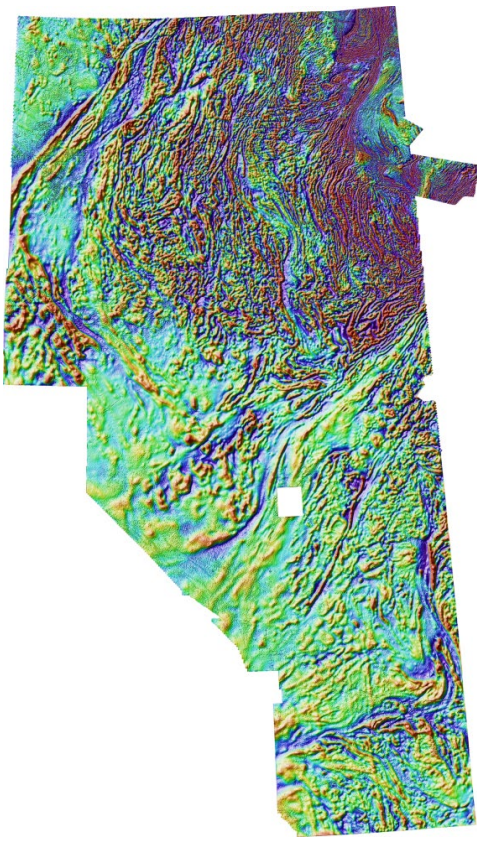

Alberta_RMIfinal_DRTP_vd_HSI_NW

Figure 4: The first vertical derivative (1VD) transform is the rate of change of the potential field in the vertical direction. Application of this filter has the effect of accentuating the shorter wavelength (higher frequency) components at the expense of longer wavelength (more regional) features.

Magnetic data-processing results images (continued)
▶ Standard filtering — Horizontal gradient magnitude

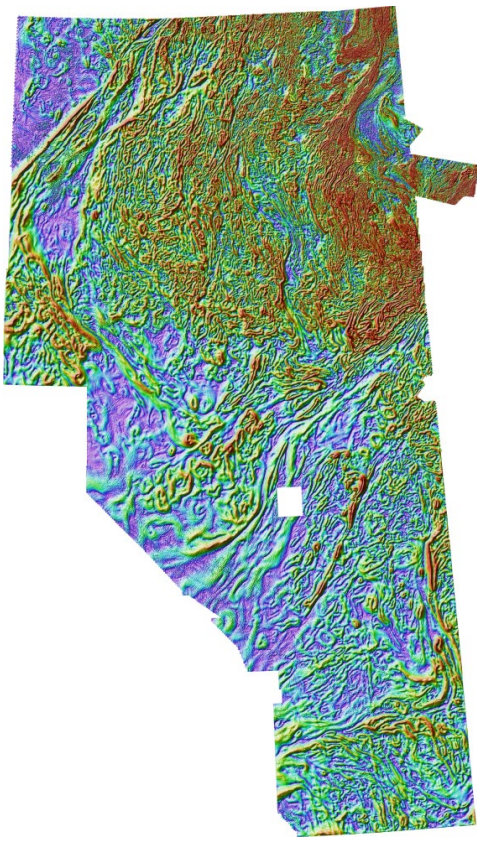

Alberta_RMIfinal_DRTP_hgm_HSI_NW

Figure 5: The horizontal gradient magnitude is calculated from the x- and y-derivatives of the data ($\sqrt{dx^2 + dy^2}$). This filter highlights the location of steep gradients in the data. Peaks in the HGM should occur at susceptibility contrasts in magnetic data and density contrasts in gravity data. These are likely to be locations of faults or contacts. Peaks will be offset in the down-dip direction for dipping bodies. The results are affected by remanent magnetization.

Magnetic data-processing results images (continued)
▶ Standard filtering — Vertical derivative minus HGM

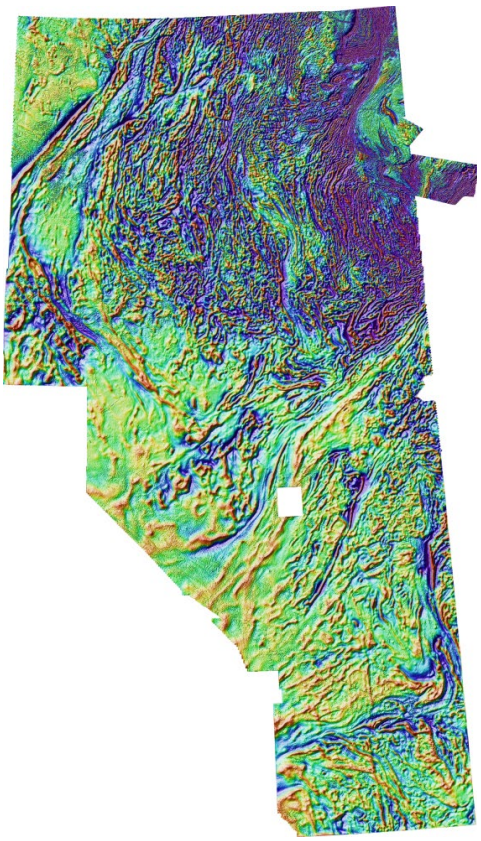

Alberta_RMIfinal_DRTP_vdmhgm_HSI_NW

Figure 6: The vertical derivative minus the HGM (VDMHGM) is a filter that accentuates the contrast in the first vertical derivative. This is useful for highlighting shallow sources in potential field data. It can also be useful when trying to pick the exact location to place a narrow magnetic unit or a narrow dense unit.

Magnetic data-processing results images (continued)

▶ Standard filtering — Tilt angle

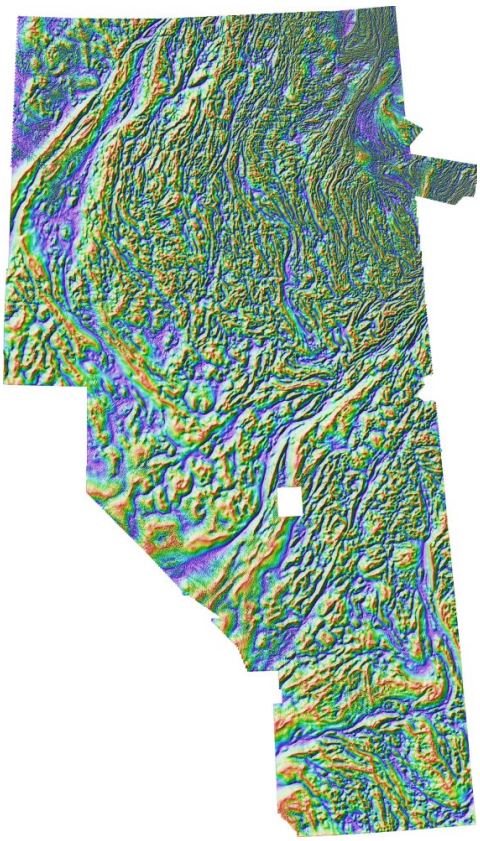

Alberta_RMIfinal_DRTP_tilt_HSI_NW

Figure 7: The tilt angle filter is the arctangent of the ratio of the vertical derivative to the horizontal gradient magnitude. This filter removes information about the amplitude of the signal, making the heights of peaks the same regardless of the susceptibility or density of the causative body. Structure and depth information are preserved. This makes it easier to see subtle features and some structures.

Magnetic data-processing results images (continued)
▶ Standard filtering — Analytic signal

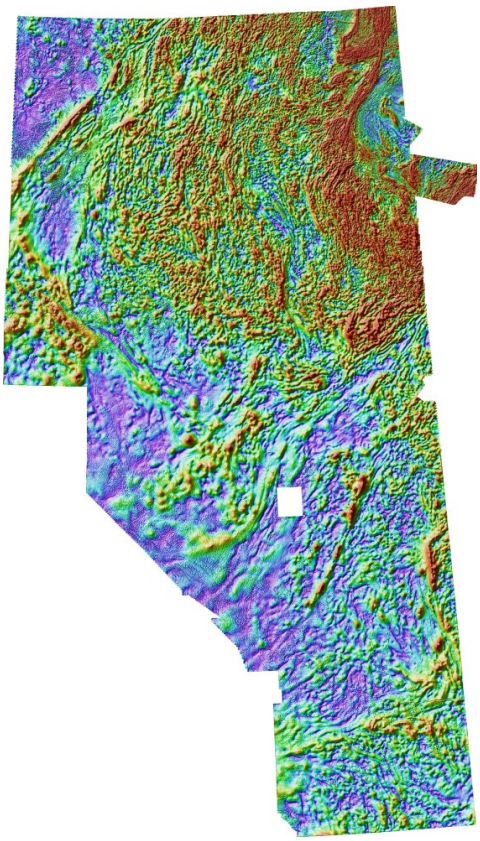

Alberta_RMIfinal_DRTP_asig_HSI_NW

Figure 8: Analytic signal of the RTP data. The analytic signal (also known as the total gradient magnitude) is calculated as $\sqrt{dx^2 + dy^2 + dz^2}$. This filter highlights the location of rapid changes in the data. Highs in the analytic signal correspond to high amplitudes in the vertical derivative (positive or negative) or high amplitudes in the horizontal gradient magnitude. Highs will occur over the top of small bodies with high susceptibility or high density contrast or at the edge of large-scale susceptibility or density contrast. Long-wavelength features are suppressed by this filter since it is based on derivative filters. This filter is relatively independent of magnetization direction and remanent magnetization.

Magnetic data-processing results images (continued)
▶ Standard filtering — Analytic signal of vertical integral

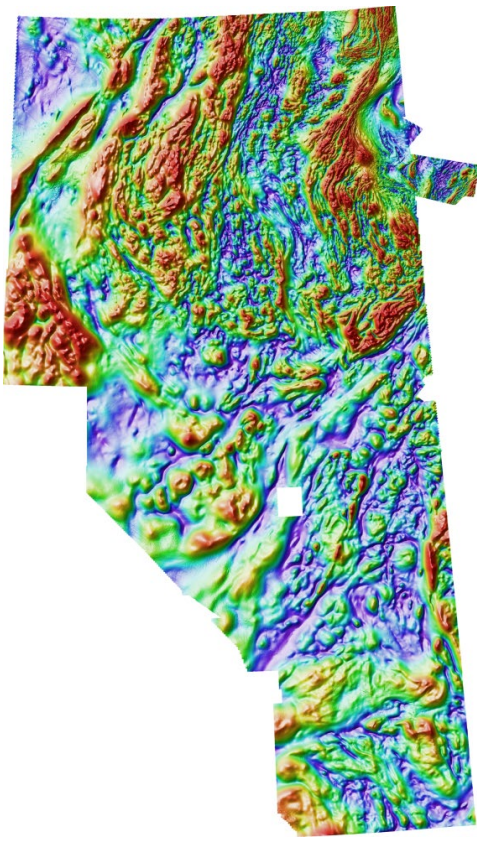

Alberta_RMIfinal_DRTP_vias_HSI_NW

Figure 9: The analytic signal filter was applied to the vertical integral of the magnetic data to produce this VIAS result. The analytic signal filter is described in the caption of **Figure 8**. Produces a grid with wavelength and amplitude characteristics that are similar to the RTP grid, but with reduced effects of remanent magnetization and magnetization direction.

Magnetic data-processing results images (continued)
▶ Standard filtering — Automatic gain control

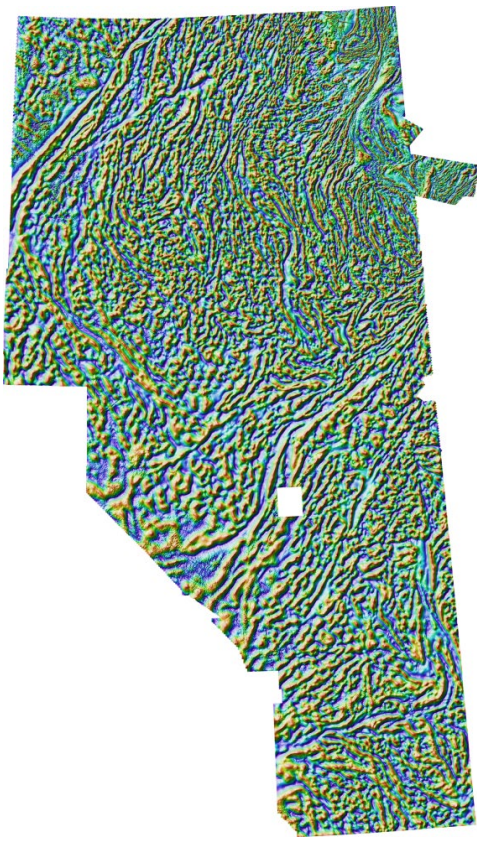

Alberta_RMIfinal_DRTP_AGC20_HSI_NW

Figure 10: The automatic gain control filter (AGC) is a means of evening out the amplitudes of anomalies. This makes more subtle features in the data visible. The filter also acts as a high-pass filter by suppressing the longer wavelengths.

Magnetic data-processing results images (continued)
▶ Standard filtering — Small-scale residual

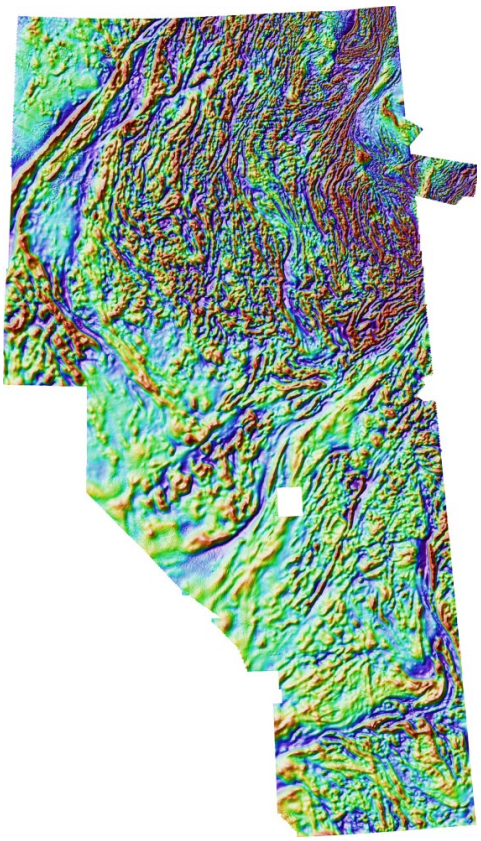

Alberta_RMIfinal_DRTP_res300_1500_HSI_NW

Figure 11: Differential upward continuation was applied to calculate the 300m-1500m residual of the RTP data in an attempt to separate sources from different depths (Jacobsen, 1987). The source depths should correspond to half of the upward continuation level. For this residual, that would be about 150m-750m depth.

Magnetic data-processing results images (continued)
▶ Standard filtering — Medium-scale residual

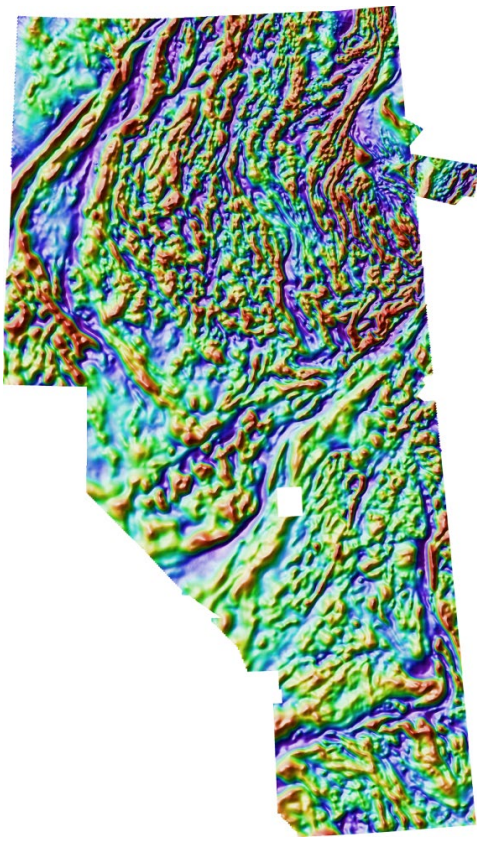

Alberta_RMIfinal_DRTP_res1500_6000_HSI_NW

Figure 12: Differential upward continuation was applied to calculate the 1500m-6000m residual of the RTP data in an attempt to separate sources from different depths (Jacobsen, 1987). The source depths should correspond to half of the upward continuation level. For this residual, that would be 750m-3000m depth.

Magnetic data-processing results images (continued)
▶ Standard filtering — Large-scale residual

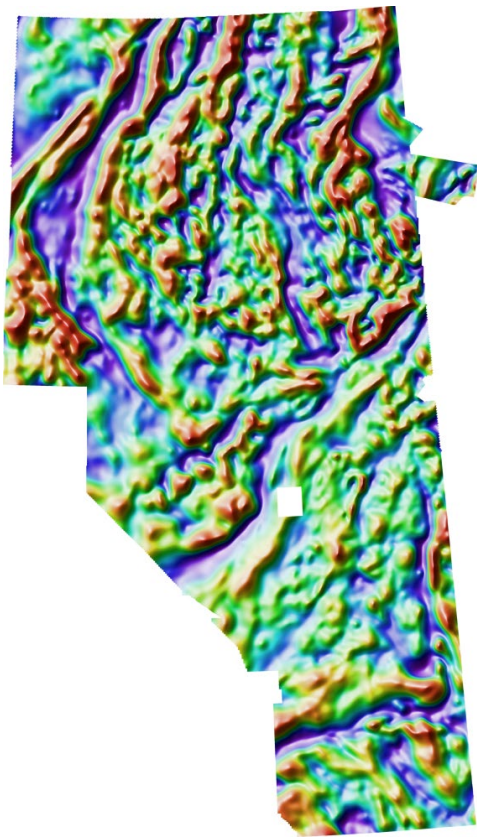

Alberta_RMIfinal_DRTP_res6000_15000_HSI_NW

Figure 13: Differential upward continuation was applied to calculate the 6000m-15000m residual of the RTP data in an attempt to separate sources from different depths (Jacobsen, 1987). The source depths should correspond to half of the upward continuation level. For this residual, that would be 3000m-7500m depth.

Magnetic data-processing results images (continued)

▶ Standard filtering — Pseudogravity

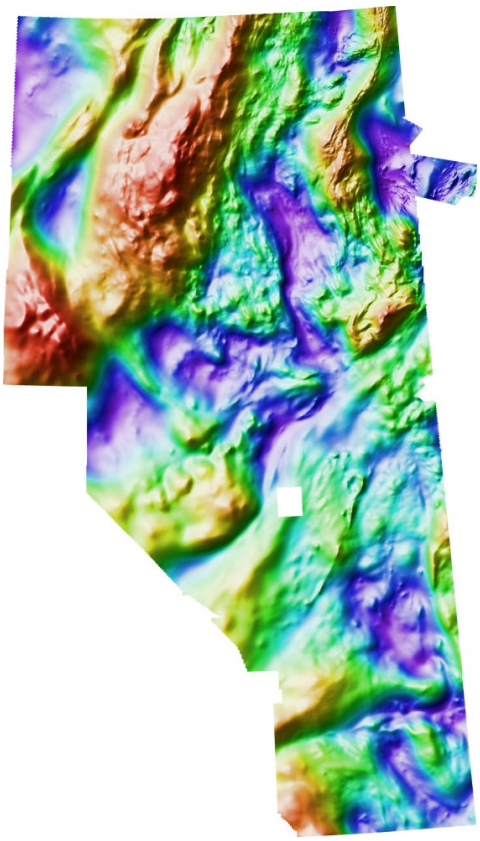

Alberta_RMIfinal_DRTP_PGrav_HSI_NW

Figure 14: Pseudogravity is generated by calculating the vertical integral of reduced-to-the-pole magnetic data and then using Poisson's relation (correlation between magnetic potential and gravitational potential) to scale the result. This generates a grid that is the expected gravity field if density were distributed in the same way as magnetic susceptibility in the project area. This is not a true gravity grid because it is highly unlikely that susceptibility and density are perfectly correlated. This filter enhances long-wavelength features and is good for highlighting large-scale features.

Magnetic data-processing results images (continued)
▶ Standard filtering — Pseudogravity residual

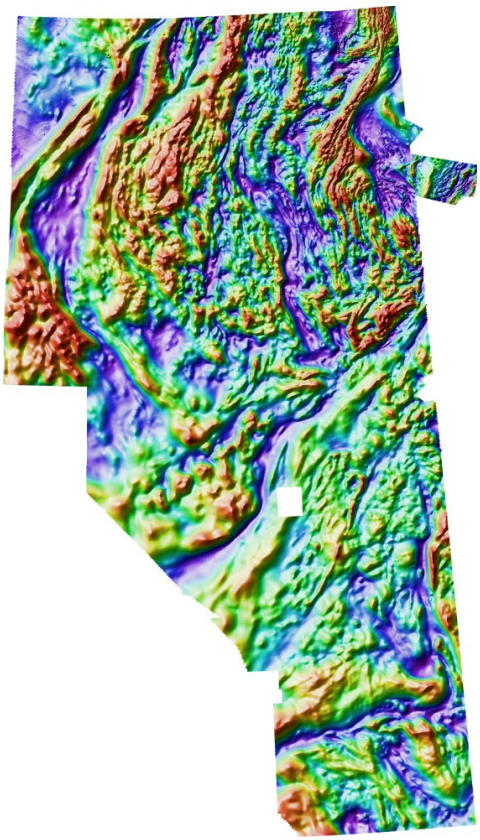

Alberta_RMIfinal_DRTP_PGravRes_HSI_NW

Figure 15: Differential upward continuation was applied to the pseudogravity grid to generate a 0-2000m residual. This removes the longest wavelength features to allow intermediate-scale features to be seen.

Magnetic data-processing results images (continued)
▶ Standard filtering — HGM of pseudogravity residual

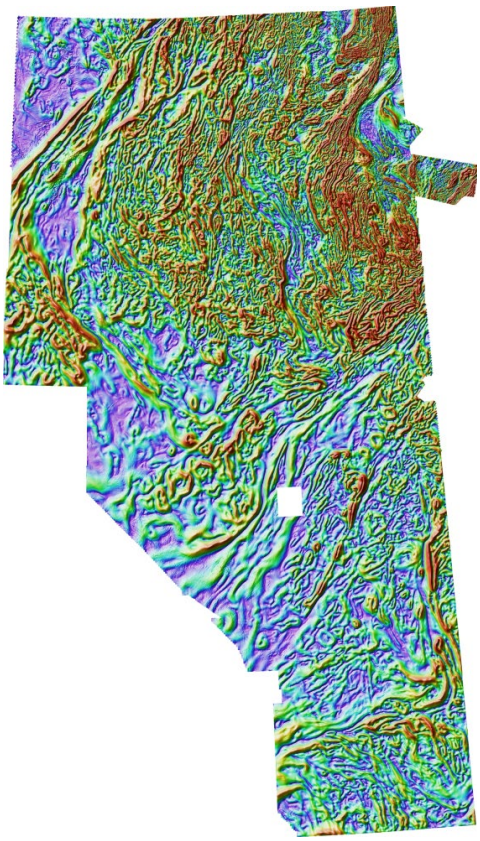

Alberta_RMIfinal_DRTP_PGravResHGM_HSI_NW

Figure 16: The horizontal gradient was calculated from the pseudogravity residual as described in the caption for **Figure 5**. The results highlight the edges of intermediate-scale features. However, this filter is affected by magnetization direction and remanent magnetization.

Magnetic data-processing results images (continued)
▶ Standard filtering images — Using ternary images

RGB

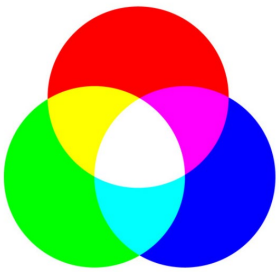

For RGB images:
Green + blue = cyan
Red + blue = magenta
Red + green = yellow
Red + green + blue = white
Low in red + green + blue = black

CMYK

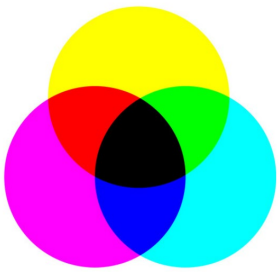

For CMY images:
Magenta + yellow = red
Cyan + yellow = green
Cyan + magenta = blue
Cyan + magenta + yellow = black
Low in red + green + blue = white

Figure 17: The information above shows how to interpret the colors in the RGB and CMY ternary images appearing in the next few figures, which are:

(i) Ternary of directional derivatives — This image encapsulates information about how steeply the gradient is changing in 3 orthogonal directions, namely the X and Y directions (within the plane of the image), and the Z direction (perpendicular to the plane of the image). All of this gradient information combines to help the observer intuitively identify the various major geological domains residing throughout the area of interest, and how these domains relate to each other.

(ii) Ternary of 1VD, tilt angle, and HGM — This image helps the observer intuitively understand where major structural features are situated, where breaks in the continuity of the magnetic 'fabric' occur, and how the textural character of the magnetic data changes from one locale to the next.

(iii) Ternary of residuals — Again, this image helps the observer intuitively understand where major structural features are situated, where breaks in the continuity of the magnetic 'fabric' occur, and how the textural character of the magnetic data changes from one locale to the next. However, features seen are generally coarser than those appearing in the ternary combining 1VD, tilt and HGM.

(iv) Ternary of RTP, VIAS, and analytic signal — This image helps the observer intuitively understand which subareas may be most affected by remanence (red locales in the CMY image).

(v) Ternary of pseudogravity results — This image combines three pseudogravity-related grids and produces an image that may assist the observer with intuitively grasping the geological affinity of features in the data.

Magnetic data-processing results images (continued)
▶ Standard filtering — Ternary of directional derivatives

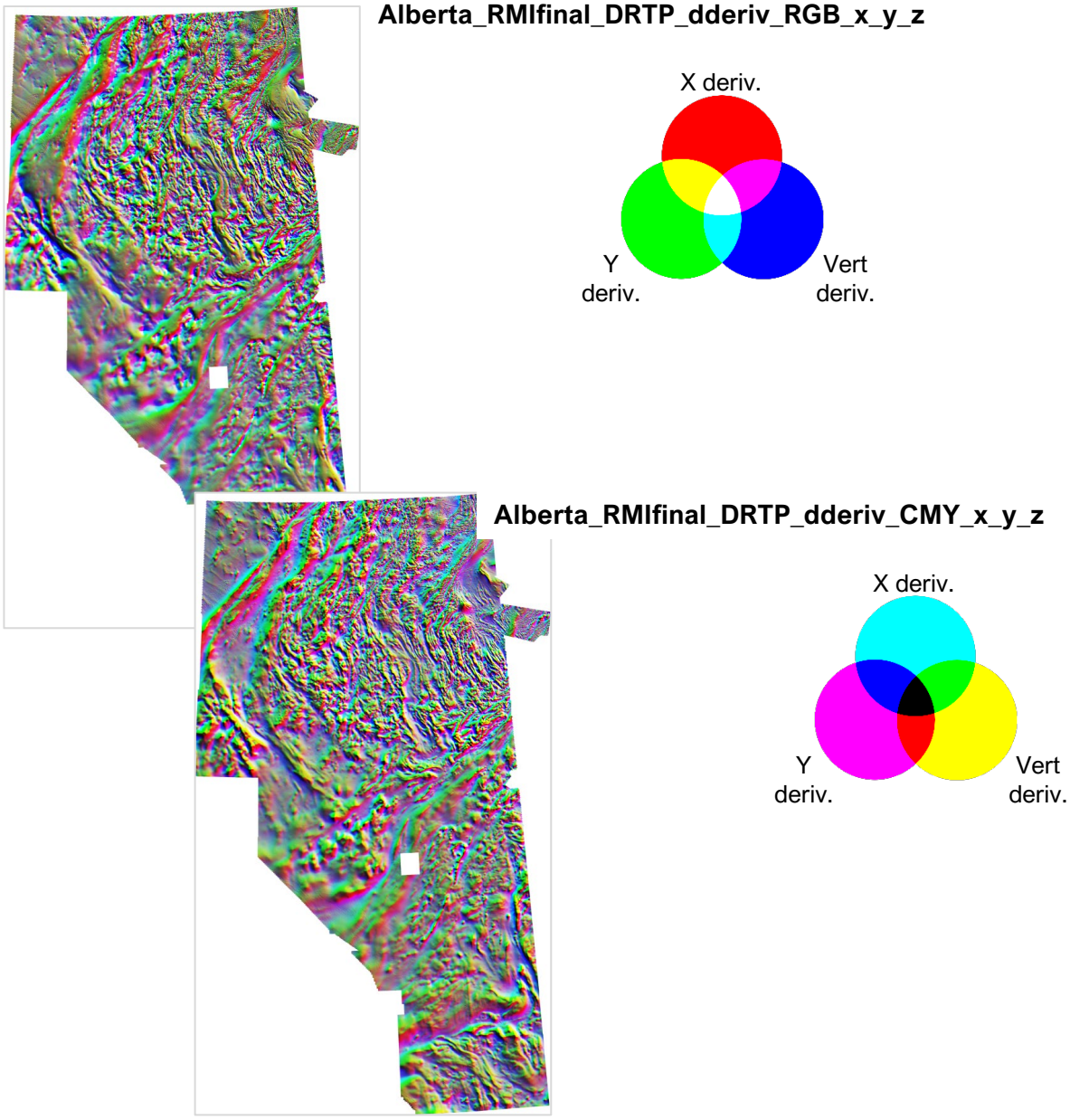

Figure 18: RGB and CMY ternary images co-displaying the X-gradient (R/C channels), Y-gradient (G/M channels), and Z-gradient (i.e., vertical derivative) (B/Y channels).

Magnetic data-processing results images (continued)

▶ Standard filtering — Ternary of 1VD, tilt, HGM

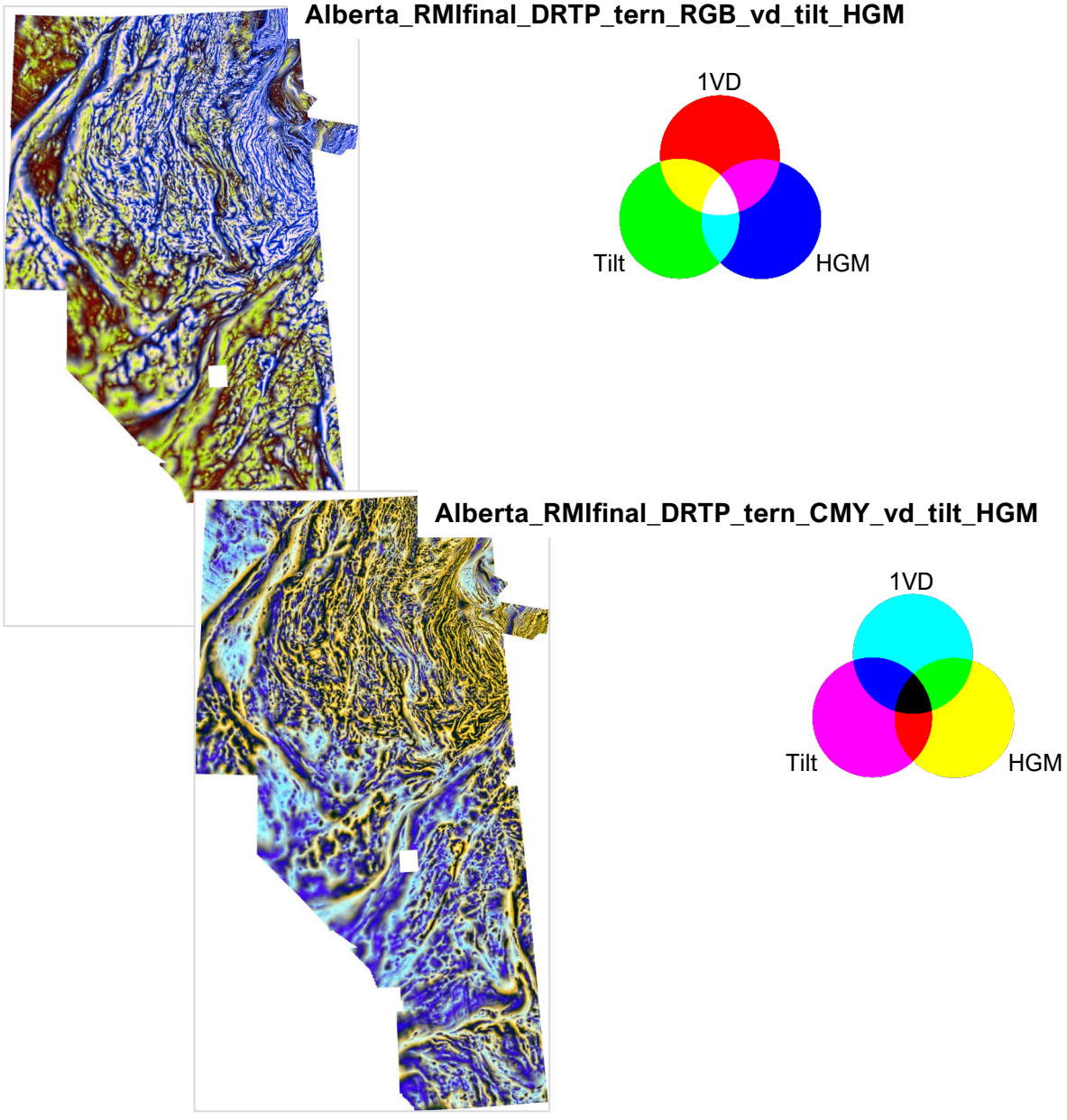

Figure 19: RGB and CMY ternary images co-displaying the vertical derivative (R/C channels), tilt angle (G/M channels), and HGM (B/Y channels).

Magnetic data-processing results images (continued)

▶ Standard filtering — Ternary of residuals

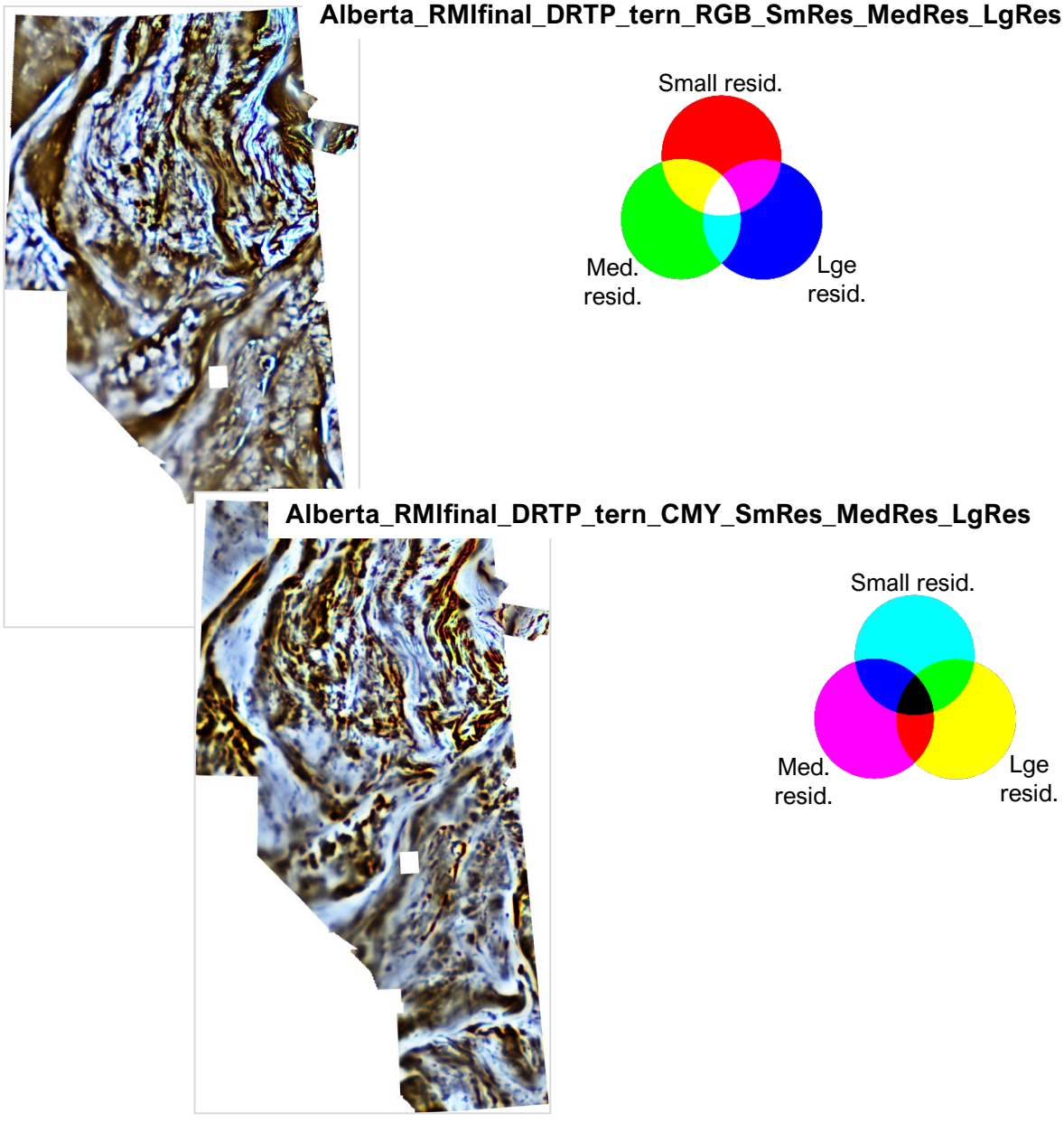

Figure 20: RGB and CMY ternary images co-displaying the small-scale (R/C channels), medium-scale (G/M channels), and large-scale residuals (B/Y channels).

Magnetic data-processing results images (continued)

▶ Standard filtering — Ternary of RTP, VIAS, Asig

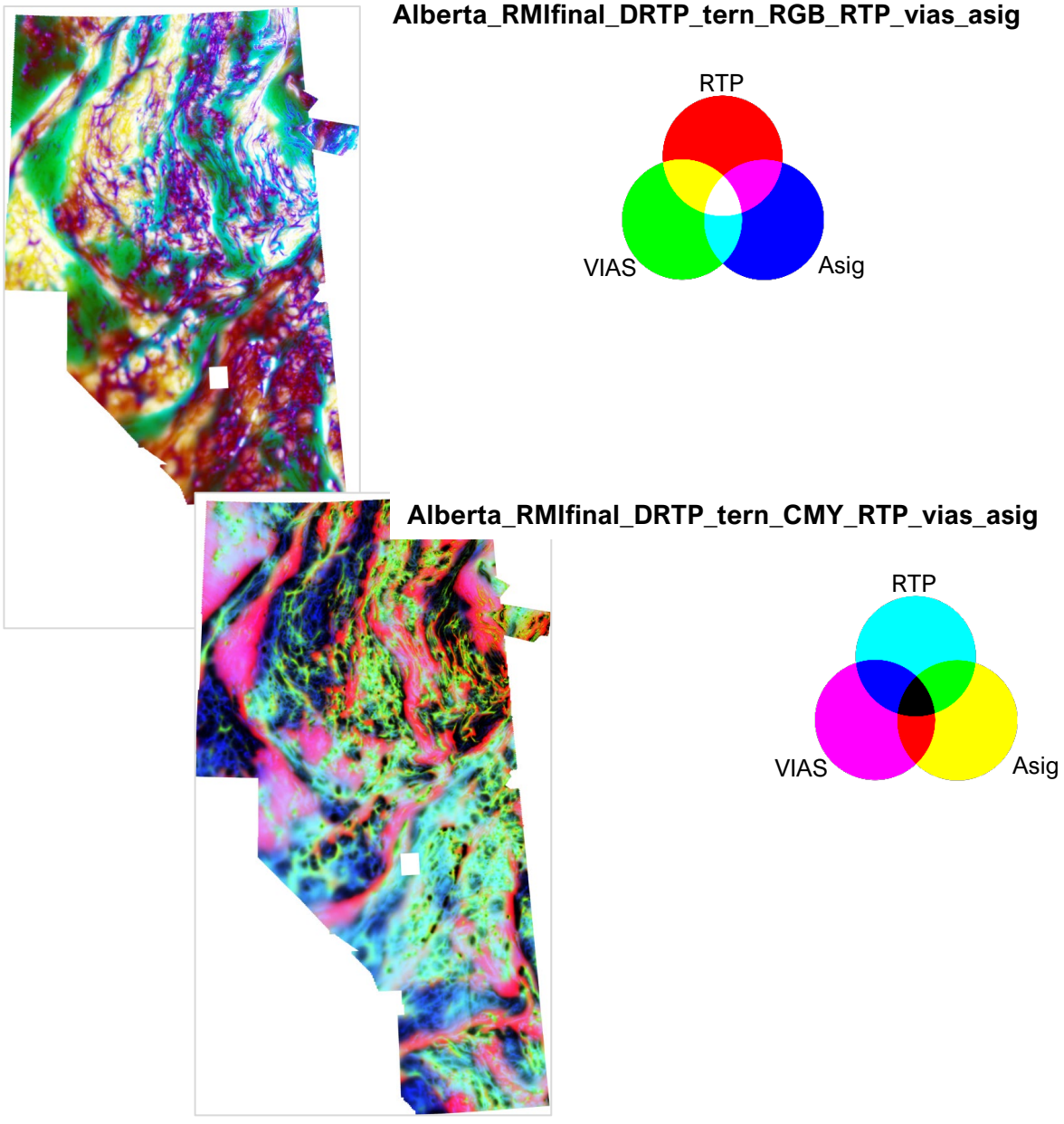

Figure 21: RGB and CMY ternary images co-displaying the RTP (R/C channels), VIAS (G/M channels), and analytic signal (B/Y channels).

Magnetic data-processing results images (continued)

▶ Standard filtering — Ternary of pseudogravity results

Alberta_RMIfinal_DRTP_tern_RGB_PGrav_PGravRes_PGravResHGM

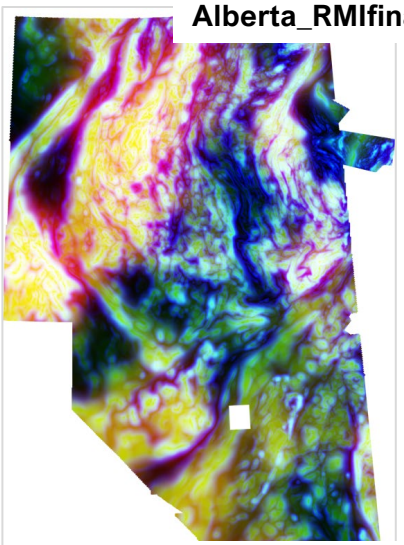

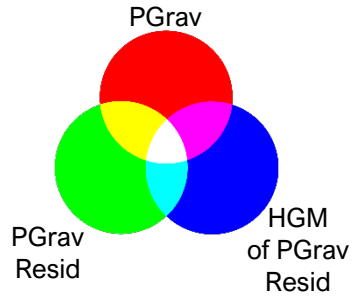

Alberta_RMIfinal_DRTP_tern_CMY_PGrav_PGravRes_PGravResHGM

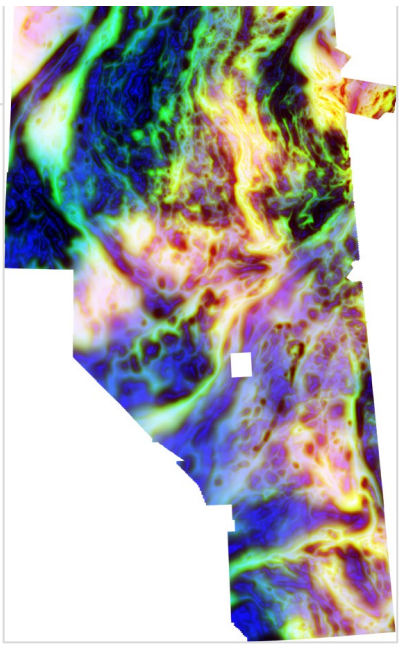

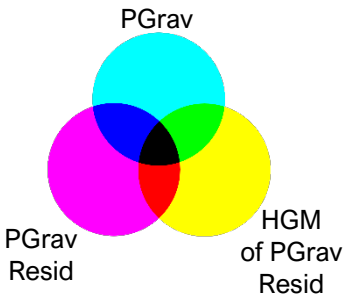

Figure 22: RGB and CMY ternary images co-displaying pseudograv (R/C channels), pseudograv residual (G/M channels), and HGM of pseudograv residual (B/Y channels).

Magnetic data-processing results images (continued)

▶ Total structure detection — Analysis of RTP

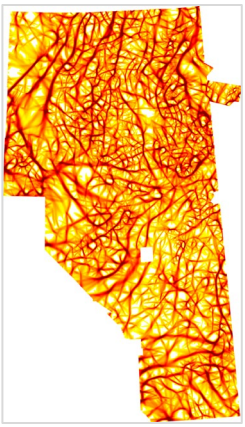

Figure 23: Representative image** showing 4000m structure detection results for the RTP data. TOP: Total structure detected. MIDDLE: Map of thresholded structural orientations. BOTTOM: Total structure in vectorized form (black lines with displayed thickness varying according to median value) over the project area's RTP image.

Alberta_RMIfinal_DRTP_Struct4000_Total

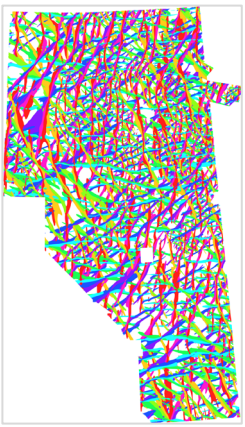

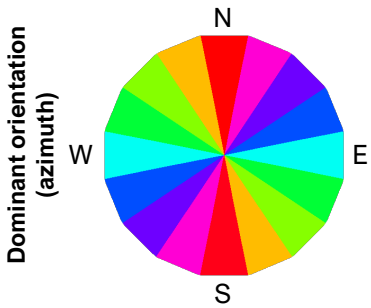

Alberta_RMIfinal_DRTP_Struct4000_OriDom_Th

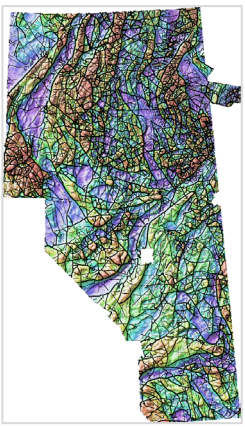

Alberta_RMIfinal_DRTP_Struct4000_Total_Vec

Alberta_RMIfinal_DRTP_HSI_NW

** *Further scales of results also delivered.*

Magnetic data-processing results images (continued)

▶ Total structure detection — Analysis of RTP

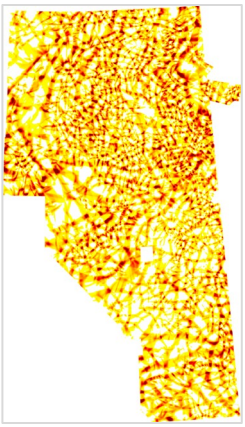

Figure 24: Representative image** showing 4000m structure detection results for the RTP data. TOP: Total structure intersections detected. MIDDLE: Intersections co-displayed with same-scale structures (line color and thickness varies according to structure's median value). BOTTOM: Intersections co-displayed with strong intersections (black-lined polygons) over gray RTP.

Alberta_RMIfinal_DRTP_Struct4000_Int

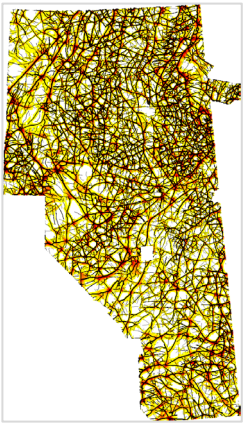

Alberta_RMIfinal_DRTP_Struct4000_Int

Alberta_RMIfinal_DRTP_Struct4000_Int_HTh_Vec

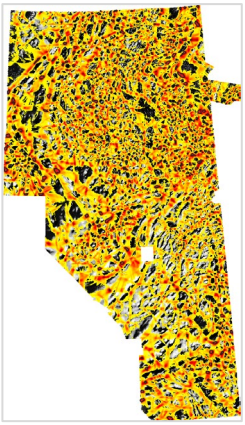

Alberta_RMIfinal_DRTP_Struct4000_Int

Alberta_RMIfinal_DRTP_Struct4000_Int_HTh_Vec

Alberta_RMIfinal_DRTP_HSI_NW (grayscale)

** *Further scales of results also delivered.*

Magnetic data-processing results images (continued)

▶ Total structure detection — Analysis of AGC

Figure 25: Representative image** showing 4000m structure detection results for the RTP's AGC. TOP: Total structure detected. MIDDLE: Map of thresholded structural orientations. BOTTOM: Total structure in vectorized form (black lines with displayed thickness varying according to median value) over the project area's RTP image.

Alberta_RMIfinal_DRTP_AGC60_Struct4000_Total

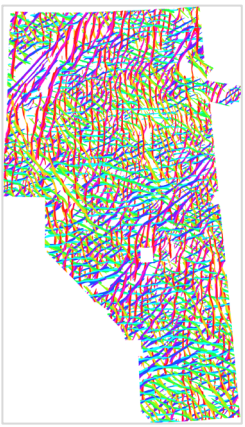

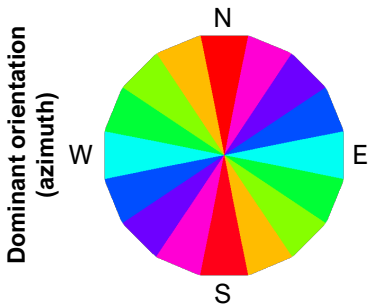

Alberta_RMIfinal_DRTP_AGC60_Struct4000_OriDom_Th

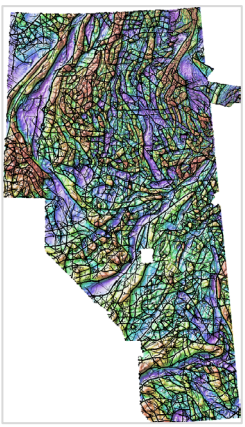

Alberta_RMIfinal_DRTP_AGC60_Struct4000_Total_Vec

Alberta_RMIfinal_DRTP_HSI_NW

** *Further scales of results also delivered.*

Magnetic data-processing results images (continued)

▶ Total structure detection — Analysis of AGC

Figure 26: Representative image** showing 4000m structure detection results for the RTP's AGC. TOP: Total structure intersections detected. MIDDLE: Intersections co-displayed with same-scale structures (line color and thickness varies according to structure's median value). BOTTOM: Intersections co-displayed with strong intersections (black-lined polygons) over gray RTP.

Alberta_RMIfinal_DRTP_AGC60_Struct4000_Int

Alberta_RMIfinal_DRTP_AGC60_Struct4000_Int

Alberta_RMIfinal_DRTP_AGC60_Struct4000_Total_Vec

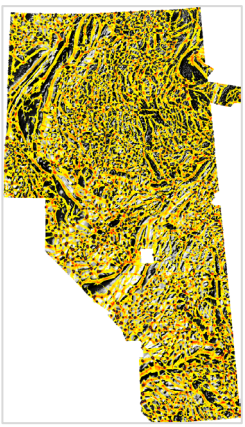

Alberta_RMIfinal_DRTP_AGC60_Struct4000_Int

Alberta_RMIfinal_DRTP_AGC60_Struct4000_Int_HTh_Vec

Alberta_RMIfinal_DRTP_HSI_NW (grayscale)

** *Further scales of results also delivered.*

Magnetic data-processing results images (continued)
▶ Parallel/cross structure — RTP fabric orientation

Alberta_RMIfinal_DRTP_Fab_Ori

Figure 27: The orientation of magnetic units was determined by taking the AGC of the RTP magnetic data and applying an anisotropic diffusion filter to highlight linear features. Ridge lines were extracted from the enhanced grid and the orientation of the ridge lines was determine. The resulting orientations were interpolated and smoothed to generate the map shown above. The green areas are dominated by WNW to NW trends. The blue and cyan areas are dominated by ENE to EW trends while the magenta indicates NE to NNE trends. The reds and oranges indicate areas that are dominated by NNW to N-trending features.

Magnetic data-processing results images (continued)

▶ Parallel/cross structure — RTP

Figure 28: Representative image** showing 4000m belt-parallel structure detection results for the RTP data. TOP: Parallel structures detected. MIDDLE: The same results in vectorized form (displayed line thickness varies according to structure's median value). BOTTOM: Vectorized results co-displayed with the RTP image.

Alberta_RMIfinal_DRTP_Struct4000_Para

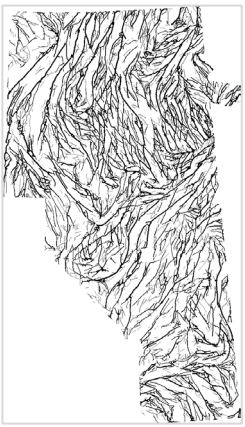

Alberta_RMIfinal_DRTP_Struct4000_Para_Vec

Alberta_RMIfinal_DRTP_Struct4000_Para_Vec

Alberta_RMIfinal_DRTP_HSI_NW

** *Further scales of results also delivered.*

Magnetic data-processing results images (continued)

▶ Parallel/cross structure — RTP

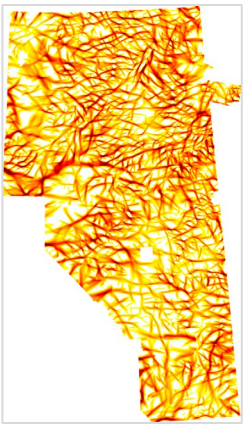

Figure 29: Representative image** showing 4000m belt-crossing structure detection results for the RTP data. TOP: Cross structures detected. MIDDLE: The same results in vectorized form (displayed line thickness varies according to structure's median value). BOTTOM: Vectorized results co-displayed with the RTP image.

Alberta_RMIfinal_DRTP_Struct4000_Cross

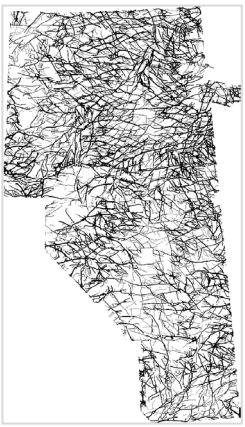

Alberta_RMIfinal_DRTP_Struct4000_Cross_Vec

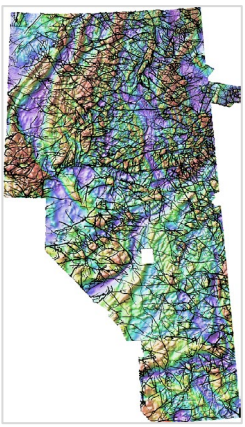

Alberta_RMIfinal_DRTP_Struct4000_Cross_Vec

Alberta_RMIfinal_DRTP_HSI_NW

** *Further scales of results also delivered.*

Magnetic data-processing results images (continued)

▶ Parallel/cross structure — AGC

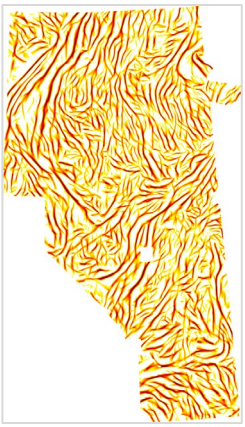

Figure 30: Representative image** showing 4000m belt-parallel structure detection results for the RTP's AGC. TOP: Parallel structures detected. MIDDLE: The same results in vectorized form (displayed line thickness varies according to structure's median value). BOTTOM: Vectorized results co-displayed with the RTP image.

Alberta_RMIfinal_DRTP_AGC60_Struct4000_Para

Alberta_RMIfinal_DRTP_AGC60_Struct4000_Para_Vec

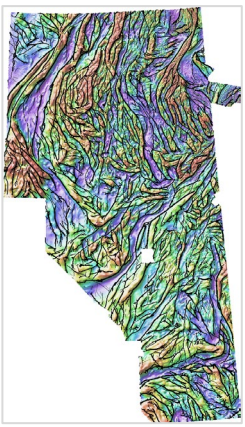

Alberta_RMIfinal_DRTP_AGC60_Struct4000_Para_Vec

Alberta_RMIfinal_DRTP_HSI_NW

** *Further scales of results also delivered.*

Magnetic data-processing results images (continued)

▶ Parallel/cross structure — AGC

Figure 31: Representative image** showing 4000m belt-crossing structure detection results for the RTP's AGC. TOP: Cross structures detected. MIDDLE: The same results in vectorized form (displayed line thickness varies according to structure's median value). BOTTOM: Vectorized results co-displayed with the RTP image.

Alberta_RMIfinal_DRTP_AGC60_Struct4000_Cross

Alberta_RMIfinal_DRTP_AGC60_Struct4000_Cross_Vec

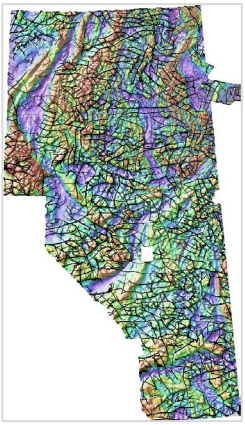

Alberta_RMIfinal_DRTP_AGC60_Struct4000_Cross_Vec

Alberta_RMIfinal_DRTP_HSI_NW

** *Further scales of results also delivered.*

Magnetic data-processing results images (continued)

▶ Radial symmetry analysis — RTP

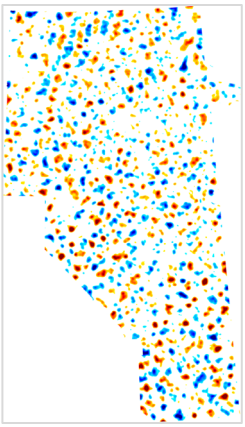

Figure 32: Representative image** showing 8000m magnitude-independent radial symmetry results for the RTP data. TOP: Radially symmetric features detected (both positive and negative anomalies). MIDDLE: Vectorized polygons representing strong anomalies obtained via thresholding. BOTTOM: Polygons co-displayed with the RTP image.

Alberta_RMIfinal_DRTP_res2000_32000_RSym8000_mi_highs_and_lows

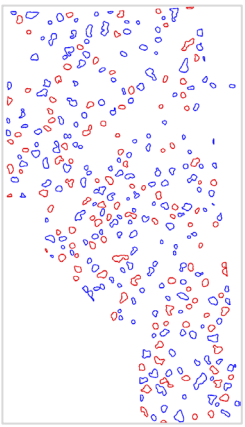

Alberta_RMIfinal_DRTP_res2000_32000_RSym8000_mi_HTh_Vec_highs

Alberta_RMIfinal_DRTP_res2000_32000_RSym8000_mi_HTh_Vec_lows

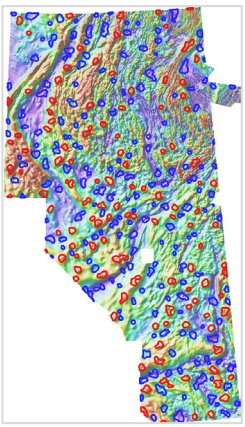

Alberta_RMIfinal_DRTP_res2000_32000_RSym8000_mi_HTh_Vec_highs

Alberta_RMIfinal_DRTP_res2000_32000_RSym8000_mi_HTh_Vec_lows

Alberta_RMIfinal_DRTP_HSI_NW

** *Further scales of results also delivered.*

Magnetic data-processing results images (continued)

▶ Depth to basement — Depth

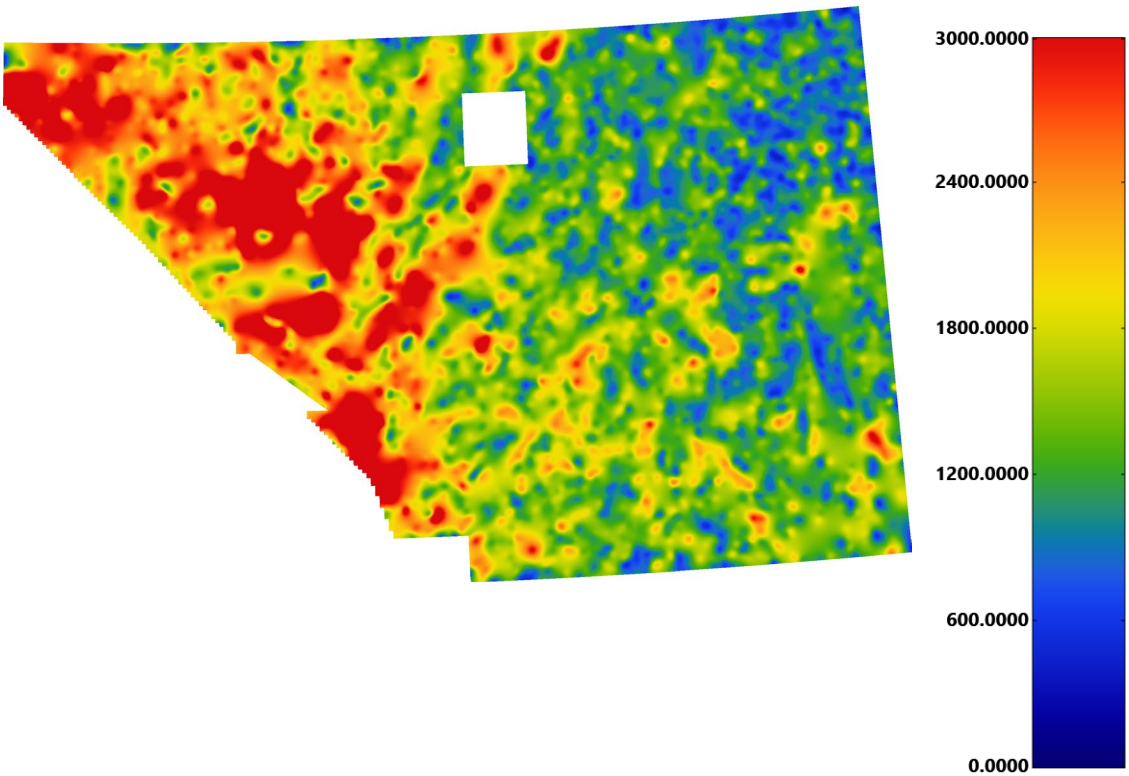

AlbertaCenter_RMI_RTP_Depth_to_Magnetic_Source

Figure 33: The depth to magnetic source results are shown colored according to the color bar on the right. The units are in meters below the topographic surface. The depths increase to the west with the magnetic rocks being buried by more than 3km in the areas with the most cover. The least cover is in the northeast. The whole area appears to have some cover present though small amounts of basement could outcrop in the NE.

Magnetic data-processing results images (continued)

▶ Depth to basement — Surface elevation

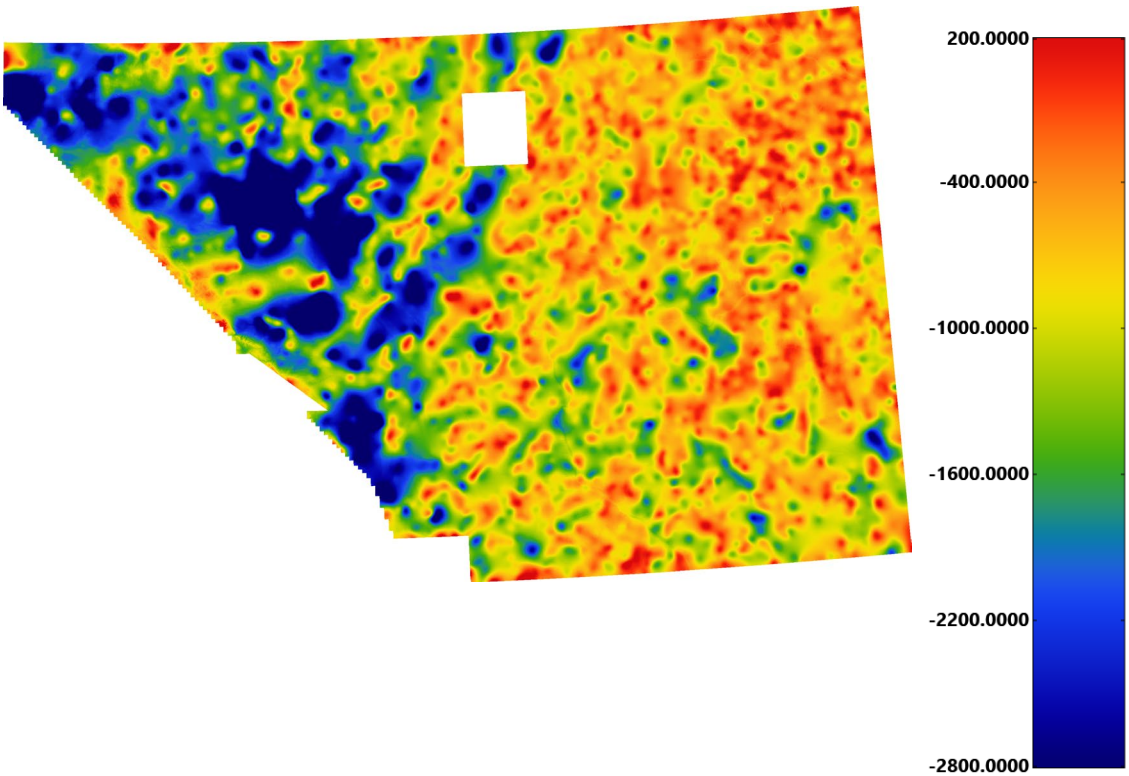

AlbertaCenter_RMI_RTP_Magnetic_Basement_Surface

Figure 34: The elevation of the magnetic basement surface is shown colored as indicated by the color bar to the right of the image. The grid is basically the inverse of the depth to source grid with the magnetic rocks close to the surface in the northeast and getting down to and RL below -2800 in parts of the west.

Appendix 1: Structure detection algorithm

The goal in developing structure detection was to move towards automated interpretation of potential field data that would be most similar to an interpretation by a person. The structure detection is a phase congruency algorithm based on oriented exponential filters (**Kovesi, 1999**).

The structure detection filter is a feature detection algorithm used to highlight ridges, valleys or edges in gridded data. The results are significantly different from other feature detection routines.

Perhaps the biggest difference is that the results are a measure of symmetry or asymmetry, irrespective of amplitude. This is because the analysis is completed using the local phase rather than the signal amplitude.

This means that features in areas of low contrast are highlighted just as well as those in areas of high contrast, as long as the frequencies are present. High values in the structure grid indicate that the structure is close to a step edge. A small step change will have a higher value than a higher amplitude change that is more gradual.

The method is also multi-scale by design. For structures to be highlighted, they must be present at more than one scale. This eliminates more-minor edges that may be present over a narrow frequency range.

The use of exponential filters to determine the scale allows for some inference as to the depth of the structures detected when the filter is applied to potential field data. The wavelength in the filename is the shallowest upward continuation level used and the approximate depth should range between 0.5 and 1 times this wavelength.

This depth estimate is based on **Jacobsen (1987)**. This method is not perfect at separating sources from different depths. It is possible to generate long-wavelength features from shallow sources as evidenced by the fact that there are long wavelength features present in radiometric data, which do not have a significant depth component. However, the method should provide a good first pass estimate of which features extend to depth and which are only surficial. It is possible for deep tapping structures to be missed if there is not a significant property contrast across them.

Appendix 1: Structure detection algorithm (continued)

The structure detection filter produces orientation grids that show the orientation of the strongest edge at a given location. When these orientation grids have been thresholded to remove low amplitude features, it's easier to see the prominent structural orientations.

References

Kovesi, P., 1999, Image Features From Phase Congruency. Videre: A Journal of Computer Vision Research, v. 1, no. 3.

Jacobsen, B.H., 1987, A case for upward continuation as a standard separation filter for potential-field maps. Geophysics, v.52, no. 8, pp. 1138-1148.

Appendix 2: Radial symmetry algorithm

The goal in developing the radial symmetry filter is a move towards automated interpretation of potential field and topographic data that would be most similar to an interpretation by a person.

The filter highlights round features (as opposed to linear features) in the data. This allows us to locate areas that have a higher likelihood of being intrusive bodies or discrete alteration zones.

We have developed several radial symmetry filters. The filter that was used for this project is a gradient-based filter that looks for points where the grid slopes away in all directions. Detected locations are magnetic highs that are discrete bodies. Discrete magnetic lows are areas where the grid slopes toward the location from all directions. This algorithm is based on **Loy and Zelinsky (2002)**.

The filter can be used in a magnitude independent (MI) or magnitude dependent (MD) mode. The MI measure is a strict measure of radial symmetry, making it a direct measure of how round an anomaly is, irrespective of the magnitude of the gradients involved there. The MD measure is the MI measure scaled according to the magnitude of the gradients in the grid.

The filter looks for features with a radius between a base radius and two times that radius. It will not locate features that are significantly smaller than the range used. The filter will highlight the center of some features that are larger than the radius range.

References

Loy G., Zelinsky A., 2002, A Fast Radial Symmetry Transform for Detecting Points of Interest. In: Heyden A., Sparr G., Nielsen M., Johansen P. (eds) Computer Vision — ECCV 2002. ECCV 2002. Lecture Notes in Computer Science, vol 2350. Springer, Berlin, Heidelberg